**UNIVERSITÀ DEGLI STUDI DI PARMA**

*Dottorato di Ricerca in Tecnologie dell'Informazione*

*XXII Ciclo*

# PHASE MODULATED LONG-HAUL OPTICAL TRANSMISSIONS WITH DIFFERENTIAL AND COHERENT RECEPTION

Coordinatore:

*Chiar.mo Prof. Carlo Morandi*

Tutor:

*Chiar.mo Prof. Alberto Bononi*

Dottorando: *Marco Bertolini*

January 2009

*A Claudia*
*Alla mia famiglia*

*“When God said ’Let there be light’he surely must have meant coherent light” (C. Townes)*

# Contents

# List of Figures

# List of acronyms

**ADC** analog-to-digital converter

**AMZI** asymmetric Mach-Zehnder interferometer

**ASE** amplified spontaneous emission

**AWGN** addictive white Gaussian noise

**BER** bit error rate

**BPSK** binary phase shift keying

**CMA** constant modulus algorithm

**CSRZ** carrier-suppressed return-to-zero

**DCF** dispersion compensating fiber

**DFB** distributed feedback

**DM** dispersion map

**DPSK** differential phase shift keying

**DQPSK** differential quadrature phase shift keying

**DSMF** dispersion slope matched fiber

**DSP** digital signal processing

**EDFA** frbium-doped fiber amplifier

**FEC** forward error correction

**FIR** finite impulse response

**GFF** gain flattening filter

**GVD** group velocity dispersion

**ISI** inter-symbol interference

**NLPN** nonlinear phase noise

**NLT** non-linear threshold

**NZ-DSF** non-zero dispersion shifted fiber

**OFDM** orthogonal frequency division multiplexing

**OOK** on-of keying

**OSNR** optical signal to niose ratio

**PBS** polarization beam splitter

**PBC** polarization beam combiner

**PDF** probability density function

**PDM** polarization division multiplexing

**PMD** polarization mode dispersion

**PMF** polarization mantaining fiber

**PRBS** pseudo-random binary sequence

**PRQS** pseudo-random quaternary sequence

**PSBT** phase shaped binary transmission

**PSK** phase shift keying

**QAM** quadrature amplitude modulation

**QPSK** quadrature phase shift keying

**ROADM** reconfigurable add-drop module

**RZ** return-to-zero

**SMF** single mode fiber

**SNR** signal to niose ratio

**SP** sensitivity penalty

**SPM** self phase modulation

**SSFM** split-step Fourier method

**WDM** wavelength division multiplexing

**XPM** cross phase modulation

**XPolM** cross-polarization modulation

# Foreword

Since the first transmission of live traffic over optical fiber by General Telephone and Electronics in 1975, the capacity of fiber based transmission systems has kept growing exponentially, almost decuplicating every four years [1]. Different technologies and techniques enabled such an incredible and continuous growth: the invention of the single mode fiber (SMF), of the erbium-doped fiber amplifier ((EDFA), the use of dispersion maps (DM), wavelength division multiplexing (WDM), and forward error correction (FEC) codes.

Over the last decade, the introduction of phase shift keying (PSK) modulation formats using direct (balanced) detection, allowed to increase the maximum reach of optical transmission systems. However the main break trough was achieved when phase modulation was first used in conjunction with coherent detection and digital signal processing (DSP) in the electronic domain. The joint use of these two techniques makes ultra-long haul, high capacity transmission possible thanks to the improved tolerances to distortion and extraordinary spectral efficiency. Fig. 1 shows the evolution over the last fifteen years of the product capacity distance (CxD, expressed in bit/s·km) of the main transmission experiments, in logarithmic scale. CxD is a common measure used to rank experimental demonstrations, that accounts both for the aggregated datarate and for the maximum reach without regeneration. The use of coherent detection and phase modulation has brought an increase of about a factor of two in the CxD products over just one year.

Even if the introduction (or the revamp, in the case of coherent detection) of these new techniques enables the rise of a new generation of optical transmission systems, it

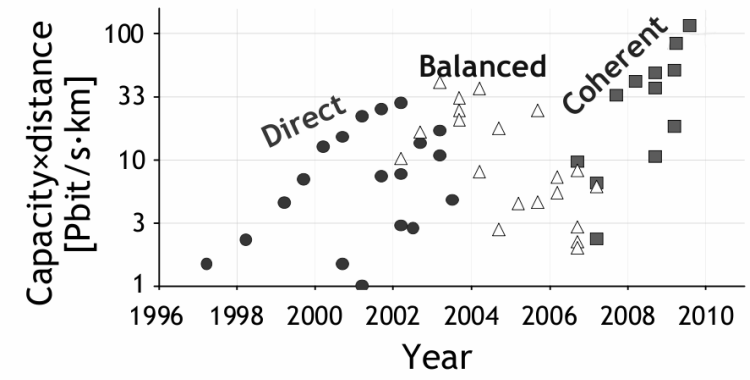


Figure 1: Evolution over time of the capacity x distance product for different reception schemes [courtesy of M. Salsi].

also poses new challenges to system designer, because new impairments (either linear or nonlinear) become dominant in these kind of transmission. Moreover, the deployment of these new technologies will happen at first in selected channels of WDM systems, and the signals will co-propagate with legacy intensity modulated (on-off keying, OOK) ones. The analysis of these peculiar "hybrid" transmission systems is required to determine and possibly mitigate the main causes of distortion. Deep theoretical, numerical and experimental studies of phase modulated systems, with balanced or coherent detection, in homogeneous or hybrid environment are underway in order to overcome the mentioned limitations.

This thesis is organized as follows. In the first chapter we will describe phase modulated optical systems, focusing on the transmitter and receiver structure and nonlinear effects peculiar to phase modulation. Chapter two retraces the history and introduces the basic concepts of coherent detection, along with the description of the most important DSP algorithms. In chapter three we present some theoretical and numerical results obtained for hybrid systems, both with direct and coherent detection. Chapter four is about the numerical and experimental study of nonlinear effects in coherent systems and the techniques to mitigate such effects. Chapter five

will briefly introduce the peculiarities of submarine transmissions and will review some experimental results when introducing coherent detection. Finally, in chapter six we will draw our conclusions.

# Chapter 1

# Phase modulation in optical communication system

## 1.1 Introduction

Since the birth of optical communications, up to around year 2000, OOK has been the only modulation format used in optical systems. This is due to the fact that turning on and off the light that comes out of a laser is the simplest way to modulate an optical signal. Also, many other technology improvements, from WDM transmissions, to the use of FEC codes, allowed to steadily increase the capacity and the reach of optical communication systems, without the need to introduce more complex modulation formats.

Over the last decade, however, a number of advanced modulation formats have been proposed, that increase the signal tolerance to optical filtering, group velocity dispersion (GVD), polarization mode dispersion (PMD), and nonlinear effects [2–4]. These formats, like duobinary and its variant phase shaped binary transmission (PSBT), or carrier-suppressed return-to-zero (CSRZ), still carry the actual information on the amplitude of the signal, but also modulate the phase of the signal. At a cost of an increased complexity of the transmitter, the tolerance of these signals to various sources of distortion is increased.

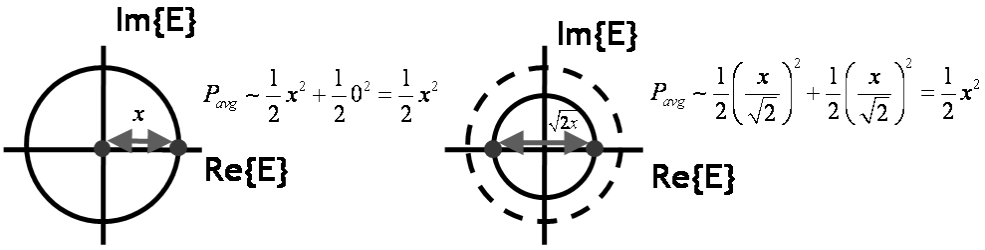


Figure 1.1: Constellation of OOK (left) and DPSK (right). The distance between the symbols is $\sqrt{2}$ larger for DPSK, yielding a 3-dB sensitivity gain.

Another approach is based on the use of phase modulation [5] (PSK), where the phase of the signal carries the information. In general, a PSK signal can be expressed in the form

$$e(t) = A_0 e^{j(2\pi f_0 t + \phi_0(t) + \frac{(m-1)\pi}{M})} \quad form = 1,2,\ldots,M, \tag{1.1}$$

where $f_0$ is the frequency of the carrier, $\phi_0(t)$ is the phase of the carrier and M is the cardinality of the alphabet. In the following we will only consider binary PSK (BPSK, $M = 2$) and quaternary PSK (QPSK, $M = 4$. To demodulate PSK signals, it is necessary to know the phase of the carrier, subtract it from the received signal and retrieve the desired information associated with the modulated phase. In direct-detection optical receivers, however, the phase of the carrier is not available, unless a complex coherent receiver is employed. Thus, if the phase of the carrier is nearly constant over two symbol times (which is generally the case in large baudrate optical systems), one can store the information onto the *phase changes* of the signal. This is why the format is called *differential* PSK. For example, in differential binary PSK (DBPSK, or DPSK), the bit "1" is associated to a phase shift of $\pi$, while the bit "0" is associated to a null phase shift. In differential quadrature PSK (DQPSK), the couples of bits "00", "01", "11" and "10" are mapped onto phase shifts between two consecutive symbols of 0, $\frac{\pi}{2}$, $\pi$, and $\frac{3\pi}{2}$.

DPSK, using a balanced reception (as we will see in the following sections), has an inherent 3dB advantage in the required optical signal to noise ratio (OSNR) at

a given bit-error rate (BER) with respect to OOK. Moreover, DPSK features a very good tolerance to nonlinear effects and thus it is well suited for long-haul transmissions. However DPSK, just like OOK and other hybrid phase/intensity modulation formats, is a binary format. This means that the maximum achievable spectral efficiency is 1 bit/s/Hz. Given an optical bandwidth in the fiber of around 4THz (the well known C band, from 1525 to 1565nm), the maximum capacity of the system is 4Tb/s. The increasing traffic that optical networks are required to sustain, requires a more efficient usage of the available bandwidth. The only solution is to resort to multilevel modulation formats. Intense study has been devoted to the simplest multilevel modulation format, DQPSK [6, 7].

In this chapter we will describe the transmitter and receiver configuration for both DPSK and DQPSK, and we will briefly introduce the peculiarities of phase modulation formats with respect to intra-channel and inter-channel nonlinear effects.

## 1.2 Transmitter Configuration

### 1.2.1 DPSK Transmitter

In the DPSK format, "0" and "1" bits are encoded as either 0 or $\pi$ phase shifts between two consecutive bits. The most obvious advantage of DPSK, compared to OOK, is that the required OSNR for a given BER is around 3dB lower for DPSK. This can be easily understood considering Fig. 1.1. Given an equal amount of output average power of the modulator, the distance between the two points of the DPSK constellation is $\sqrt{2}$ times bigger than the distance between the two OOK points. For binary formats, The BER depends on the distance between the two points of the constellation. To achieve the same BER, OOK thus requires a power 2 times higher ($\sqrt{2}$ times bigger amplitude) than DPSK and this translates into a 3dB OSNR penalty.

To generate a DPSK signal, there are two possible approaches [5]. One is to use a simple phase modulator, while the other is to resort to Mach-Zehnder modulators used for OOK modulation, by suitably choosing the driving signals. In both cases, the modulator can be optionally followed by a return-to-zero (RZ) pulse carver if RZ format is desired. The transmitter configurations are depicted in Fig. 1.2(a).

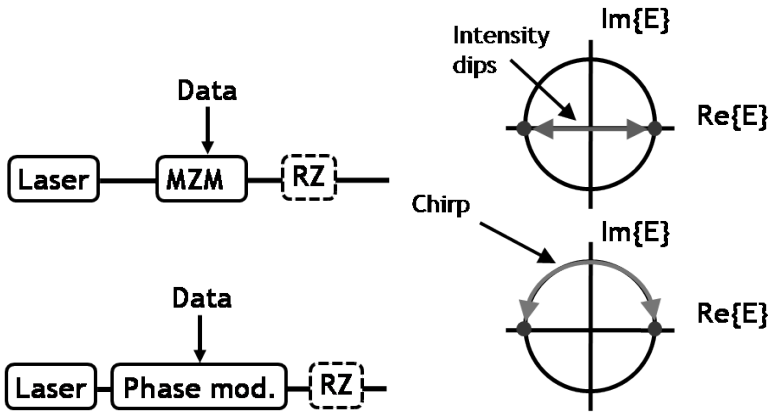


(a) (b)

Figure 1.2: Transmitter configurations (left) and transitions (right) for a DPSK signal generated using a Mach-Zehnder modulator (MZM,top) or a phase modulator (bottom).

When a phase modulator is used to generate the DPSK signal, only the phase of the signal is modified according to the driving voltage applied to the modulator, while the amplitude of the optical signals remains exactly constant (See Fig. 1.2(b)). However, due to the non ideality of the driving signal, the phase changes are not instantaneous and thus the modulator introduces chirp on the signal [8]. If not carefully designed, the chirp interacts with the GVD introducing distortion and making unattractive the use of a phase modulator.

A Mach-Zehnder modulator only acts on the amplitude of the incoming optical signal, but inverting the sign of the amplitude is equivalent to modulate the phase by $\pi$. Fig. 1.3 compares the driving signals required to generate OOK and DPSK using a Mach-Zehnder. When OOK modulating, the driving signal is biased at the middle between a minimum and a maximum of the Mach-Zehnder transfer function; then a voltage (commonly known as $V_\pi$) is applied such that the signal can swing between the minimum (light off, “0”) and the maximum (light on, “1”). When DPSK modulating, the driving signal is biased at a minimum and a voltage of $2 \times V_\pi$) is applied.

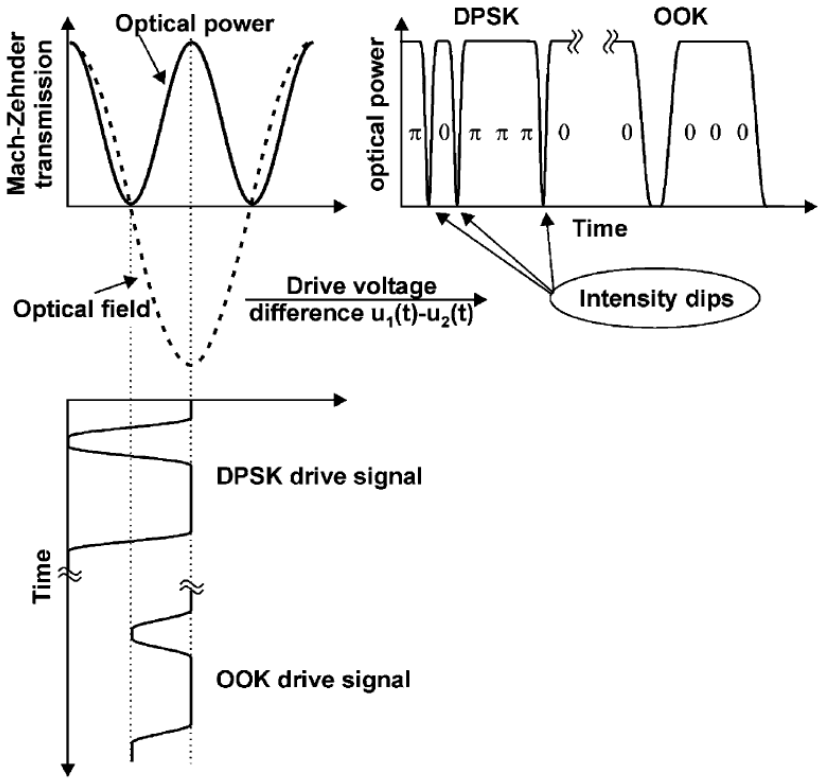


Figure 1.3: Driving signals for OOK and DPSK modulation using a Mach-Zehnder and resulting transmitted signals (reproduced from [5]).

This way the signals swings between to consecutive maxima which have the same amplitude but a phase shifted by $\pi$.

The result is that the amplitude of the DPSK is not constant (see Figs. 1.2(b),1.3), since at each transition the driving voltage crosses the minimum of the transfer function. This generates the characteristic “intensity dips” at the border of the bits where a transition happens. On the other hand, the phase shift is instantaneous, since it happens exactly when the signal crosses the minimum of the transfer function. This basically eliminates the chirp in the output signal. Moreover, when using phase mod-

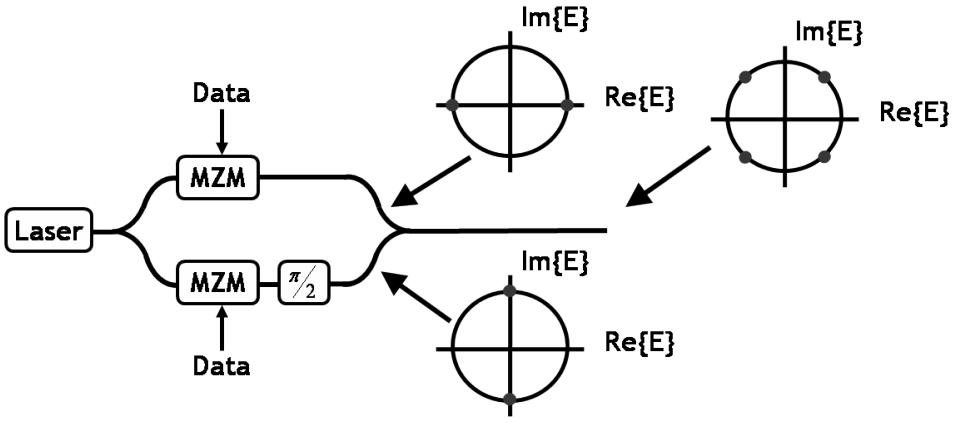


Figure 1.4: Dual parallel Mach-Zehnder modulator structure for DQPSK modulation.

ulators, the phase of the signal is proportional to the driving signal and every imperfection of the modulating waveform gets mapped to the phase of the signal. When using a Mach-Zehnder, the phase of the modulated signal is not affected by these imperfection which are in contrast mapped onto the amplitude. However, since in the DPSK format the information is stored into the phase of the signal, rather than into the amplitude, these distortion have a very limited impact on the performance of the system [3].

### 1.2.2 DQPSK Transmitter

The DQPSK transmitter is composed of two parallel Mach-Zehnder modulators inserted into a "Super Mach-Zehnder" structure, represented in Fig. 1.4. The upper arm of the super-structure contains a Mach-Zehnder modulator that DPSK-modulates the signal. The lower branch is similar, but the modulator is followed by an element that rotates the phase of the signal by $\frac{\pi}{2}$. At the output the two signals are recombined and, as long as perfect quadrature addition is assured the phase of the resulting signal can take the values $\{0, \frac{\pi}{2}, \pi, \frac{3\pi}{2}\}$. This complex transmitter structure must be integrated, in order to assure phase stability of the modulated signal. This modulator is commonly known as "dual parallel Mach-Zehnder modulator" or "QI modulator"

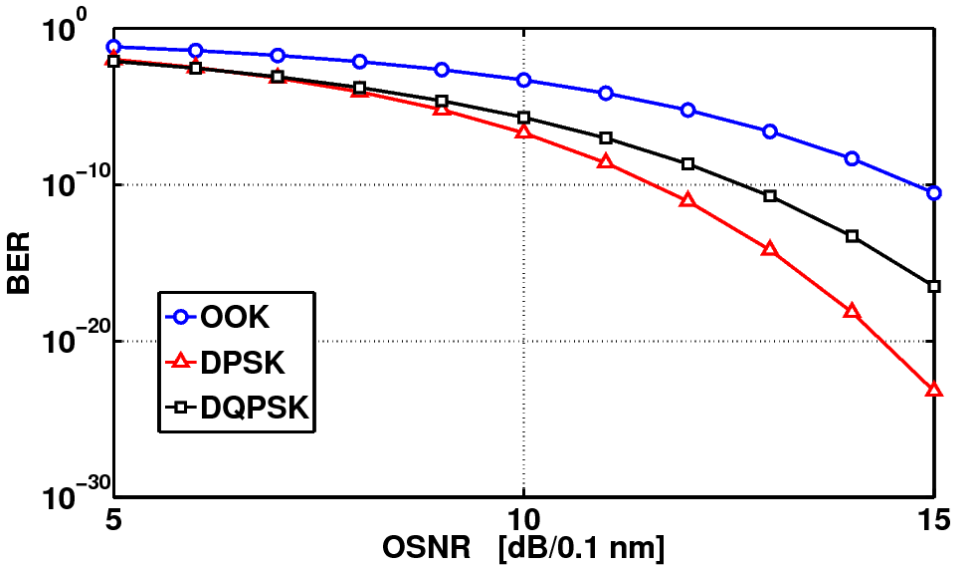


Figure 1.5: BER vs. OSNR at 0.1nm curves for OOK, DPSK and DQPSK formats at 10Gb/s.

and, coupled with the use of multilevel driving signals, can be used to generate every desired multilevel constellation.

DQPSK sensitivity at a given BER is worse than DPSK, but still better than OOK. The reduced tolerance to noise is however traded with an increased spectral efficiency than can be in theory as high as 2b/s/Hz. Fig. 1.5 shows the sensitivity curves of BER vs. OSNR at 0.1nm for OOK, DPSK and DQPSK.

## 1.3 Receiver Configuration

### 1.3.1 DPSK

A standard DPSK receiver is depicted in Fig. 1.6(a). It is composed of an optical filter ($B_o$) that selects the channel, followed by an asymmetric Mach-Zehnder interferometer (AMZI). The two outputs of the AMZI are then detected by a couple of

balanced photodiodes, and then filtered by an electric filter ($B_e$, used to filter out the out-of-band noise) before being sampled.

In order to understand the working principle of the DPSK receiver, it is first necessary to describe the AMZI. The AMZI (Fig. 1.6(b)) is a 2x2 device, composed of the cascade of an optical coupler (C), a delay component (D) and another optical coupler at the output. The transfer function of an optical coupler, with 50% splitting ratio is

$$\begin{bmatrix} \frac{1}{\sqrt{2}} & \frac{j}{\sqrt{2}} \\ \frac{j}{\sqrt{2}} & \frac{1}{\sqrt{2}} \end{bmatrix}, \tag{1.2}$$

being $j$ the imaginary unit. The delay component introduces a delay $T_0$ equal to the duration of a symbol and (optionally) a phase shift of $\varphi_0$ in the lower arm. The transfer function of this component is

$$\begin{bmatrix} e^{-j2\pi T_0 f} & 0 \\ 0 & e^{-j\varphi_0} \end{bmatrix}. \tag{1.3}$$

The total transfer function of the AMZI is thus

$$\begin{aligned} H_{AMZI}(f) &= \begin{bmatrix} \frac{1}{\sqrt{2}} & \frac{j}{\sqrt{2}} \\ \frac{j}{\sqrt{2}} & \frac{1}{\sqrt{2}} \end{bmatrix} \begin{bmatrix} e^{-j2\pi T_0 f} & 0 \\ 0 & e^{-j\varphi_0} \end{bmatrix} \begin{bmatrix} \frac{1}{\sqrt{2}} & \frac{j}{\sqrt{2}} \\ \frac{j}{\sqrt{2}} & \frac{1}{\sqrt{2}} \end{bmatrix} \\ &= \frac{1}{2} \begin{bmatrix} e^{-j2\pi T_0 f} - e^{-j\varphi_0} & j(e^{-j2\pi T_0 f} + e^{-j\varphi_0}) \\ j(e^{-j2\pi T_0 f} + e^{-j\varphi_0}) & e^{-j\varphi_0} - e^{-j2\pi T_0 f} \end{bmatrix}. \end{aligned} \tag{1.4}$$

The AMZI used in DPSK receivers has $\varphi_0 = 0$. The input signal $e_{in}(t)$, having the same expression as in eq. (1.1) with $M$=2 and Fourier transform $E_{in}(f)$, is injected only on the lower port; the two output signals are

$$\begin{aligned} \begin{bmatrix} E_{out,c}(f) \\ E_{out,d}(f) \end{bmatrix} &= \frac{1}{2} \begin{bmatrix} e^{-j2\pi T_0 f} - e^{-j\varphi_0} & j(e^{-j2\pi T_0 f} + e^{-j\varphi_0}) \\ j(e^{-j2\pi T_0 f} + e^{-j\varphi_0}) & e^{-j\varphi_0} - e^{-j2\pi T_0 f} \end{bmatrix} \begin{bmatrix} 0 \\ E_{in}(f) \end{bmatrix} \\ &= \frac{1}{2} \begin{bmatrix} jE_{in}(f)(e^{-j2\pi T_0 f} + 1) \\ E_{in}(f)(1 - e^{-j2\pi T_0 f}) \end{bmatrix} = \begin{bmatrix} E_{in}(f) H_{AMZI,21} \\ E_{in}(f) H_{AMZI,22} \end{bmatrix}. \end{aligned} \tag{1.5}$$

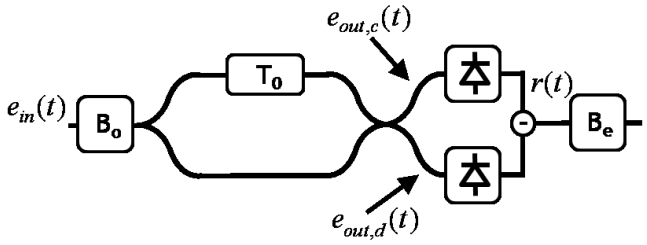


(a)

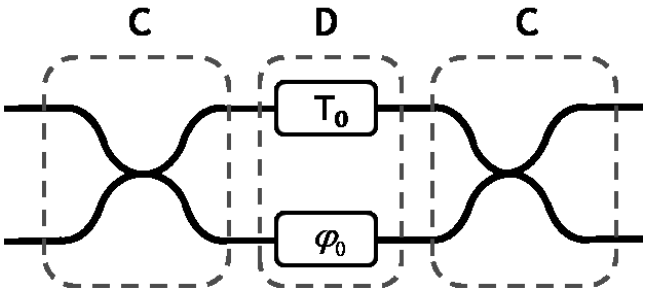


(b)

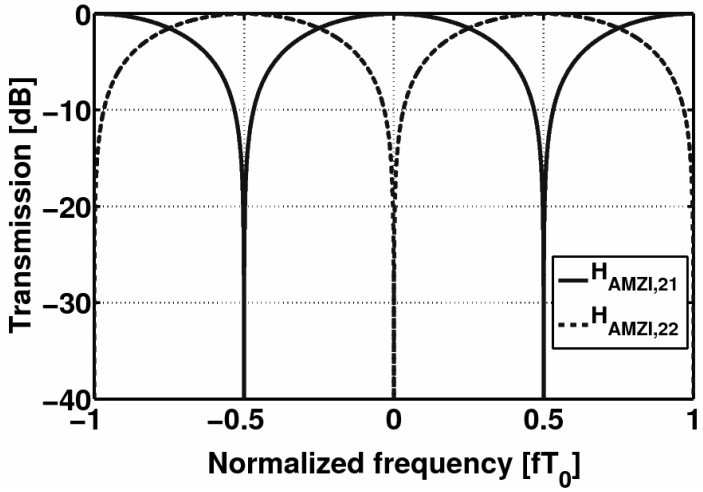


(c)

Figure 1.6: Standard DPSK receiver structure (a), building blocks of an AMZI (b) and transfer functions of the upper and lower output ports of the AMZI used for DPSK demodulation.

The transfer function of the elements $H_{AMZI,21}$ and $H_{AMZI,22}$ are depicted in Fig. 1.6(c). Taking the inverse Fourier transform

$$\begin{bmatrix} e_{out,c}(t) \\ e_{out,d}(t) \end{bmatrix} = \frac{1}{2}\begin{bmatrix} j(e_{in}(t)+e_in(t-T_0)) \\ e_{in}(t)-e_in(t-T_0) \end{bmatrix} \tag{1.6}$$

the signal at the input of the electric filter is

$$\begin{aligned} r(t) &\propto |\frac{j}{2}(e_{in}(t)+e_in(t-T_0))|^2 - |\frac{1}{2}e_{in}(t)-e_{in}(t-T_0)|^2 \\ &= Re\{e_{in}(t)e^*_{in}(t-T_0)\} \\ &= A_0^2 Re\{e^{j\Delta\theta}\} = A_0^2 cos(\Delta\theta) \end{aligned} \tag{1.7}$$

where we assumed that the carrier phase is constant over the two symbols and we called $\Delta\theta$ the phase difference between the two consecutive bits. When $\Delta\theta$=0, $r(t)$=1, while when $\Delta\theta$=$\pi$, $r(t)$=-1. Using a decision threshold fixed at 0, one can recover the transmitted bits.

### 1.3.2 DQPSK

The DQPSK receiver, depicted in Fig. 1.7(a), is basically composed of two parallel DPSK receivers with an added phase shift of $\pm\frac{\pi}{4}$ on the lower arms. Following the same calculations as in (1.2)-(1.5) and using $\varphi_0 = \pm\frac{\pi}{4}$, one finds that the received currents at the electric filters are:

$$\begin{aligned} r_I(t) &= \left|\frac{j}{2}(e_{in}(t)e^{\frac{-j\pi}{4}} + e_in(t-T_0))\right|^2 - \left|\frac{1}{2}e_{in}(t)e^{\frac{-j\pi}{4}} - e_in(t-T_0)\right|^2 \\ &= Re\{e_{in}(t)e_in^*(t-T_0)e^{\frac{-j\pi}{4}}\} \\ &= A_0^2 Re\{e^{j(\Delta\theta-\frac{\pi}{4})}\} = A_0^2 cos\left(\Delta\theta - \frac{\pi}{4}\right) \\ r_Q(t) &= \left|\frac{j}{2}(e_{in}(t)e^{\frac{j\pi}{4}} + e_in(t-T_0))\right|^2 - \left|\frac{1}{2}e_{in}(t)e^{\frac{j\pi}{4}} - e_in(t-T_0)\right|^2 \\ &= Re\{e_{in}(t)e_in^*(t-T_0)e^{\frac{j\pi}{4}}\} \\ &= A_0^2 Re\{e^{j(\Delta\theta+\frac{\pi}{4})}\} = A_0^2 cos\left(\Delta\theta + \frac{\pi}{4}\right). \end{aligned} \tag{1.8}$$

The four possible values of $\Delta\theta$ are $\{0, \frac{\pi}{2}, \pi, \frac{3\pi}{2}\}$. The respective values of the couple $[r_I(t), r_Q(t)]$ are

$$\begin{cases} \Delta\theta = 0 & \Rightarrow \quad [r_I(t), r_Q(t)] = \frac{1}{\sqrt{2}}(1,1) \\ \Delta\theta = \frac{\pi}{2} & \Rightarrow \quad [r_I(t), r_Q(t)] = \frac{1}{\sqrt{2}}(1,-1) \\ \Delta\theta = \pi & \Rightarrow \quad [r_I(t), r_Q(t)] = \frac{1}{\sqrt{2}}(-1,-1) \\ \Delta\theta = \frac{3\pi}{2} & \Rightarrow \quad [r_I(t), r_Q(t)] = \frac{1}{\sqrt{2}}(-1,1) \end{cases} \tag{1.9}$$

and thus, setting the decision thresholds to 0 for both the vector elements, one can recover the transmitted bits.

## 1.4 Nonlinear Effects in PSK transmissions

When an optical signal propagates into a fiber, the refractive index of the core of the fiber varies, depending on the instantaneous intensity of the signal. This effect is known as *Kerr nonlinearity* and it is the cause of the main nonlinear effects in fiber propagation [9–11].

Basically, the intensity variations of the signal modulate the phase of the signal itself via the refractive index. This phase modulation, in conjunction with a non-null dispersion, causes pulse broadening and, ultimately, inter-symbol interference (ISI).

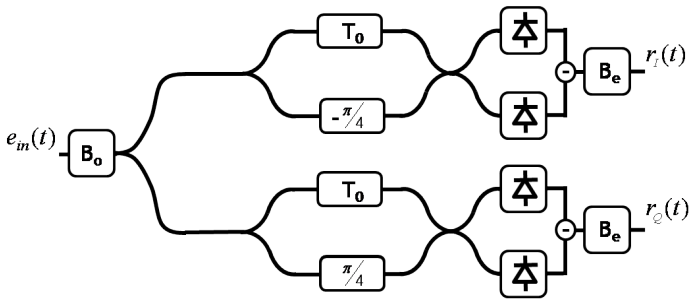


(a)

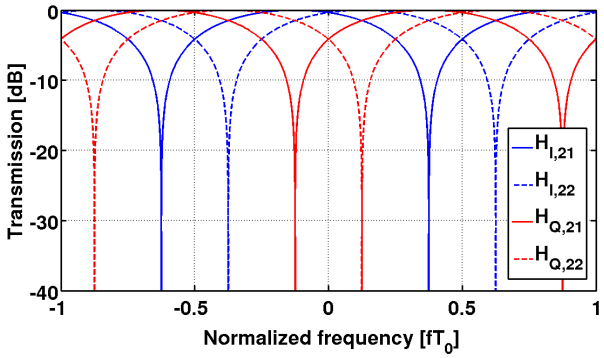


(b)

Figure 1.7: Standard DQPSK receiver structure (top) and transfer functions of the upper and lower output ports of the two AMZI (I,Q) used for DQPSK demodulation (bottom).

In WDM systems, the intensity variations of every channel do not only modulate its phase, but also modulate the phase of the neighboring channels. The first effect is called self phase modulation (SPM), while the second is known as cross phase modulation (XPM).

The intensity of PSK modulated signals is more constant than in OOK signals, because the only intensity variations are due to the distortions of the signal that would be otherwise constant in every symbol slot (or at least at the center of every symbol slot for RZ pulses). The effect of both SPM and XPM is thus reduced with respect to

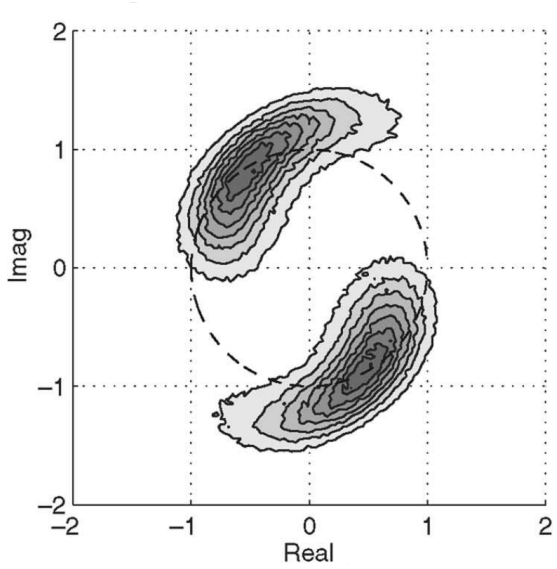


Figure 1.8: Effect of nonlinear phase noise on the PDF of the received ASE noise.

intensity modulated signals [12, 13]. However in PSK signals, another effect should be accounted for. The noise accumulated along the propagation,caused by optical amplification, can induce very rapid (shorter than the symbol time) and completely random variations of the intensity which get directly mapped on the phase of the signal through SPM. This signal-noise interaction is called *Gordon-Mollenauer effect* [14] or nonlinear phase noise (NLPN), and it is a very important source of distortion for PSK, especially for differentially decoded ones (like DPSK and DQPSK). In fact the phase gets randomized from symbol to symbol, while the basic assumption of differential detection is that the unmodulated phase of the signal is nearly constant over two symbol times.

The same reasoning can be extended to the noise generated by neighboring channels in WDM systems. In this case the noise-induced intensity variations on the other channels of the WDM comb modulate the phase of the channel through XPM. This effect is especially important for systems with high spectral efficiency (es. 10Gb/s on a 50GHz grid).

The Gordon-Mollenauer effect has been studied in many works, both theoretical [13,15–17] and experimental [18,19]. The main result is that, when NLPN is present, the noise gets colored. This means that the assumptions of addictive white Gaussian noise (AWGN) is not valid and thus both in numerical simulation and experiments, the technique of "noise loading", i.e. adding noise before the receiver in order to obtain the desired OSNR, can cause incorrect estimation of the performance of a system. It is thus very important to always account for the interaction of signal and noise along the propagation when studying DPSK/DQPSK systems. Fig. 1.8 shows the effect of NLPN on the contour plot of the probability density functions (PDF) of two received symbols in a DPSK system.

# Chapter 2

# Optical coherent detection

An alternative to direct detection, combined with intensity modulation or phase modulation, is the so called coherent detection. This demodulation technique owes its name to the fact that the receiver needs the knowledge of the phase of the carrier wave to demodulate the signal, and thus the coherence of the carrier plays an important role.

Coherent detection was already studied during the 1980s [20–25] but the advent of optical amplifiers a the beginning of the 1990s delayed the commercial deployment of such systems. In this chapter we will introduce the basic concepts of coherent detection, will review their evolution, and finally will focus on the more recent implementations in combination with electronic DSP.

## 2.1 Basic Concepts

The main idea behind optical coherent detection is to combine the incoming signal with an unmodulated laser (called *local oscillator*) in order to improve the performance of the receiver. To understand the working principle, let's consider the signal we want to demodulate as

$$E_s = A_s e^{-j(\omega_0 t + \phi_s)}, \tag{2.1}$$

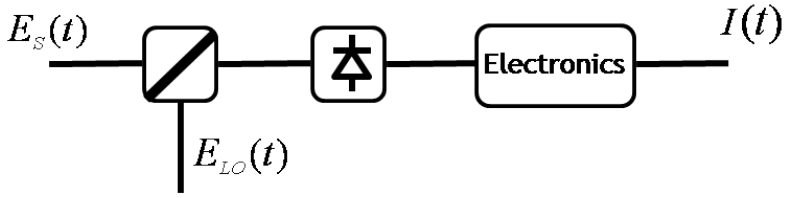


Figure 2.1: Simplest structure of an homodyne coherent receiver.

where $\omega_0$ is the carrier frequency and $A_s$ and $\phi_s$ are the amplitude and the phase of the signal. The expression for the local oscillator is

$$E_{LO} = A_{LO} e^{-j(\omega_{LO} t + \phi_{LO})}, \tag{2.2}$$

where $\omega_0$ is the local oscillator frequency and $A_{LO}$ and $\phi_{LO}$ are the amplitude and the phase of the signal. We assume that the two signals are perfectly co-polarized and that the responsivity of the photodetector is 1. If the two signals are combined as depicted in Fig. 2.1, the photo current is thus

$$\begin{aligned} I(t) &= |E_s + E_{LO}|^2 \\ &= P_s + P_{LO} + 2\sqrt{P_s P_{LO}} cos(\omega_{IF} t + \phi_s - \phi_{LO}), \end{aligned} \tag{2.3}$$

where $P_s = A_s^2$,$P_{LO} = A_{LO}^2$ and $\omega_{IF} = \omega_0 - \omega_{LO}$. We refer to the case of $\omega_{IF} = 0$ as *homodyne detection*, while if $\omega_{IF} \neq 0$, we talk about *heterodyne detection*. For homodyne reception, the photocurrent is

$$I(t) = P_s + P_{LO} + 2\sqrt{P_s P_{LO}} cos(\phi_s - \phi_{LO}) \tag{2.4}$$

and clearly, provided that $\phi_{LO}$ is known, we have access to both the phase and the amplitude of the received signal. With coherent reception it is thus possible to modulate the signal in amplitude, phase or frequency or a combination of them. In absence of amplified spontaneous emission ( ASE) noise generated by optical amplifiers, the

variance of the noise at the receiver is given by the sum of the variances of shot noise ($\sigma_s^2$) and thermal noise ($\sigma_t^2$) ( [8], Chap. 4).

$$\sigma_s^2 = 2q(I+I_d)\Delta f, \quad \sigma_T^2 = \frac{4k_BT}{R_L}F_n\Delta f, \tag{2.5}$$

where $q$ is the electron charge, $I_d$ is the dark current of the photodiode, $\Delta f$ is the effective noise bandwidth of the receiver. $k_B$ is the Boltzmann constant, $T$ is the temperature in kelvin degrees, $R_L$ is the load of the resistor and finally $F_n$ is the factor by which thermal noise is enhanced by the receiver circuits.

Assuming that $\phi_s - \phi_{LO}$ is 0 (or possibly $\pi$, in case of BPSK modulation) over a symbol time (i.e. the carrier and the local oscillator are phase locked), the signal to noise ratio (SNR) is thus

$$SNR = \frac{4P_sP_{LO}}{2q(P_{LO}+I_d)\Delta f + \sigma_T^2}, \tag{2.6}$$

where we assumed that we removed the DC component from the received signal and $P_{LO} \gg P_s$, and thus $I \simeq P_{LO}$. It is clear that increasing $P_{LO}$ one can make the contribution of thermal noise to the total noise small with respect to shot noise. This is the so called "shot-noise limited operation" regime which is desirable for devices like standard *p-i-n* photodiodes whose performance is limited by thermal noise. If we consider the heterodyne case, the photo current is

$$I(t) = P_s + P_{LO} + 2\sqrt{P_sP_{LO}}cos(\omega_{IF}t + \phi_s - \phi_{LO}). \tag{2.7}$$

In this case, we can still achieve the shot noise limited regime, but with a sensitivity penalty with respect to homodyne reception of 3dB. The received signal is in fact reduced by a factor of two when averaging the rapidly varying $cos^2(\omega_{IF})$ over one symbol time (recall average of $cos^2(\theta) = \frac{1}{2}$). In exchange for this reduced sensitivity, the phase locking of the carrier and the local oscillator is not a strict requirement in heterodyne receivers like it was in homodyne receivers, even if the phase noise of both lasers should be moderate in order to avoid penalty. This relaxed requirements make heterodyne receivers much more suitable for practical implementation.

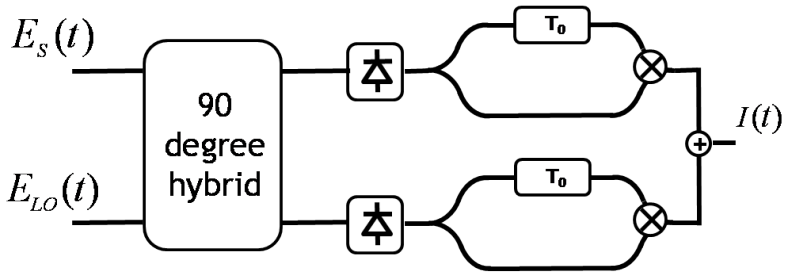


Figure 2.2: Phase diversity coherent receiver for DPSK modulation format.

### 2.1.1 Phase and polarization diversity coherent receivers

A very important source of sensitivity reduction for coherent receivers is phase noise, generated both by the transmitter laser and the local oscillator. The received photocurrent gets distorted when fluctuations of either $\phi_s$ or $\phi_{LO}$ happen, both in homodyne and in heterodyne detection (see Eq. 2.4, 2.7), even if the heterodyne case is less affected. This poses stringent requirements on the linewidths of the lasers used in coherent systems (the larger the linewidth, the larger the phase noise generated by a laser).

A possible solution is to use the so called phase-diversity receivers [26–28]. Such receivers aim at generating a photocurrent that doesn't depend on the phases $\phi_s$ and $\phi_{LO}$, using more than one photodetector. Fig. 2.2 shows the structure of a phase diversity receiver for DPSK modulation format. These receivers use optical components called "90 degrees optical hybrid", that combine the input signals in phase and in quadrature. Let the signal ($E_s$) and the local oscillator ($E_{LO}$) have the expressions

$$\begin{aligned} E_s(t) &= A_s f_s(t) e^{j(\omega_0 t+\phi_s)} \\ E_{LO}(t) &= A_{LO} e^{j(\omega_0 t+\phi_{LO})}, \end{aligned} \tag{2.8}$$

where $A_s, \phi_s, A_{LO}, \phi_{LO}$ are the amplitude and phase of the signals, $\omega_0$ is their frequency (assumed equal) and $f(t)$ can be $\pm 1$ depending on the transmitted BPSK symbol. Referring to Fig. 2.2, the outputs of the 90 degrees hybrid are:

$$\begin{aligned} E_{out,1} &= \frac{1}{2}(E_s + E_{LO}) \\ E_{out,2} &= \frac{1}{2}(E_s + jE_{LO}). \end{aligned} \tag{2.9}$$

Thus, the output of the two photodiodes are

$$\begin{aligned} I_U(t) &= \frac{P_s + P_{LO}}{2} + \sqrt{P_s P_{LO}} f_s(t) cos(\phi_s - \phi_{LO}) \\ I_L(t) &= \frac{P_s + P_{LO}}{2} + \sqrt{P_s P_{LO}} f_s(t) sin(\phi_s - \phi_{LO}), \end{aligned} \tag{2.10}$$

where $P_L$ and $P_s$ are the powers of the local oscillator and the signal at the input of the hybrid. Now let us drop the DC terms, multiply the received currents by their replica delayed by one symbol time $T_0$ and sum. Assuming that the phase of both lasers is constant over two symbol times, one gets

$$\begin{aligned} I(t) &= P_s P_{LO} f_s(t) f_s(t - T_0) \left\{ cos^2(\Delta\phi) + sin^2(\Delta\phi) \right\} \\ &= P_s P_{LO} f_s(t) f_s(t - T_0). \end{aligned} \tag{2.11}$$

The final current is independent of the phase noise of the lasers, provided that the phase variations are slow compared to the symbol time.

The other main source of sensitivity reduction in these coherent receivers is polarization mismatch between the local oscillator and the transmitter laser. This is not a problem in direct detection schemes, because the photodiodes detect both the polarizations of the signal. However in coherent receivers, the intensity of the beating of the two signals is proportional to the angle ($\theta$) between their two states of polarization. If they are orthogonal ($\theta = \frac{\pi}{2}$), the output signal disappears (complete fading). One possible solution is to track the value of $\theta$ and try to force it to 0, however this requires complex feedback control techniques that increase the complexity of the system.

Another approach is to resort to the so called *polarization diversity receivers* [29–31] whose operation is independent of the states of polarization of the signals.

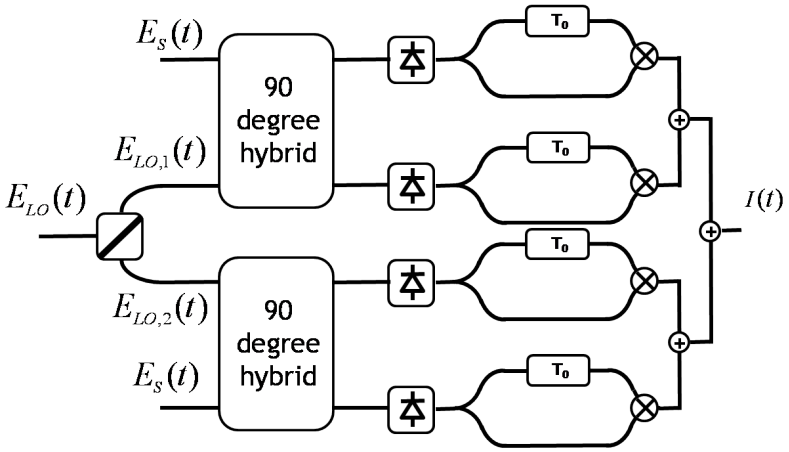


Figure 2.3: Phase and polarization diversity coherent receiver for DPSK modulation format.

This technique can be used in combination with phase diversity reception in order to obtain a receiver tolerant to both phase and polarization fluctuations. Fig. 2.3 depicts a phase and polarization diversity receiver for DPSK modulation. The input signals of the two optical hybrids are the same as in Eq. (2.8), with the difference that the amplitude of the local oscillator is multiplied by the splitting factor of the polarization beam splitter (PBS) $\sqrt{\alpha}$ on one arm and by $\sqrt{1-\alpha}$ on the other arm

$$\begin{aligned} E_{LO,1} &= \sqrt{\alpha} A_{LO} e^{j(\omega_0 t + \phi_{LO})} \\ E_{Lo,2} &= \sqrt{1-\alpha} A_{LO} e^{j(\omega_0 t + \phi_{LO})}. \end{aligned} \tag{2.12}$$

Using the same notations as for the phase diversity receiver, the final current is

$$
\begin{aligned}
I(t) &= \alpha P_s P_{LO} f_s(t) f_s(t-T_0) cos^2(\Delta\phi) + \\
&= \alpha P_s P_{LO} f_s(t) f_s(t-T_0) sin^2(\Delta\phi) + \\
&= (1-\alpha) P_s P_{LO} f_s(t) f_s(t-T_0) cos^2(\Delta\phi) + \\
&= (1-\alpha) P_s P_{LO} f_s(t) f_s(t-T_0) sin^2(\Delta\phi) + \\
&= \alpha P_s P_{LO} f_s(t) f_s(t-T_0) + (1-\alpha) P_s P_{LO} f_s(t) f_s(t-T_0) \\
&= P_s P_{LO} f_s(t) f_s(t-T_0) \qquad (2.13)
\end{aligned}
$$

which is clearly independent of both the splitting ratio $\alpha$ (which in turn is a function of the angle $\theta$) and the phase noise.

### 2.1.2 The reason of the abandon

The main reason that caused at the beginning of the 1990s the abandon of coherent optical communications was the invention of EDFAs. In presence of optical amplification, in fact, the variance of the noise at the receiver is given by the sum of the variances expressed in Eq. (2.5), plus the contribution of ASE noise. This last term gets largely dominant and it is independent of the demodulation scheme; thus the sensitivity improvement given by coherent reception with respect to direct detection is largely reduced, making this technique far less attractive.

Moreover, the complexity of the required optical components at the receiver (optical hybrid, PBS, etc.) increased the cost of the transceiver. As a consequence, coherent reception was unattractive from an economic point of view in absence of clear performance improvement or at least strong reduction of the complexity of the overall optical system.

## 2.2 Current Optical Coherent Receivers

The rebirth of coherent optical communications at the beginning of years 2000 was possible thanks to the exponential growth of computing performance of silicon based-processors guaranteed by Moore's law. Today fairly inexpensive, very complex and

very high speed DSP processors are available on the market and allow to exploit the great advantage of coherent reception: the fact that both the amplitude and the phase of the transmitted signal are available at the receiver (see Eq. (2.4)). With an adequate amount of processing power it is thus possible to compensate for both linear and deterministic nonlinear effects in the electrical domain. This allows to reduce the need for complex optical compensators and to move nearly all the complexity of the optical transmission line at the transceiver. Moreover, coherent polarization diversity reception makes practical transmissions on both polarizations, thus doubling the spectral efficiency.

For these reasons, coherent reception in conjunction with electronic DSP has been a very hot research topic for the last few years. Both 40Gb/s [32–36] and 100Gb/s transmissions [37–40] have been demonstrated using coherent reception. Also, ultra-long haul transmissions have been achieved at both 40Gb/s and 100Gb/s [41–45] paving the way for undersea coherent optical communications. Ultra-high spectral efficiency have been reported [46–48] strongly increasing the amount of information that can be squeezed into the C-band. Finally, it is worth to note that 40Gb/s transceivers based on PDM-QPSK are already commercially available [49], while 100Gb/s ones are expected to hit the market very soon.

Usually when using coherent detection, the data are transmitted on both polarizations (polarization division multiplexing PDM) since, as we will see in this chapter, the detection is always performed using polarization diversity in order to be able to compensate for the fiber birefringence. Thus PDM doesn't introduce increased complexity at the receiver and can double the spectral efficiency, independently of the selected modulation format.

Many modulation formats have been used in combination with coherent detection, based both on PSK (BPSK, QPSK, 8-PSK, etc.) and quadrature amplitude modulation (8-QAM, 16-QAM, 64-QAM, etc.). Aside of standard single-carrier transmissions, also orthogonal frequency division multiplexing (OFDM) can be used with coherent receiver [50]. This modulation technique is often used in the wireless domain and allows for extremely high spectral efficiency coupled with great tolerance to linear impairments.

However, among all the possible formats, QPSK combined with PDM has been the more studied, especially at 100Gb/s. Using four 25Gb/s binary streams, one can pack 100Gb/s in a 50GHz channel, reaching a notable spectral efficiency or 2b/s/Hz. Moreover PDM-QPSK has proved to be a very good choice with respect to tolerance to fiber nonlinearities at such high bitrates. In the course of this section we will briefly describe the current more common configuration of the coherent receiver (which is the same for all modulation formats), while in the next one we will focus on the DSP algorithms used in the receiver, with special attention to the ones used for PDM-QPSK.

Fig. 2.4 shows the "coherent mixer" that is used today in coherent optical systems to recover the phase and amplitude of the received signal and to convert it to the electronic domain. It is basically a polarization and phase diversity receiver that uses four balanced photodiodes to detect the light and isolate the beating between the carrier and the local oscillator.

We assume that the received signal carries information on both polarizations and thus has the form

$$\begin{aligned} \overrightarrow{E_r}(t) &= E_{rx}\widehat{\mathbf{x}} + E_{ry}\widehat{\mathbf{y}}, \\ E_{rx} &= A_{rx}(t)e^{j(\omega_r t+\varphi_x(t)+\varphi_{n,x}(t))} \\ E_{ry} &= A_{ry}(t)e^{j(\omega_r t+\varphi_y(t)+\varphi_{n,y}(t))} \end{aligned} \tag{2.14}$$

and $\varphi_x(t), \varphi_y(t)$ are the modulated phases while $\varphi_{n,x}(t), \varphi_{n,y}(t)$ represent the phase noise of the carrier on the two polarizations. The local oscillator can be represented as

$$E_{LO} = A_{LO}e^{j(\omega_{LO}t+\varphi_{n,LO}(t))}, \tag{2.15}$$

where $\varphi_{n,LO}(t)$ is the phase noise associated with the local oscillator. Each PBS splits in two the power of the incident light and rotates the phase by $\frac{\pi}{2}$. The quarter wave plate (QWP) rotates by $\frac{\pi}{2}$ half of the linearly polarized light coming from the local oscillator. This way the polarization of the local oscillator becomes circular at

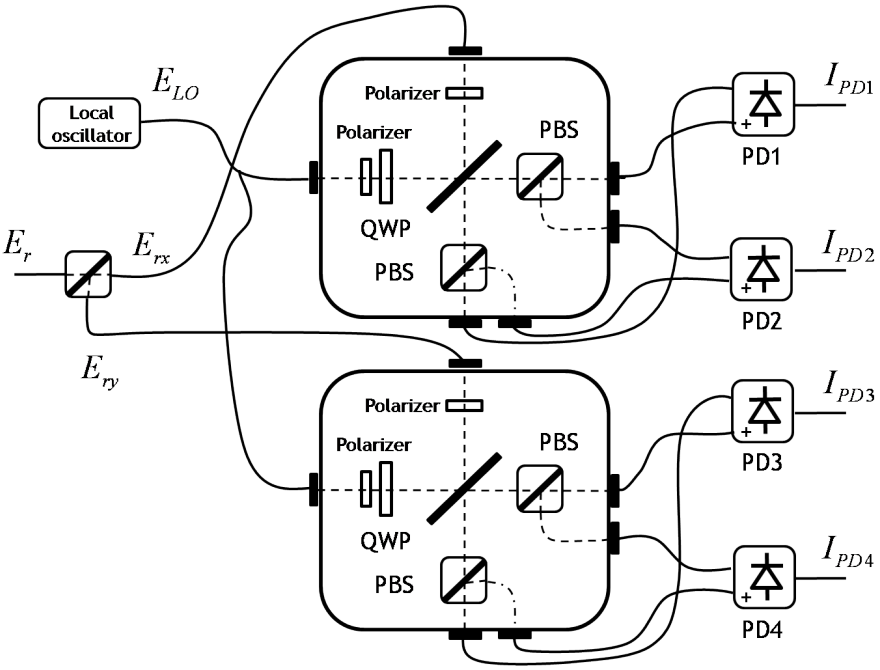


Figure 2.4: Detailed scheme of a coherent mixer for phase and polarization diversity coherent receivers for PDM transmissions connected to four balanced photodiodes.

the output of the QWP. At the eight output ports of the coherent mixer the electric fields of the received signals are thus:

$$
\begin{aligned}
E_{r1+} &= \frac{1}{2\sqrt{2}} E_{rx} e^{j\frac{\pi}{2}} \qquad E_{r3+} = \frac{1}{2\sqrt{2}} E_{ry} e^{j\frac{\pi}{2}} && \text{Shifted by one reflection} \\
E_{r1-} &= \frac{1}{2\sqrt{2}} E_{rx} \qquad E_{r3-} = \frac{1}{2\sqrt{2}} E_{ry} && \text{Not shifted} \\
E_{r2+} &= \frac{1}{2\sqrt{2}} E_{rx} e^{j\frac{\pi}{2}} \qquad E_{r4+} = \frac{1}{2\sqrt{2}} E_{ry} e^{j\frac{\pi}{2}} && \text{Shifted by one reflection} \\
E_{r2-} &= \frac{1}{2\sqrt{2}} E_{rx} e^{j\pi} \qquad E_{r4-} = \frac{1}{2\sqrt{2}} E_{ry} e^{j\pi} && \text{Shifted by two reflections,}
\end{aligned}
\tag{2.16}
$$

while the electric fields of the local oscillator are

$$\begin{aligned}
E_{LO1+} = E_{LO3+} &= \frac{1}{2\sqrt{2}} E_{LO} e^{j\frac{\pi}{2}} && \text{Shifted by QWP} \\
E_{LO1-} = E_{LO3-} &= \frac{1}{2\sqrt{2}} E_{LO} e^{j\pi} && \text{Shifted by QWP and one reflection} \\
E_{LO2+} = E_{LO4+} &= \frac{1}{2\sqrt{2}} E_{LO} e^{j\pi} && \text{Shifted by two reflections} \\
E_{L=2-} = E_{LO4-} &= \frac{1}{2\sqrt{2}} E_{LO} e^{j\frac{\pi}{2}} && \text{Shifted by two reflection.}
\end{aligned} \tag{2.17}$$

Thus the resulting photocurrents are

$$\begin{aligned}
I_{PD1+} &\propto \left| \frac{1}{2\sqrt{2}} E_{rx} e^{j\frac{\pi}{2}} + \frac{1}{2\sqrt{2}} E_{LO} e^{j\frac{\pi}{2}} \right|^2 \\
&= \frac{1}{8} |A_{rx}|^2 + \frac{1}{8} |A_{LO}|^2 + \frac{1}{4} A_{rx} A_{LO} cos\left[(\omega_r - \omega_{LO})t + \varphi_{rx}(t)\right] \\
I_{PD1-} &\propto \left| \frac{1}{2\sqrt{2}} E_{rx} + \frac{1}{2\sqrt{2}} E_{LO} e^{j\pi} \right|^2 \\
&= \frac{1}{8} |A_{rx}|^2 + \frac{1}{8} |A_{LO}|^2 - \frac{1}{4} A_{rx} A_{LO} cos\left[(\omega_r - \omega_{LO})t + \varphi_{rx}(t)\right],
\end{aligned} \tag{2.18}$$

where $\varphi_{rx}(t) = \varphi_y(t) + \varphi_{n,y}(t) - \varphi_{n,LO}(t)$ is the modulated phase plus the difference between the phase of the two lasers. The final photocurrent at the output of the first balanced photodiodes is thus

$$I_{PD1} = I_{PD1+} - I_{PD1-} = \frac{1}{2} A_{rx} A_{LO} cos\left[(\omega_r - \omega_{LO})t + \varphi_{rx}(t)\right] \tag{2.19}$$

and repeating the calculations for the other three photodiodes one gets

$$
\begin{aligned}
I_{PD2} &= I_{PD2+} - I_{PD2-} = \frac{1}{2} A_{rx} A_{LO} sin\left[(\omega_r - \omega_{LO})t + \varphi_{rx}(t)\right] \\
I_{PD3} &= I_{PD3+} - I_{PD3-} = \frac{1}{2} A_{ry} A_{LO} cos\left[(\omega_r - \omega_{LO})t + \varphi_{ry}(t)\right] \\
I_{PD4} &= I_{PD4+} - I_{PD4-} = \frac{1}{2} A_{ry} A_{LO} sin\left[(\omega_r - \omega_{LO})t + \varphi_{ry}(t)\right]
\end{aligned} \tag{2.20}
$$

and finally

$$
\begin{aligned}
I_{PD1} + jI_{PD2} &= \frac{1}{2} A_{rx} A_{LO} e^{j\left[(\omega_r - \omega_{LO})t + \varphi_{rx}(t)\right]} \\
I_{PD3} + jI_{PD4} &= \frac{1}{2} A_{ry} A_{LO} e^{j\left[(\omega_r - \omega_{LO})t + \varphi_{ry}(t)\right]}.
\end{aligned} \tag{2.21}
$$

If one can estimate both the frequency detuning $(\omega_r - \omega_{LO})$ and the phase noise of the lasers $\varphi_{n,y}(t) - \varphi_{n,LO}(t)$ both the amplitude and the phase of the signals on both polarizations are available at the decision gate, since the amplitude of the local oscillator $A_{LO}$ is constant.

## 2.3 DSP Algorithms

In this section we will analyze the sequence of DSP functions used to recover the phase and the amplitude of a 100Gb/s PDM-QPSK signal and eventually compensate for linear impairments like GVD and PMD. Many of these functions are common to any modulation format, while others require slight modifications. However conceptually the steps required to recover the transmitted information from the photocurrents is the same, independently of the selected format. Also, we will always consider a 112Gb/s signal, since optical transmission systems use FEC codes that require an overhead that is typically 12% for such high bitrates.

Fig. 2.5 shows the diagram of the DSP processing in an optical coherent receiver. First the photocurrents are sampled by four analog-to-digital converters (ADC) clocked at twice the symbolrate (Nyquist rate) to avoid aliasing. For 112Gb/s PDM-QPSK the

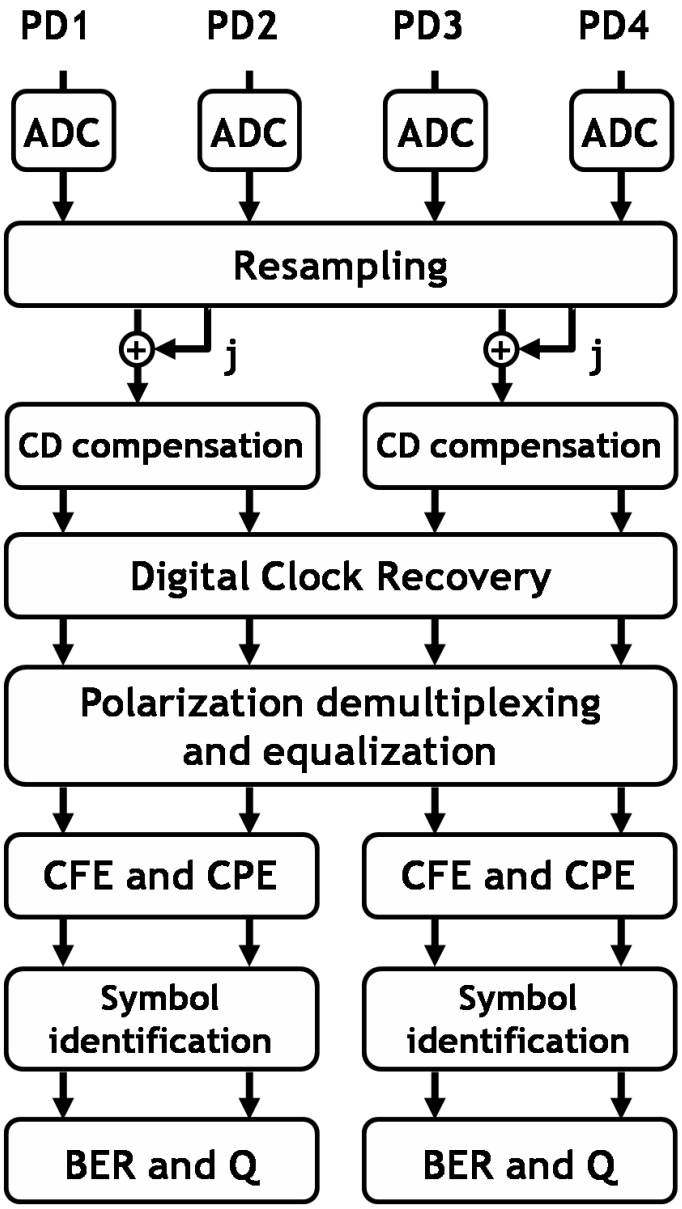


Figure 2.5: Function diagram for DSP processing in a PDM-QPSK coherent receiver.

baudrate is 28Gbaud since every symbol carries four bits (two bits per QPSK symbol over each polarization) and the required sampling rate is 56Gbaud, which is very close to the limit of current technology. Then the acquired samples are resampled in order to compensate for the slight clock mismatch between the transmitter and the ADCs and obtain exactly two samples per symbol. The two sample streams are summed in quadrature for each polarization to implement the function expressed by Eq. (2.21).

### 2.3.1 Dispersion compensation

The first step required to recover the signal is to compensate for the cumulated chromatic dispersion. If we neglect nonlinearities, the effect of chromatic dispersion on the propagation of a pulse can be modeled with the following differential equation [51]:

$$\frac{\partial E(z,t)}{\partial z} = j\frac{D\lambda^2}{4\pi c}\frac{\partial^2 E(z,t)}{\partial t^2} \tag{2.22}$$

where $z$ is the length of the link, $t$ is the time variable in the frame moving with the pulse, $\lambda$ if the wavelength of the line, c is the speed of light and $D$ is the GVD coefficient of the fiber. Taking the Fourier transform of Eq. 2.22, we find that the transfer function of the GVD in the frequency domain is

$$G(z,\omega) = e^{-j\frac{Dz\lambda^2}{4\pi c}\omega^2}. \tag{2.23}$$

To compensate for the dispersion it is thus necessary to implement the inverse filter $G_c(z,\omega) = \frac{1}{G(z,\omega)}$, whose impulse response is given by the inverse Fourier transform of $G_c(z,\omega)$

$$g_c(z,t) = \sqrt{\frac{jc}{D\lambda^2 z}}e^{-j\overbrace{\frac{\pi c}{D\lambda^2 z}}^{\phi(t)}t^2}. \tag{2.24}$$

This impulse response cannot be implemented using digital filters, since it has infinite duration and it passes all the frequencies, yielding aliasing no matter the sam-

pling frequency used. The solution is to truncate the impulse response to a finite duration. If we sample every T seconds, then the Nyquist frequency is $\omega_n = \frac{\pi}{T}$ and to avoid aliasing we need that $-\omega_n \leq \omega \leq \omega_n$. The angular frequency of the impulse response is

$$\omega = \frac{\partial \phi(t)}{\partial t} = \frac{2\pi c}{D\lambda^2 z} t \tag{2.25}$$

and thus the length of the impulse response should be at least

$$-\frac{|D|\lambda^2 z}{2cT} \leq t \leq \frac{|D|\lambda^2 z}{2cT}. \tag{2.26}$$

Given this criterion, the impulse response can be implemented using a finite impulse response (FIR) filter whose $N$ taps are [51]

$$a_k = \sqrt{\frac{jcT^2}{D\lambda^2 z}} e^{-j\frac{\pi cT^2}{D\lambda^2 z}k^2} \qquad -\left\lfloor \frac{N}{2} \right\rfloor \leq k \leq \left\lfloor \frac{N}{2} \right\rfloor, \qquad N = 2\left\lfloor \frac{|D|\lambda^2 z}{2cT^2} \right\rfloor + 1. \tag{2.27}$$

This is an upper bound on the number of taps that can be reduced without introducing an additional penalty, especially if windowing of the finite impulse response is applied. As a reference, to compensate for $Dz$=1000ps/nm of cumulated dispersion at b$\lambda$ ~1550nm, the required number of taps is around $N = 0.02B^2$ where $B^2$ is the baudrate of the signal in Gbaud.

After the dispersion compensation, clock recovery should be implemented, since the sampling time is not synchronized with the signal [52–54]. Fig. 2.6 shows the polar diagram of a dual polarization signal right after dispersion compensation. The two polarizations are still mixed together and no carrier and phase recovery has been performed; it is impossible to identify the detected symbols

### 2.3.2 Polarization demultiplexing

The effect of fiber birefringence is to rotate the main polarization axes of the signal. The rotation is frequency dependent in presence of PMD and can be modeled by a Jones matrix. The objective of polarization demultiplexing is to estimate the Jones

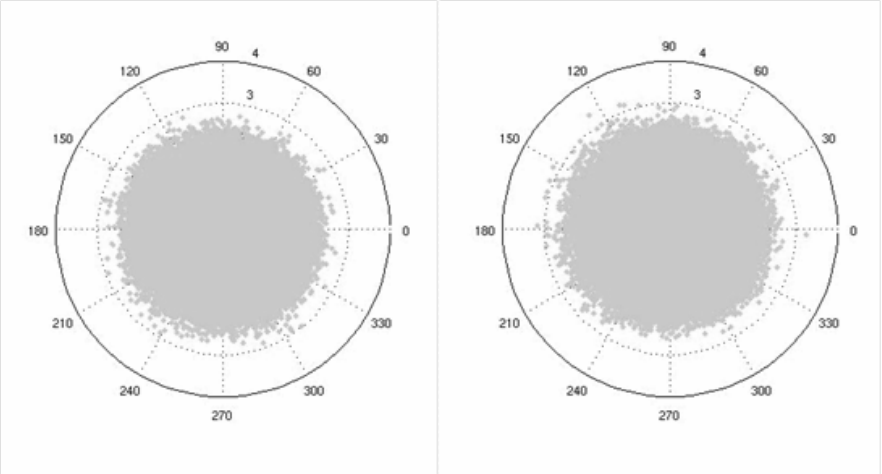


Figure 2.6: Polar diagram of a PDM-QPSK signal after dispersion compensation [courtesy of G. Charlet].

matrix associated with the system and multiply the signal by its inverse in order to recover the two transmitted polarizations. The Jones matrix is also time dependent due to many effects like temperature change, vibrations, physical stress and so on; thus the estimating and compensating scheme must be in general adaptive.

The problem of digital polarization demultiplexing was first posed in [55] and it is carefully described in [51]. Using the formalism of multiple input multiple output systems, given the input samples $E_{x,in}$, $E_{y,in}$, the outputs samples are

$$\begin{aligned} E_{x,out} &= \mathbf{h}_{xx}^T \cdot E_{x,in} + \mathbf{h}_{xy}^T \cdot E_{y,in} \\ E_{y,out} &= \mathbf{h}_{yx}^T \cdot E_{x,in} + \mathbf{h}_{yy}^T \cdot E_{y,in}, \end{aligned} \tag{2.28}$$

where $\mathbf{h}_{xx}, \mathbf{h}_{xy}, \mathbf{h}_{yx}, \mathbf{h}_{yy}$ are adaptive filters having $M$ taps that represent the four elements of the inverse Jones matrix. The taps of the filters must be updated in order to find the correct inverse matrix (during the acquisition) and then track the variations of the channels. A desirable feature of the demultiplexing algorithm is that it shouldn't rely on the knowledge of the data to update the taps. This property avoids the use

of training sequences at the beginning or during a transmission. The non-data-aided algorithms are also called *blind* algorithms, and they usually exploit some properties of the signal.

For PSK modulation in general, the property in question is that, in absence of distortions, the received signal has a constant modulus. Thus a widely used algorithm to invert the Jones matrix of the channel is the constant modulus algorithm (CMA) [56]. Assuming that the modulus is unitary, the CMA tries to minimize the mean square error $\langle \varepsilon_{xy}^2 \rangle$ of $\varepsilon_{xy} = 1 - |E_{xy,out}|^2$. The gradient of the error with respect to the elements of the inverse Jones matrix, represented by the filter taps, should thus tend to zero

$$\frac{\partial \langle \varepsilon_x^2 \rangle}{\partial \mathbf{h}_{xx}} = 0; \quad \frac{\partial \langle \varepsilon_x^2 \rangle}{\partial \mathbf{h}_{xy}} = 0; \quad \frac{\partial \langle \varepsilon_y^2 \rangle}{\partial \mathbf{h}_{yx}} = 0; \quad \frac{\partial \langle \varepsilon_y^2 \rangle}{\partial \mathbf{h}_{yy}} = 0. \tag{2.29}$$

Applying the stochastic gradient algorithm one gets the following updating rules for the filters

$$\begin{aligned}
\mathbf{h}_{xx}^{(k)} &= \mathbf{h}_{xx}^{(k-1)} + \mu \varepsilon_{xx} E_{x,out} E_{x,in}^* \\
\mathbf{h}_{xy}^{(k)} &= \mathbf{h}_{xy}^{(k-1)} + \mu \varepsilon_{xy} E_{x,out} E_{y,in}^* \\
\mathbf{h}_{yx}^{(k)} &= \mathbf{h}_{yx}^{(k-1)} + \mu \varepsilon_{yx} E_{y,out} E_{x,in}^* \\
\mathbf{h}_{yy}^{(k)} &= \mathbf{h}_{yy}^{(k-1)} + \mu \varepsilon_{yy} E_{y,out} E_{y,in}^*,
\end{aligned} \tag{2.30}$$

where $\mu$ is the convergence parameter. Using a number of taps $M$ high enough, very huge amounts of PMD can be compensated for in the electric domain without any additional penalty. Moreover, if the amount of GVD compensated by the previous filter slightly underestimate/overestimate the real GVD of the link, the CMA can compensate for an amount of dispersion that depends again on the number of taps, but is tipically around $\pm$1000ps/nm. Finally CMA can also increase the tolerance to optical filtering, since it tries to invert the transfer function of the filter [34].

CMA has been successfully applied to modulation formats that do not have a constant modulus [56, 57], like QAM. However in these cases the performance of

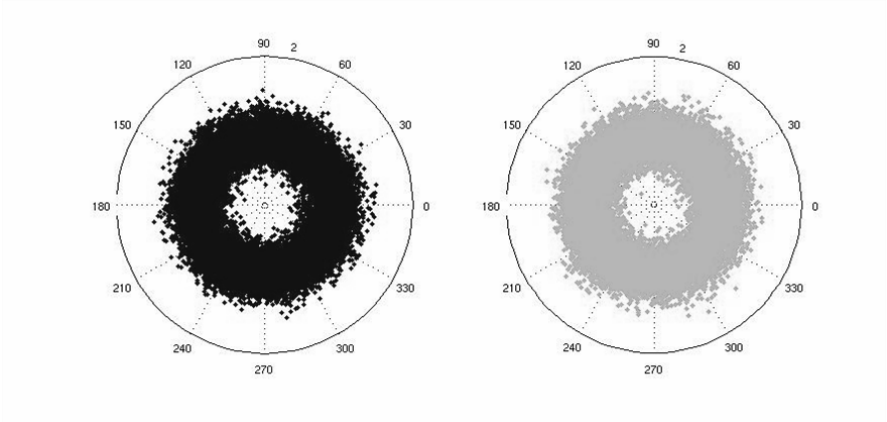


Figure 2.7: Polar diagram of a PDM-QPSK signal after polarization demultiplexing. The polarizations are separated but the symbols are still unidentifiable [courtesy of G. Charlet].

the algorithm tends to degrade and it should be modified to cope with variable amplitudes. A possible variation of CMA is the multiple modulus algorithm proposed in [58], where the signal modulus is compared to the three possible values assumed by a 16-QAM signal and the lowest error is selected.

Fig. 2.7 shows the polar diagram of the signal after polarization demultiplexing, commonly known as “donuts”. Now the two polarizations are correctly recovered, but in order to be able to identify the modulated phase of the signal, frequency and phase estimation should be carried out.

### 2.3.3 Carrier frequency and phase estimation

The recovery of frequency and phase of the carrier is the last signal processing step required to recover the transmitted signal. After dispersion compensation and polarization demultiplexing (assuming ideal operation), the processed samples, on both polarizations, are in the form

$$E_{x,y}(k) = Ae^{j(\Delta\omega(k)+\theta_s(k)+\theta_c(k))} + n_k, \tag{2.31}$$

where k is the the symbol, $\Delta\omega(k)$ is the frequency offset between the carrier and the local oscillator, $\theta_s, \theta_c$ are the phase of the transmitted signal and the phase noise of the carrier and the local oscillator and $n_k$ is the additive noise. The first step is to estimate $\Delta\omega(k)$ and take the signal to the baseband, then phase estimation is performed. However, since the presented frequency estimation algorithm is based on the same principles as the phase estimation algorithm we will start from the latter.

Assuming that the frequency offset has been removed, that the additive noise is absent and considering a QPSK signal, taking the fourth power of the received samples, calculating the argument and dividing by four, one gets

$$\frac{arg\left(E_{x,y}^4(k)\right)}{4} = \theta_c(k), \tag{2.32}$$

since $e^{4j\theta_s(k)} = 1$ for every possible QPSK symbol. This is a perfect estimator of the phase noise that can be later subtracted, recovering the modulated phase. However, in presence of additive noise, the estimator becomes (assuming small-signal approximation for the noise)

$$\begin{aligned} \frac{arg\left(E_{x,y}^4(k)\right)}{4} &= \theta_c(k) + 4arg\left(e^{3\theta_s(k)+3\theta_c(k)}n_k\right) + o(n_k^2) \\ &= \theta_c(k) + \delta(\theta_c(k), n_k) + o(n_k^2), \end{aligned} \tag{2.33}$$

where $\delta(\theta_c(k), n_k)$ is a small quantity that depends on the OSNR. It is apparent that the estimator is no longer accurate in presence of noise. If we assume that the carrier phase is constant, a possible technique to reduce the variance of the estimation error is to average the estimated phase over $M$ symbols

$$\theta_{c,est}(k) = \frac{1}{4}arg\left\{\sum_{k=1}^{M} E_{x,y}^4(k)\right\}. \tag{2.34}$$

This way, if the phase noise is constant, the variance of the estimation error is reduced by a factor equal to $M$. However, since the carrier phase noise is not constant, the averaging introduces an error that grows when the length of the averaging window $M$ grows. Thus the optimal length $M$ is a trade-off between the OSNR and the

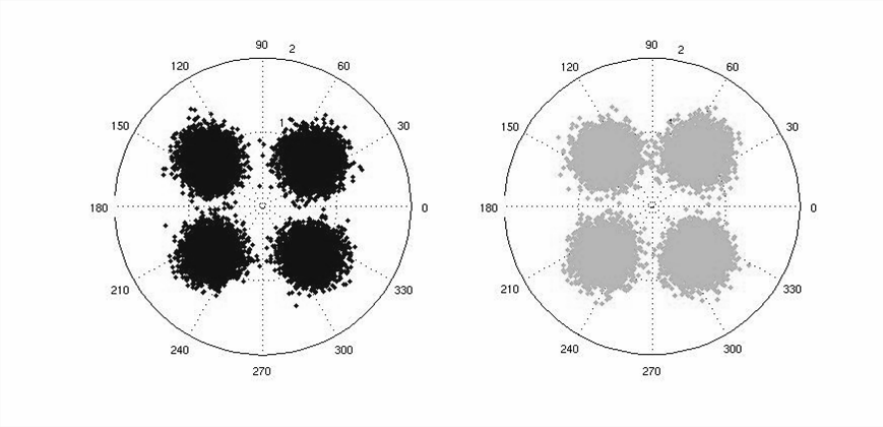


Figure 2.8: Polar diagram of a PDM-QPSK signal after frequency and phase estimation. The symbols are recovered and threshold based decision is now possible [courtesy of G. Charlet].

variance of the phase noise, i.e. the linewidth of the lasers. Large linewidths require short filters, while low OSNRs require long filters. The presented algorithm is the well known "Viterbi&Viterbi" algorithm [59]. Since the estimated phase is forced to be $-\frac{\pi}{4} \leq \theta_{c,est}(k) \leq \frac{\pi}{4}$ there is a four-fold phase ambiguity and differential encoding is mandatory to avoid error propagation.

Viterbi&Viterbi is a feedforward algorithm that doesn't require training sequences and relies on the properties of the QPSK signals. An improvement of the original algorithm, where all the weight of the averaging window are equal, consists of using a Wiener filter [60], that is the optimal filter according to estimation theory [61]. Viterbi&Viterbi can be extended to any PSK format by simply elevating the received signal to a power equal to the constellation alphabet (power $N$=2 for BPSK, $N$=8 for 8-PSK and so on) and can also be modified to be applicable to QAM signals [58, 62].

The same principle of Viterbi&Viterbi can be used to estimate the frequency offset between the carrier and the local oscillator ($\Delta\nu$) [63]. If two signals have a detuning of $\Delta\nu$, the phase shift between two consecutive symbols due to the frequency

offset is

$$\Delta\varphi = 2\pi\Delta\nu T, \tag{2.35}$$

where $T$ is the sampling time. If one multiplies the received samples by the complex conjugate of the previous symbol, the result is a complex number whose phase is equal to the difference in phase of the two. In general the phase noise between two consecutive symbols can be safely considered constant; thus, using the Viterbi&Viterbi algorithm it is possible to remove the modulated phase and to estimate $\Delta\varphi$. The detuning can be then compensated by simply adding to every symbol a phase shift equal to

$$\varphi_k = k\Delta\varphi T, \tag{2.36}$$

where $k$ is the running symbol index. In general the variations of the frequency offset between the two lasers are very slow, thus the estimation of the phase shift $\Delta\varphi$ can be improved by averaging over a very large number of symbols (es. 500 or 1000). Fig. 2.8 shows the polar diagram after phase and frequency estimation. The transmitted symbols are clearly visible. Placing decision thresholds at 0 on both in-phase and quadrature components allows to identify the symbols and comparing the received sequence with the transmitted one, BER and $Q^2$-factor can be calculated.

# Chapter 3

# Nonlinear effects in hybrid PSK-10Gb/s OOK transmission systems

In order to make the deployment of 40 and 100Gb/s services in optical terrestrial networks cost effective, high datarate channels must be loaded on an already existing WDM infrastructure designed for 10Gb/s OOK channels with a channel spacing down to 50GHz. The main limitation of PSK formats operated in a *hybrid* scenario, i.e., with two or more different formats mixed on the WDM comb, lies in its limited tolerance to XPM caused by neighboring intensity-modulated OOK channels. Both simulation and experiments [64–68] have already established that this is the main impairment on QPSK channels in QPSK/OOK hybrid systems.

In this chapter we will first compare by means of Monte Carlo simulations the performance of PDM-QPSK and DQPSK in a hybrid scenario [69, 70], then we will analyze what is the impact of replacing 10Gb/s OOK channels with 10Gb/s DPSK channels with simplified receiver [71, 72] and finally we will present a simple model of the interactions among OOK and QPSK channels through XPM [73, 74].

## 3.1 PDM-QPSK and DQPSK nonlinear tolerance in hybrid systems

In this section we compare through numerical simulations the tolerance to nonlinear effects of DQPSK at 40Gb/s and PDM-QPSK at 40 and 80Gb/s when surrounded by 10Gb/s OOK channels.

### 3.1.1 Numerical setup

We tested a 5-channel system on a 50GHz grid that propagates along a dispersion managed (DM) system composed of 20x100km spans of Teralight fiber ($D$=8ps/nm/km, $\alpha$=0.2dB/km, $\gamma$=1.7$\frac{1}{\mathrm{W}\cdot\mathrm{km}}$at1550nm) and SMF ($D$=16ps/nm/km, $\alpha$=0.2dB/km, $\gamma$=1.3$\frac{1}{\mathrm{W}\cdot\mathrm{km}}$ at 1550nm). All the results refer to the central channel. We separately verified that increasing the number of channels does not cause significant variations of performance [66]. The line was composed of 20 identical spans, each comprising transmission and linear compensating fibers, followed by an amplifier with flat gain and a noise figure of 6dB. Purely linear pre-/post-compensating fibers were inserted before/after the transmission link.

The even channels were always NRZ-OOK modulated at a bitrate of 10Gb/s (10Gbaud). The odd channels were in turn 40Gb/s DQPSK (20Gbaud), 40Gb/s PDM-QPSK (10Gbaud) or 80Gb/s PDM-QPSK (20Gbaud). The OOK channels were modulated using pseudo-random binary sequences (PRBS) with different seeds and length $2^9$ , while the DQPSK and PDM-QPSK were modulated using a pseudo-random quaternary sequence (PRQS) of length $4^5$. All channels had the same average power and were synchronous at the input of the pre- fiber. We verified that inserting random delays among channels shows very limited impact thanks to the decorrelation induced by pre-compensating and in-line fibers. OOK channels were copolarized with one polarization of coherent channels in PDM-QPSK configuration.

The propagation of signal and ASE noise along the fibers was modeled using a variable step-size split step Fourier method (SSFM), that takes into account all linear and non-linear effects, except PMD. The maximum nonlinear phase rotation per step

was 3mrad which we verified to be small enough for the considered system.

The DQPSK channel was received using a second order superGaussian optical filter with 3-dB bandwidth 2×baudrate (20 or 40GHz), followed by a standard receiver and a 5th order Bessel filter with 3-dB bandwidth 0.65×baudrate (6.5 or 13GHz) [17]. The PDM-QPSK receiver used the same filters, and was composed of two coherent mixers (one for each polarization), used to combine the signal with the local oscillator, followed by four balanced photodetectors and the DSP unit. The incoming signal is sampled at twice the symbol-rate and no quantization is performed. The receiver was the same as described in [34], with no digital dispersion compensation.

For each configuration, we measured the $Q^2$-factor as a function of the average launched power $P_{in}$, for three different values of residual dispersion per span, $D_{in}$=12.5, 25, and 50ps/nm both using Teralight [69] and SMF. The $Q^2$-factor was computed from Monte Carlo simulations of the bit error rate (BER) in order to account for nonlinear phase noise, which is often neglected [75]. The simulations were stopped when the relative estimation error on BER reached 20% with a Gaussian confidence of 95%, providing in each case at least 100 error counts. The precompensating fiber cumulated dispersion was -292, -411 and -649ps/nm for the three tested $D_{in}$ respectively when using Teralight fiber, and -488, -607 and -844 ps/nm when using SMF. These values were chosen using the "*straight line rule*" [76]. The dispersion of the post-compensating fiber was optimized for a QPSK transmission using Karhunen-Loéve method [17], assuming white noise. Typically the residual total dispersion was close to 0 and in every tested case it was within the range [-40;40] ps/nm.

In such systems, the main nonlinear impairment was found to be the XPM due to 10Gb/s OOK channels on 40Gb/s-80Gb/s channels [66].Though not reported here, we ran single channel simulations for DQPSK and 80Gb/s PDM-QPSK configurations with Teralight fiber. We verified that cross-channel effects are dominant. Among these, four-wave mixing is negligible because of the sizable in-line dispersion. Hence XPM is by far the dominant non-linear effect.

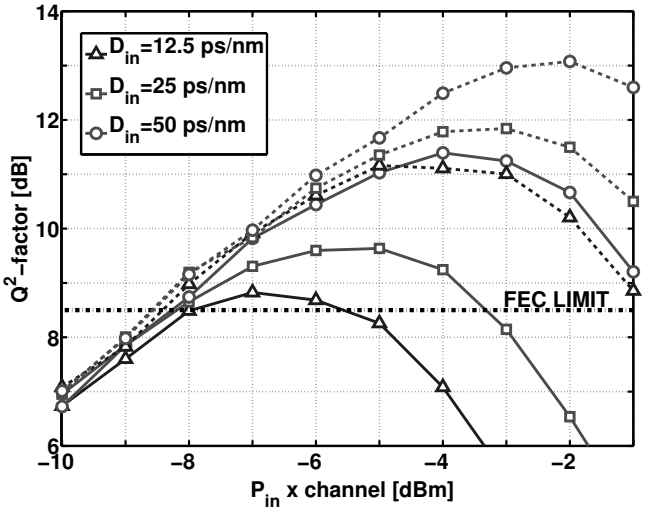


Figure 3.1: $Q^2$-factor vs. $P_{in}$ for DQPSK at 40Gb/s with 10Gb/s OOK neighboring channels. Dashed lines with SMF fiber, solid lines with Teralight.

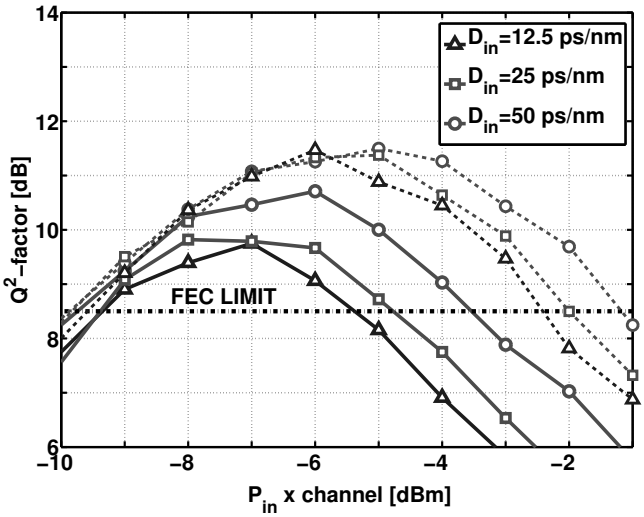


Figure 3.2: $Q^2$-factor vs. $P_{in}$ for PDM-QPSK at 40Gb/s with 10Gb/s OOK neighboring channels. Dashed lines with SMF fiber, solid lines with Teralight.

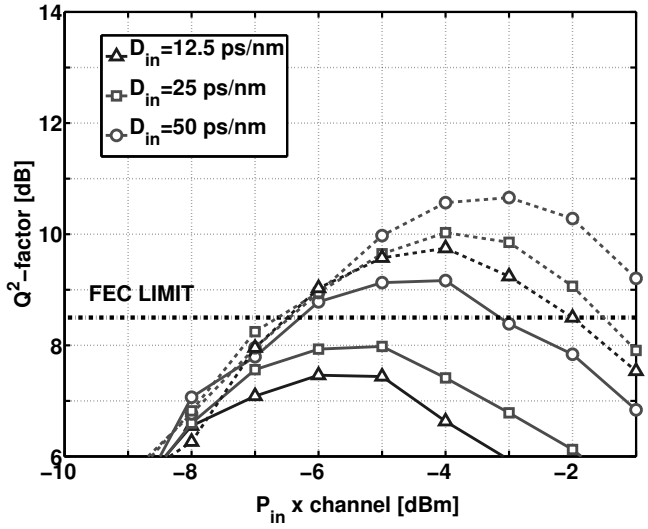


Figure 3.3: $Q^2$-factor vs. $P_{in}$ for PDM-QPSK at 80Gb/s with 10Gb/s OOK neighboring channels. Dashed lines with SMF fiber, solid lines with Teralight

### 3.1.2 Results

Figs. 3.1, 3.2, 3.3 sketch the measured $Q^2$-factor vs. launched power for the configurations under investigation. The best performance is always obtained with SMF fiber which is not surprising since increasing the dispersion is known to reduce XPM. Also the use of SMF reduces the impact of $D_{in}$ (the $Q^2$-factor curves for SMF are closer than for Teralight), thus relaxing the dispersion mapping constraints. From a comparison of Fig. 3.1 and Fig. 3.2, we note that the best $Q^2$-factor is better for the DQPSK case ($\sim$0.8dB with Teralight and $\sim$1.5dB with SMF). 40Gb/s PDM-QPSK shows an enhanced optical signal-to-noise ratio (OSNR) sensitivity in the linear region on the left of the maximum $Q^2$-factor. On the other hand DQPSK shows a superior nonlinear threshold (NLT, defined as $P_{in}$ per channel at best $Q^2$-factor). Fig. 3.3 shows that 80Gb/s PDM-QPSK suffers from a reduced OSNR sensitivity due to its higher bitrate ($\sim$3dB in $Q^2$-factor at $P_{in}$=-8dBm) and for low values of $D_{in}$ the nonlinear penalties are enhanced, compared to 40Gb/s PDM-QPSK. However the NLT is bet-

Table 3.1: Improvement of the best $Q^2$-factor [dB] when using 100GHz spacing on Teralight fiber

| | DQPSK 40G | PDM-QPSK 40G | PDM-QPSK 80G |
|---|---|---|---|
| $D_{in}$=12.5 ps/nm | 1.96 | 0.78 | 0.33 |
| $D_{in}$=25 ps/nm | 2.24 | 1.17 | 0.24 |
| $D_{in}$=50 ps/nm | 2.12 | 0.83 | 0.24 |

ter than 40Gb/s PDM-QPSK ($\sim$2 dB with both fibers). Over such a long distance this configuration cannot offer adequate performance. However with a careful DM (higher values of $D_{in}$) and on shorter links (1000$\div$1500km), PDM-QPSK could be a good candidate for 80Gb/s or even 100Gb/s channel upgrades.

We also investigated the effect of increasing the channel spacing from 50 to 100GHz on a Teralight fiber. Table 3.1 reports the improvement of the best $Q^2$-factor for the considered configurations.

As expected the $Q^2$-factor is always better at 100GHz, but this effect is more evident for DQPSK ($\sim$2dB) than for 40 or 80Gb/s PDM-QPSK ($\sim$1 and $\sim$0.3dB, respectively). A possible solution to improve PDM-QPSK robustness against SPM and XPM is to improve the phase estimation algorithm. In our simulations, we used a Viterbi&Viterbi [34]. The number of samples used to average the phase ($M$) was 7. Fig. 3.4 shows the performance of the 40Gb/s PDM-QPSK+OOK system, using $D_{in}$=25ps/nm and Teralight fiber, for different values of $M$. $M$=7 is near the optimum for low values of $P_{in}$, but gives a penalty of almost 1dB for $P_{in}$=-4dBm. Using smaller values of $M$ (es. 3) could thus reduce the impact of XPM, but could be insufficient to provide a decisive improvement. On the other hand, the DSP unit allows for a suboptimal DM design. Comparing Figs. 3.1 and 3.2 for $D_{in}$=12.5ps/nm with Teralight fiber, we see that the $Q^2$-factor of PDM-QPSK is decreased by 2dB w.r.t. $D_{in}$=50ps/nm, while the $Q^2$-factor of DQPSK is 4.5dB smaller. The enhanced tolerance of PDM-QPSK is due to the constant modulus algorithm (CMA) used at the receiver that acts as a generic adaptive equalizer, thus relaxing the impact of DM [34].

We conclude this section showing in Fig. 3.5 the NLT as a function of $D_{in}$ using

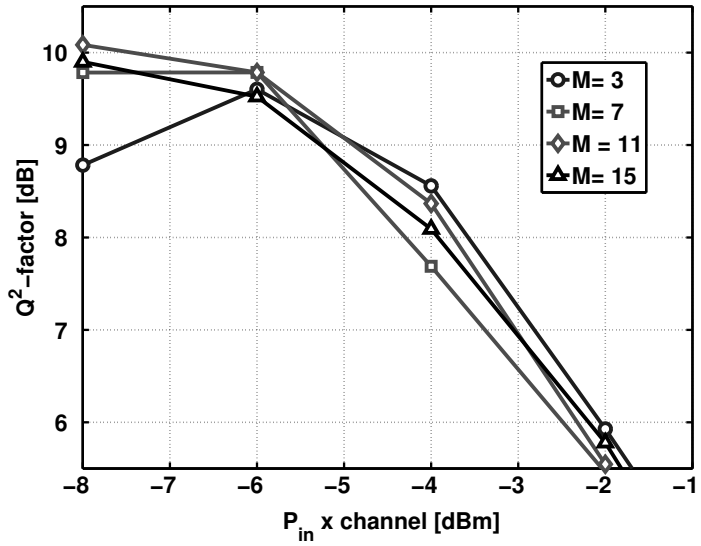


Figure 3.4: $Q^2$-factor vs. $P_{in}$ of PDM-QPSK at 40Gb/s + OOK, $D_{in}$=25 ps/nm on Teralight fiber for four different values of $M$.

Teralight fiber. These curves are obtained by interpolating the available values of $Q^2$-factor vs $P_{in}$. The NLT always grows for increasing values of $|D_{in}|$, because residual in-line dispersion reduces the dominant XPM impairment. The NLT of 40Gb/s PDM-QPSK is the lowest but its value is little dependent on $D_{in}$ (1dB). On the other hand, the NLT for 40Gb/s DQPSK and 80Gb/s PDM-QPSK is higher, but it decreases by more than 3 and 2.5dBm, respectively, at $D_{in}$=0.

## 3.2 Use of 10Gb/s NF-DPSK to reduce XPM in hybrid systems

In this section we evaluate the benefit when changing the modulation format of the 10Gb/s OOK channels located next to a 40Gb/s DQPSK channels to DPSK, and to receive them using a narrow optical filter (narrow filter DPSK, NF-DPSK) [77–79]. The rationale is that DPSK is an almost constant amplitude format and thus the XPM

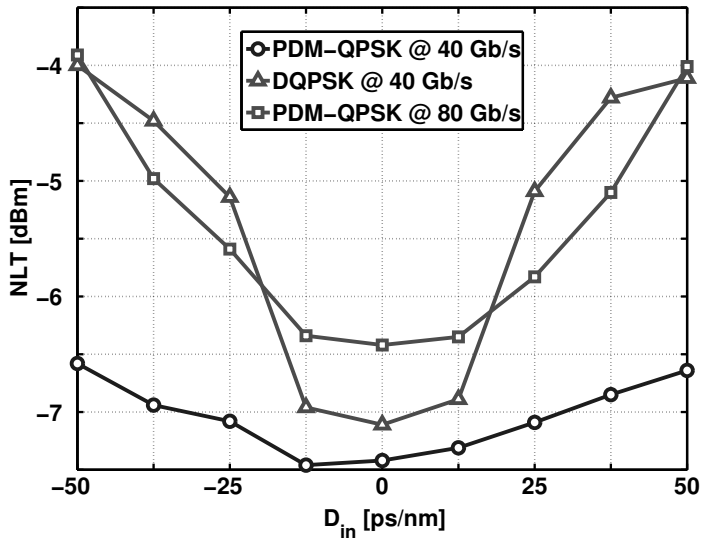


Figure 3.5: NLT vs. $D_{in}$ of the 3 examined configurations on Teralight fiber.

generated on the DQPSK channels should be reduced. On the other hand one may fear that inter-channel NLPN [15], i.e. the XPM generated by the amplitude noise of DPSK channels on the 40G channels, could be the dominant impairment. Numerical Monte Carlo (MC) simulations accounting for NLPN are carried out to support our proposal.

Before focusing on the parameters used in the simulations, we will describe the necessary modifications in the transmitter and receiver to upgrade OOK channels to NF-DPSK. At the transmitter, a DPSK electronic precoder must be added and the bias of the Mach-Zehnder modulator must be set to the null point: the drive voltage can be doubled or left unaltered ($V_\pi$, instead of $2 \times V_\pi$ ), since it gives only a small penalty on performance [5] which is easily compensated by the improved sensitivity of NF-DPSK. This gain is due to the narrow optical filter employed at the receiving side which is very effective in rejecting the amplified spontaneous emission noise [78]. The best filter is Gaussian shaped with bandwidth $\simeq 0.65\times$baudrate [79]. The filter is very narrow, thus wavelength tracking must be put in place to cope with the drift of

the laser over the whole lifespan. The proposed solution requires to replace 10Gb/s linecards; this is an additional cost, but the components are very similar to those used in OOK linecards and thus the upgrade cost should be limited. Moreover, if upgraded 40Gb/s channels are packed together, only the two OOK linecards next to the 40Gb/s channels block should be replaced by NF-DPSK linecards.

### 3.2.1 Numerical setup

We now discuss the numerical setup of the hybrid system. The system under test was composed of 5 channels, with 50GHz spacing, launched over a link comprising a pre-compensating fiber, a variable number of identical spans and a post-compensating fiber before the receiver. Each span was the concatenation of a transmission fiber (either non-zero dispersion shifted fiber, NZ-DSF or Teralight), a compensating fiber and an amplifier. The odd channels were always DQPSK modulated at 40Gb/s (20Gbaud) with full drive voltage ($2 \times V_\pi$) using a PRQS of length $4^5$, while the even ones were in turn OOK or NF-DPSK modulated using a PRBS of length $2^9$. All the results refer to the central (DQPSK) channel. We separately verified that increasing number of channels does not significantly impact the performance. The propagation was modeled using SSFM method, accounting for all linear and non linear impairments but PMD. The maximum nonlinear phase rotation per step was 3mrad. The amplifiers along the line had flat gain and a noise figure of 6 dB.

Initially we tested both hybrid configurations by simulating transmission over $25 \times 100$ km spans of NZ-DSF fiber (loss $\alpha$=0.2dB/km, dispersion $D$=4ps/nm/km at 1550nm, slope $S$=0.085ps/nm$^2$/km, effective area $A_{eff}$=72$\mu$m$^2$ , nonlinear coefficient $n_2$=2.7$\times 10^{-20}$m$^2$/W) or Teralight fiber ($\alpha$=0.2dB/km, $D$=8ps/nm/km at 1550nm, $S$=0.058ps/nm$^2$/km, $A_{eff}$=65$\mu$m$^2$, $n_2$=2.7$\times 10^{-20}$m$^2$/W) and measuring the sensitivity penalty (SP) vs. back to back at BER $10^{-5}$ as a function of both the average launched power per channel $P_{in}$ and the in-line residual dispersion per span, $D_{in}$ . The dispersion of the pre-compensating fiber was chosen using the rule in [76], while the overall cumulated dispersion was optimized in the range [-600;600] ps/nm, by acting on the post-compensating fiber.

The BER of the central DQPSK channel 3 was computed using Karhunen-Loéve

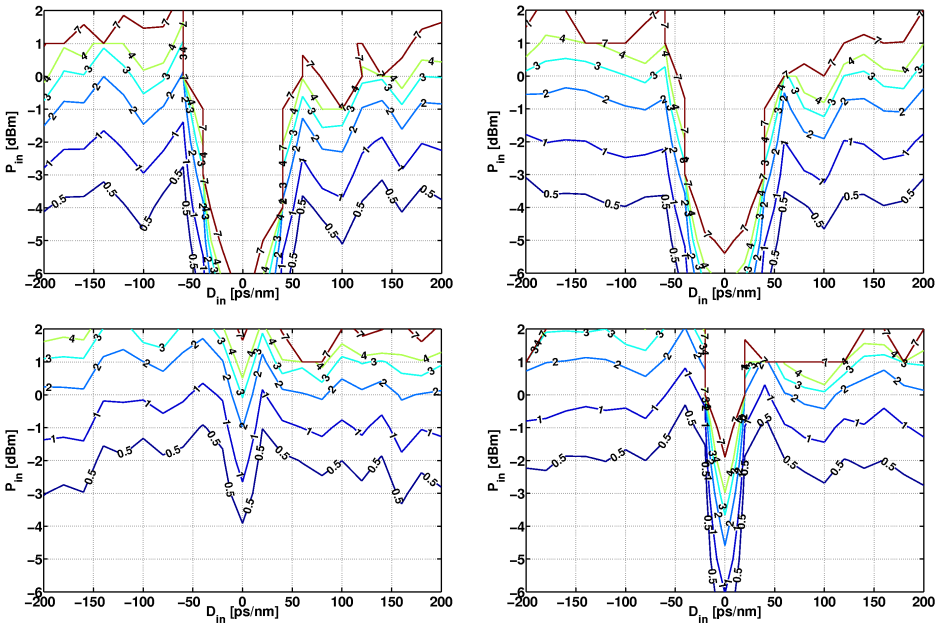


Figure 3.6: Sensitivity penalty [dB] vs. $P_{in}$ and $D_{in}$ for the central (3rd, DQPSK) channel over a NZ-DSF (left) or a Teralight (right) fiber. Channels 1, 3, 5 are DQPSK. Channels 2, 4 are OOK (top) or NF-DPSK (bottom).

(KL) method [17], thus assuming noiseless transmission and a noisy amplifier before the receiver, yielding the same amount of noise as 25 amplifiers. These semi-analytical simulations are very fast, enabling the exploration of a wide parameters range, but assume that the noise at the receiver is white, i.e. the effect of NLPN is not taken into account.

### 3.2.2 Results

Fig. 3.6 depicts the contour plots of SP vs. $P_{in}$ and $D_{in}$. When the even channels are OOK modulated (top), for values of $|D_{in}|$ up to $\simeq$ 50ps/nm the performance is heavily degraded. When we use NF-DPSK (bottom), this range is strongly reduced. For the

NZ-DSF case (bottom left), there is a negligible penalty for $P_{in} \leq -3$dBm, while for higher values of $P_{in}$ the penalty diverges only when $|D_{in}| \leq 20$ps/nm. Moreover, even for higher values of $D_{in}$, NF-DPSK still shows a gain of $\simeq$1dB in SP. The results obtained for the Teralight case (bottom right) are very similar to the NZ-DSF case, except for a larger penalty around $D_{in} \simeq 0$ps/nm, even at low values of $P_{in}$. This behavior clearly shows that the main nonlinear impairment is XPM. What happens is that the power variations of OOK channels induce phase shifts on the DQPSK channel through XPM, thus distorting the DQPSK phase, i.e. the carried information. On the other hand, NF-DPSK features a more constant amplitude in comparison to OOK, so that the XPM induced phase rotation is almost constant and can be in part canceled by the differential decoding.

We also repeated these simulations using either 10Gb/s OOK or NF-DPSK on odd channels and 40Gb/s DQPSK on the even ones and measured the performance of the central channel 3. Both configurations yield similar BER and negligible penalties, thus we can conclude that the system reach is limited only by 40Gb/s DQPSK channels, while 10Gb/s channels pose no design issues.

To account exactly for NLPN, we next simulated a $25 \times 100$km system in both OOK and NF-DPSK configurations, using noisy amplifiers along the line. We measured the $Q^2$-factor of the central DQPSK channel vs. $P_{in}$, for four different values of $D_{in}$ (12.5, 25, 50, 100ps/nm) and for two different types of transmission fiber, (NZ-DSF and Teralight). Again, the dispersion of the pre-compensating fiber was chosen using the rule in [76], while the post-compensating fiber was such that the total cumulated dispersion was 0. The $Q^2$-factor was derived from the BER computed using the standard Monte Carlo algorithm. The simulations ended when the relative error on the estimated BER reached 20% with a Gaussian confidence of 95%. At least 100 errors were counted for every estimated BER value.

Figure 3.7 shows the $Q^2$-factor as a function of $P_{in}$ for the four different values of $D_{in}$ on both fibers. When comparing curves at the same $D_{in}$, the performance of the reference signal of the hybrid DQPSK/NF-DPSK system is better by at least $\simeq$2dB than the DQPSK/OOK one, for values of in-line dispersion up to 50ps/nm. For higher values, neighboring NF-DPSK and OOK channels give similar impairments. Also

note that the dependence of the performance on the value of $D_{in}$ is clearly stronger in the OOK case.

Focusing on the case of NZ-DSF fiber (top), we can say that, provided that the value of $D_{in}$ is larger than 25ps/nm, the system with NF-DPSK channels works close to its optimum. This constraint is further relaxed employing fibers with higher $D$, like Teralight (bottom). When using OOK, instead, the value of $D_{in}$ must be at least 100ps/nm to provide the same results, no matter the type of fiber used. It is worth to notice that at $D_{in}$=100ps/nm, NF-DPSK and OOK provide very similar performance over almost the whole considered range of powers. This evidence suggests that when using this dispersion management, the inter-channel effects are well suppressed.

Finally, we conclude this section trying to clarify the role of NLPN and how its effect compares with that of XPM. We thus repeated the simulations of Fig. 3.7, by fixing the average input power $P_{in}$ to -2 dBm and extending the study to the following values of $D_{in}$: -100, -50, -25, -12.5, 0, 12.5, 25, 50, and 100ps/nm. We isolated the impact of NLPN by computing the BER with Monte Carlo (NLPN "on") and Karhunen-Loéve (NLPN "off") methods. Fig. 3.8 shows the DQPSK central channel $Q^2$-factor vs. $D_{in}$ for DQPSK/NF-DPSK (circles) and DQPSK/OOK (squares) both computed using Monte Carlo (solid) and Karhunen-Loéve (dashed) algorithms. The difference between the Monte Carlo and Karhunen-Loéve curves is the NLPN penalty. This penalty is stronger for positive values of $D_{in}$ . When neighboring channels are OOK, the penalty is almost negligible since the effect of XPM is largely dominant; when using NF-DPSK channels, the NLPN causes a slightly larger penalty and it can become the dominant impairment since the effect of XPM is strongly reduced. Summarizing, the amplitude of NF-DPSK is more constant than the amplitude of OOK and produces a more constant XPM phase shift on the DQPSK signal, which the differential receiver can partially cancel. At the same time NLPN cannot be removed at the receiver because it generates almost independent phase shifts on neighboring bits. Moreover NLPN acts on every bit because the power of the NF-DPSK signals is never null. However the overall balance is in favor of NF-DPSK, since the XPM penalty is higher than the NLPN penalty.

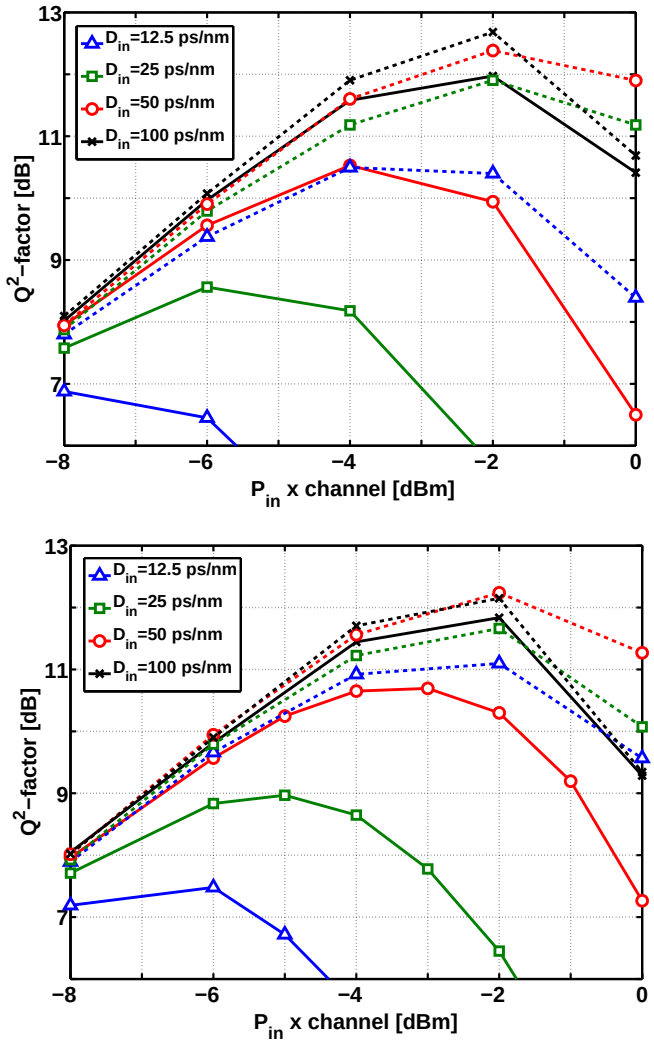


Figure 3.7: DQPSK $Q^2$-factor vs. $P_{in}$ for four values of $D_{in}$ on NZ-DSF (top) or Teralight (bottom) fiber. Even channels OOK (solid lines) or NF-DPSK (dashed lines).

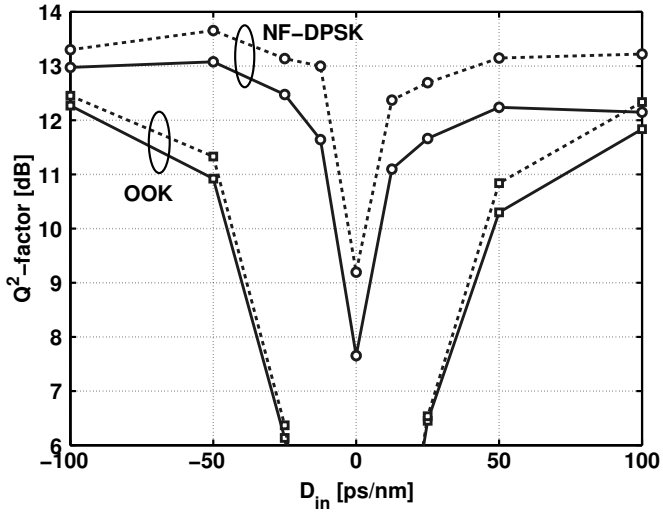


Figure 3.8: DQPSK $Q^2$-factor vs. $D_{in}$ @ $P_{in}$=-2dBm on a Teralight fiber. Even channels OOK (squares) or NF-DPSK (circles). Solid lines with NLPN, dashed lines with white noise.

## 3.3 OOK-induced XPM on high speed DQPSK/PDM-QPSK channels

As stated in the previous sections, both simulations and experiments have demonstrated that in QPSK/OOK systems the main nonlinear impairment on QPSK channels is the XPM caused by neighboring OOK channels. To explain this evidence, two analytical models have been proposed for such hybrid systems to estimate the penalty on DPSK and DQPSK channels. A first model [80] builds on previous work of Ho on DPSK [81] and is based on explicit formulas of the PDF of the received phase. A second model [82, 83] is based instead on explicit formulas of the PDF of the electrical current, and works only when the intensity fluctuations caused by XPM are dominant. Recent work by Vassilieva [84] also showed that the impact of XPM is reduced when the baudrate of the upgraded DQPSK channels is increased, and the reason was attributed to the increased OOK bit walk-off seen by the DQPSK channels when their symbol time gets reduced.

In this section, a simple theoretical framework is presented that models the interactions among OOK and QPSK channels through XPM. The framework is an extension of the work in [80]. The main novelties are: (i) a rigorous estimation of XPM in a dispersion managed (DM) setting, including pre-compensation, post-compensation and in-line compensation, and a new theoretical formulation that makes it possible to simply extend the calculations to any DM link with arbitrary dispersion/power profile; (ii) simple analytical fits of the sensitivity penalty versus phase offset variance for both incoherent and coherent reception; (iii) the extension of results to the coherent QPSK format with feed-forward phase estimation; and (iv) a thorough verification of the theoretical sensitivity penalty against SSFM simulations.

### 3.3.1 BER with phase noise

We start from standard results on the BER evaluation for PSK modulated signals in the presence of both additive noise and a phase offset [85], and tailor them to find the BER of our upgraded optical (D)QPSK channels with XPM induced phase noise, similarly to the work in [86, 87]. In our optical system, the received optical field $\tilde{E}(t)$

is the sum of a propagation-distorted signal component $\tilde{A}(t)$ and ASE noise $\tilde{m}(t)$ cumulated along the dispersion-managed line. In normal operating conditions, the XPM far exceeds the ASE-induced nonlinear phase noise [14] on the QPSK channels and is by far the dominant impairment [66–68]. Moreover thanks to the effect of walk-off, the XPM tends to have Gaussian statistics by the central limit theorem, since it is the sum of the contributions of many different symbols of the interfering signals.

In the case of DQPSK modulation, the receiver consists of an optical filter followed by a delay interferometer and balanced photo-detection [87]. The BER of a DQPSK signal affected by both additive circular Gaussian noise and the XPM Gaussian phase noise process $\Delta\phi$, and received by an interferometric receiver, can be expressed as [81].

$$\mathrm{BER} = \frac{3}{8} - \frac{\rho}{4} e^{-\rho} \sum_{n=1}^{\infty} \left[ I_{\frac{n-1}{2}}\left(\frac{\rho}{2}\right) + I_{\frac{n+1}{2}}\left(\frac{\rho}{2}\right) \right]^2 \frac{\sin(n\frac{\pi}{4})}{n} e^{-\frac{\mathrm{Var}[\Delta\phi]}{2} n^2} \tag{3.1}$$

where $I_\alpha(x)$ is the modified Bessel function of fractional index $\alpha$, and $\rho$ is the SNR, with the noise variance evaluated over the one-sided bandwidth of the optical filter. From (3.1) we find the following novel best-fit of the sensitivity penalty (SP) at a given reference back-to-back BER:

$$SP \cong -8.5\mathrm{Log}_{10}(1 - \rho_{ref}\mathrm{Var}[\Delta\phi(t)]). \tag{3.2}$$

where $\rho_{ref}$ is the SNR that achieves the reference BER, namely $\rho_{ref}$=61.7 at BER=$10^{-9}$, and $\rho_{ref}$=31.4 at BER=$10^{-5}$.

In the case of coherent reception, for simplicity we assume the local oscillator is aligned with the polarization of the incoming signal, and the optical filter bandwidth is the same as for the DQPSK receiver. We assume the frequency of the local oscillator is matched to that of the incoming signal (homodyne case), and the feed-forward phase estimation error is still denoted as $\Delta\phi$. Since in this case no additive optical noise is present on the local oscillator field, the BER of the QPSK channel affected

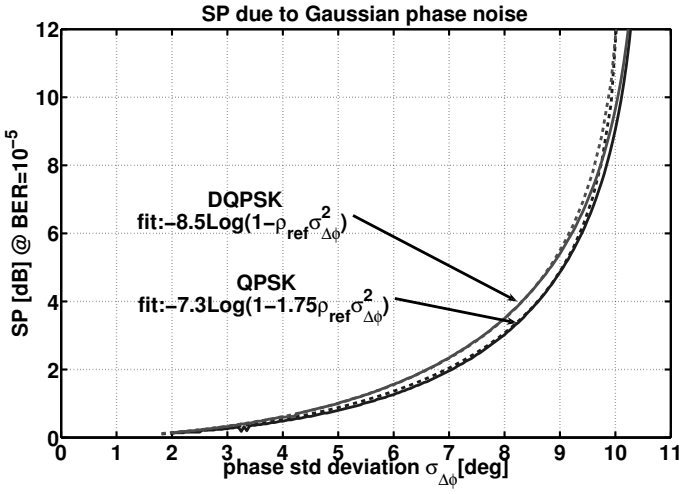


Figure 3.9: Sensitivity penalty at BER=$10^{-5}$ vs. standard deviation of phase error $\sigma_{\Delta\phi} = \sqrt{\mathrm{Var}[\Delta\phi]}$ . Solid lines: "Blachman" formulas (3.1) for DQPSK and (3.3) for coherent QPSK. Dashed lines: best fits (3.2) and (3.4).

by a Gaussian phase error $\Delta\phi$ can be computed, similarly to the DQPSK case as:

$$\mathrm{BER} = \frac{3}{8} - \frac{1}{2}\sqrt{\frac{\rho}{\pi}}e^{-\rho/2}\sum_{n=1}^{\infty}\left[I_{\frac{n-1}{2}}(\frac{\rho}{2}) + I_{\frac{n+1}{2}}(\frac{\rho}{2})\right]\frac{\sin(n\frac{\pi}{4})}{n}e^{-\frac{\mathrm{Var}[\Delta\phi]}{2}n^2}. \qquad (3.3)$$

Similarly to the DQPSK case, we obtain the following novel best-fit of the SP obtained from (3.3) at a reference back-to-back BER:

$$SP \cong -7.3\mathrm{Log}_{10}(1 - 1.75\rho_{ref}\mathrm{Var}[\Delta\phi(t)]) \qquad (3.4)$$

where for QPSK we have $\rho_{ref}$=36.0 at BER=$10^{-9}$, and $\rho_{ref}$=18.1 at BER=$10^{-5}$. The goodness of fit of (3.2) and (3.4) is shown in Fig.3.9 at a reference BER=$10^{-5}$. The fit both at BER=$10^{-3}$ and at BER=$10^{-9}$, not reported, is essentially as good as here.

In order to effectively use equations (3.2) and (3.4), we need to calculate the variance of the phase error induced by XPM, which can be computed as: $\mathrm{Var}[\Delta\phi(t)] =$

$\int_{-\infty}^{\infty} C_{\Delta\phi}(f)\mathrm{d}f$,where $C_{\Delta\phi}(f) \triangleq \mathscr{F}\{E[\Delta\phi(t-\tau)\Delta\phi(t)] - E[\Delta\phi(t)]^2\}$ is the power spectral density (PSD), i.e. the Fourier transform ($\mathscr{F}$) of the autocovariance of $\Delta\phi(t)$.

### 3.3.2 IM-XPM filters

To obtain $C_{\Delta\phi}(f)$ we will extend a well-established small-signal model for estimating the intensity-modulation (IM) to XPM conversion in DM WDM optical links [88, 89]. Our extended model includes the effect of pre-, post-, and in-line compensating fibers, and does take into account the GVD-induced pump distortion, along the lines of the "improved" IM-XPM-IM filters described in [90–92] and well suited for 40Gb/s OOK transmissions, whose simplified version, applicable to 10Gb/s OOK systems, was first published in [93–95] and later experimentally verified in [96]. We will then use the obtained results to calculate the variance induced on the phase of DQPSK/QPSK signals by neighboring OOK channels. Following the mathematical derivation in Appendix A, we can relate the Fourier transform of the XPM of the received reference channel $s$, $\Theta_{XPM}(\omega)$, to the Fourier transform of the input power $P_p(0,\omega)$ of "pump" channel $p$ as: $\Theta_{XPM}(\omega) = H_{XPM,p}(\omega)P_p(0,\omega)$, where the IM-XPM filter has expression:

$$H_{XPM,p}(\omega) = -\frac{\Phi_{NL}}{2P_{in,p}}\left\{e^{-j\frac{\omega^2}{2}\beta_r}H_p(\omega) + e^{j\frac{\omega^2}{2}\beta_r}H_p^*(-\omega)\right\} \tag{3.5}$$

where $\Phi_{NL}$ is the average cumulated nonlinear phase of the pump channel, $P_{in,p}$ is the pump average input power, $\beta_r$ [ps$^2$] is the dispersion accumulated over the entire DM link (including pre-, in-line and post-compensation) and $H_p(\omega)$ is a filter whose expression is given in the Appendix A. This same result can be obtained using a general approach based on a regular perturbation of the dispersion-managed nonlinear Schroedinger equation [97]. Most importantly, in [97] it is shown that the filter $H_p(\omega)$ in (3.5) is a simple function of the so called *DM link kernel*, a quantity that determines all performance metrics of the DM link. Hence, when moving to a DM system with a different dispersion and/or power profile, it is enough to update the expression of the kernel and thus of filter $H_p$, without having to directly recompute the IM-XPM filter. Note that only the simplest case of such IM-XPM filter, namely

the case of full in-line compensation, was used in [80] using the approximate filter in [81]. Also, note that the presented model can be extended to take into account even the effect of SPM on both pump and probe, along the lines of the method developed in [98].

To verify the accuracy of the analytical filter, we compared it to the "true" filter, obtained from simulations using the SSFM method as follows. We sent two signals along a DM system, composed of a linear pre-compensating fiber, $N$=15 identical spans with linear dispersion compensation at the end of each span, and finally a post-compensating fiber. The transmission fiber was a NZ-DSF with dispersion $D_{tx}$=3.83ps/(nm·km). The dispersion of the pre-compensating fiber was selected according to the "straight line rule" [76, 99] as: $D_{pre} = -\frac{D_{tx}}{\alpha} - \frac{N-1}{2}D_{in}$, where three different values of the residual in-line dispersion per span were used: $D_{in}$=[0, 50, 100]ps/nm. The post-compensation $D_{post}$ was such that the total cumulated dispersion $D_{tot} = D_{pre} + ND_{in} + D_{post}$ was zero. At the line input, the "probe" channel was CW, while the "pump", at a frequency distance $\Delta f$=50GHz from the probe, was sinusoidally modulated in power as $p_p(0,t) = P_{in,p}(1 + m_p \cos(\omega_m t))$, with power modulation index $m_p$=0.9. The average nonlinear phase cumulated by both channels along the link was $0.3\pi$. At the receiver, no optical/electrical filtering was added.

In the SSFM, the FFT time window contained 6.4nsec with 320 time samples/nsec, and the maximum nonlinear phase rotation per space-step was set to 1mrad. We only simulated the effect of XPM, i.e., we turned off self-phase modulation (SPM) and four-wave mixing (FWM).

From the Fourier transform of the transmitted power of pump channel $P_p(0,f)$ and that of the received probe phase $\Theta_{XPM}(f)$, we numerically computed the IM-XPM filter as $H_{XPM,p}(f_m) = \frac{\Theta_{XPM}(f_m)}{P_p(0,f_m)}$, being $f_m$ the sinusoidal modulation frequency. Fig. 3.10 shows the IM-XPM filter amplitude in dB for both theory (solid) and simulation (dots). The frequency is normalized to the baudrate of the OOK channels $R_{OOK}$=10Gbaud. The plots of the amplitude versus frequency can be interpreted by recalling from the Appendix A that the IM-XPM filter $H_{XPM,p}$ results from the composition of two factors: (1) a walk-off factor (A.6) which gives $H_{XPM,p}$ a typical

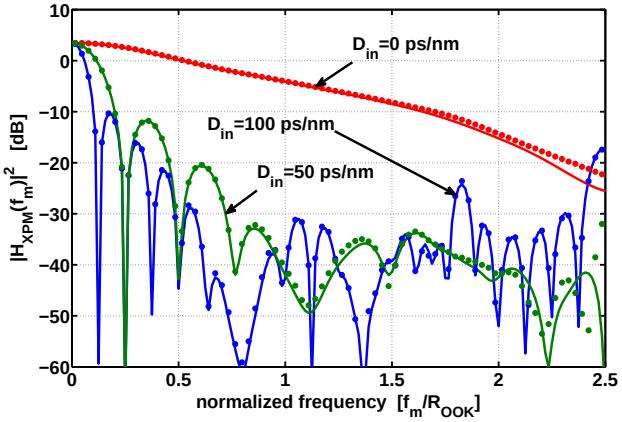


Figure 3.10: IM-XPM filter amplitude $10\log_{10}|H_{XPM,p}(f_m)|^2$ versus normalized frequency $f_m/R_{OOK}$, with $R_{OOK}$=10GHz. 15-span NZ-DSF system, $D_{pre}$=SLR, $D_{\text{tot}}$=0 and three values of in-line dispersion per span $D_{in} = [0, 50, 100]$ps/nm. Nonlinear phase $0.3\pi$. Pump-probe spacing $\Delta f$=50GHz. Dots: SSFM simulated filter; Solid line: analytical filter (3.5).

low-pass behavior, as seen at full in-line compensation $D_{in}$=0; (2) an interference factor (A.5), which introduces oscillations in frequency and notches in $|H_{XPM,p}|$ whose frequencies decrease for increasing $D_{in}$, as visible in the figure when the in-line dispersion is non-zero.From the comparison of simulation and theory we note that the predictions of the analytical filter are in very good agreement with SSFM simulations, but the precision of the filter tends to worsen at higher frequencies.

### 3.3.3 Phase Variance Evaluation

Having now an accurate filter that describes how the power fluctuations on a single OOK channel are impressed on the phase of the probe PSK signal, the overall XPM can be written as a superposition of the XPM stemming from the individual OOK channels: $\Theta_{XPM}(f) = \sum_{\substack{p=-N \\ p\neq 0}}^{N} H_{XPM,p}(f)P_p(0,f)$, having assumed that the probe channel $s$=0 has $N$ OOK pump channels to its right and $N$ to its left. The power spectral

density of the XPM process is: $C_{XPM}(f) = \sum_{\substack{p=-N \\ p\neq 0}}^{N} |H_{XPM,p}(f)|^2 C_{OOK}(f)$, where we used the independence of the OOK channels, and where $C_{OOK}(f)$ is the PSD of the intensity of each of the input OOK signals, which, for non-return to zero (NRZ) OOK modulation is

$$C_{OOK}(f) = \left(\frac{P_{\text{in,p}}}{R_{OOK}}\frac{r-1}{r+1}\right)^2 \text{sinc}^2(\frac{f}{R_{OOK}}) \tag{3.6}$$

where $r > 1$ is the extinction ratio. Now, the PSD $C_{\Delta\phi}(f)$ needed for the variance calculation is related to $C_{XPM}(f)$ according to the specific demodulator structure. Assume the upgraded channel at a baudrate of $R_s = 1/T_s$ [Gbaud] is DQPSK modulated. The receiver consists of an optical filter followed by a delay-demodulation interferometer with balanced detection. Hence the phase error to be used in the BER formula (3.1) for the reference channel $s$ is the difference $\Delta\phi(t) = \theta_{XPM}(t) - \theta_{XPM}(t - T_s)$. Taking Fourier transforms one gets: $\Delta\Phi(\omega) = \Theta_{XPM}(\omega)H_D(\omega)$, where the differential phase filter is $H_D(\omega) = 1 - e^{-j\omega T_s}$, with $|H_D(\omega)|^2 = 4\sin^2(\frac{\omega}{2R_s})$. Hence $C_{\Delta\phi}(f) = C_{XPM}(f)|H_D(f)|^2$, so that

$$\text{Var}[\Delta\phi] = \sum_{\substack{p=-N \\ p\neq 0}}^{N} \int_{-\infty}^{\infty} C_{OOK}(f) \cdot |H_{XPM,p}(f)|^2 \, |H_D(f)|^2 \text{d}f \tag{3.7}$$

and we note that the integrand must have Hermitian symmetry, so that the integral is twice that on positive frequencies. Since the optical filter also gives a spectral shaping to the phase, it is sufficient to restrict the range of integration to the bandwidth $B_o$ of the optical filter [81]. Also, it can be shown that $H_{XPM,-p}(f) = H^*_{XPM,p}(f)$, so that finally the variance expression simplifies to

$$\text{Var}[\Delta\phi] = 2\sum_{p=1}^{N} 2\int_0^{B_o} C_{OOK}(f) \, |H_{XPM,p}(f)|^2 \, |H_D(f)|^2 \text{d}f \,. \tag{3.8}$$

Note that, when we can approximate $\omega + p\Delta\omega \cong p\Delta\omega$, then from (A.7) $H_p(\omega) = H_p^*(-\omega)$ and thus from (3.5) we get (see Appendix A): $|H_{XPM,p}(\omega)|^2 \cong (\frac{N\gamma}{\alpha})^2 |I_p(\omega p\Delta\omega)|^2 |H_{Wp}(\omega p\Delta\omega)|^2 \cos(\frac{\omega^2}{2}\beta_r)$ which is the approximate expression

used by Ho ( [81], eq. (9), where $\beta_r = 0$ is assumed). Such an approximation, while reasonable at 100GHz channel spacing, becomes more critical at 50GHz spacing.

We next assume the reference channel $s$ is QPSK modulated and demodulated using a coherent receiver, with feed-forward phase estimation based on the Viterbi and Viterbi (V&V) algorithm [59]. We also assume the feed-forward phase estimation error $\Delta\phi(t)$ is dominated by the XPM rather than by the phase induced by the ASE on the received signal. Namely, the phase error (or "offset") to be used in the BER formula (3.3) is the difference $\Delta\phi(t) = \theta_{XPM}(t) - \hat{\theta}_{XPM}$, where as in [60] we assume the estimated XPM comes from a linear processing of the sampled values at the $M$ previous symbol times ( [60], eqs. (15),(27)):

$$\hat{\theta}_{XPM} = \frac{\sum_{m=1}^{M} \theta_{XPM}(t - mT_s)}{M} = \frac{\sum_{m=1}^{M} \arg\left[\tilde{E}(t - mT_s)^4\right]}{4M}. \tag{3.9}$$

This is less performant but simpler to analyze than the optimal V&V phase estimator [33]: $\hat{\theta} = \frac{1}{4}\arg\left[\frac{1}{M}\sum_{m=1}^{M}\tilde{E}(t - mT_s)^4\right]$. The difference between the two estimators is most striking when the fields $\tilde{E}(t - mT_s)$ have widely different amplitudes and thus SNRs $\rho_m$ at the different symbol times. However, when treating penalties stemming from XPM, it is enough to consider the case of equal SNRs, in which case the V&V and the estimator (3.9) are quite similar. Using (3.9), we see that the phase error is a linear filtering of the XPM process: $\Delta\phi(t) = \theta_{XPM}(t) \otimes h_D(t)$, where $\otimes$ denotes convolution, and the filter impulse response is $h_D(t) = \delta(t) - \frac{1}{M}\sum_{m=1}^{M}\delta(t - mT_s)$ so that its frequency response is:

$$H_D(\omega) = 1 - \frac{1}{M}\sum_{m=1}^{M} e^{-j\omega mT_s}. \tag{3.10}$$

When $M$=1 we get the same differential filter as in the DQPSK case with delay demodulation treated in the previous section. Using expression (3.10) for what we call the "generalized" differential filter, the variance of the phase error is still given by (3.8).

The dependence of XPM on the DM link parameters comes through the IM-XPM filter (A.5). However, as we can see from (3.8), the variance of XPM also

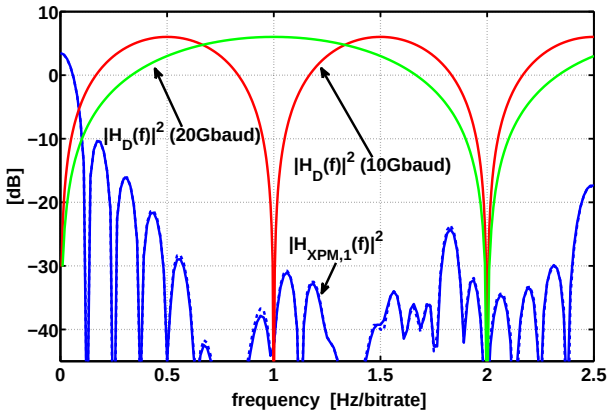


Figure 3.11: Plot of $|H_{XPM,1}(f)|^2$ and $|H_D(f)|^2$ versus normalized frequency $f/R_{OOK}$, with $R_{OOK}$=10GHz, for DQPSK at 10 and 20Gbaud. 15-span NZ-DSF system, $D_{in}$=100ps/nm, $D_{pre}$=SLR, $D_{tot}$=0. Nonlinear phase $0.3\pi$. Channel spacing $\Delta f$=50GHz.

depends on the phase estimation filter $H_D(\omega)$. For the same 15-span DM line as in the previous section with $D_{in}$=100ps/nm with minimum channel spacing of 50GHz, Fig. 3.11 depicts both $|H_{XPM,p}(\omega)|^2$ with $p$=1 (pump-probe spacing 50GHz), and $|H_D(\omega)|^2$ for a DQPSK reference channel modulated at both 10Gbaud (20Gb/s) and 20Gbaud (40Gb/s). The frequency axis is normalized to the bitrate of the pump OOK channel.

It is clear that if the baudrate of the DQPSK channel increases, $H_D(\omega)$ gets more effective in suppressing the low frequencies of the XPM spectrum $C_{OOK}(f)|H_{XPM,p}(f)|^2$. This result can also be easily understood by reasoning in the time domain: if DQPSK and OOK have the same baudrate, the XPM contributions on adjacent symbols are almost independent and the effect of differential detection cannot help. On the other hand, if the baudrate of DQPSK increases, every OOK symbol induces the same XPM over more and more DQPSK symbols, which are thus correlated. In this case differential detection can partially suppress the XPM contributions.

Fig. 3.12 shows $|H_D(\omega)|^2$for coherent QPSK at a baudrate of 20Gbaud, when

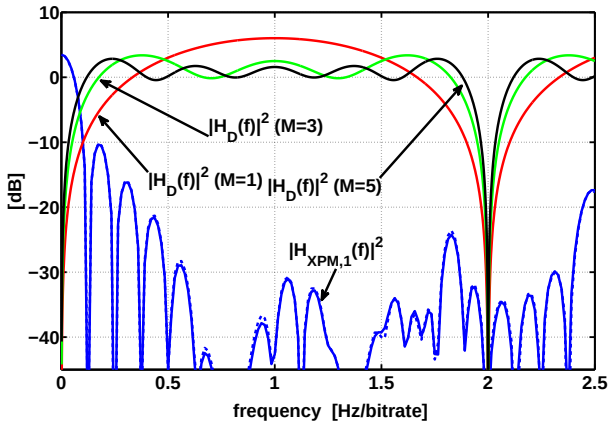


Figure 3.12: Plot of $|H_{XPM,1}(f)|^2$ and $|H_D(f)|^2$ for coherent QPSK at 20Gbaud, varying the number of phase estimation samples $M$. 15-span NZ-DSF system, $D_{in}$=100ps/nm, $D_{pre}$=SLR, $D_{tot}$=0. Nonlinear phase $0.3\pi$. Channel spacing $\Delta f$=50GHz.

the phase is estimated over $M$=1, 3 or 5 symbols. Increasing $M$ has the effect of reducing the cut-off frequency of $H_D(\omega)$, thus increasing the XPM variance. It is a known fact that in absence of strong nonlinearities and when ASE noise dominates over the phase noise of the transmitting laser, a higher $M$ yields a better performance [60]. In the nonlinear regime, on the contrary, $M$ must be reduced to improve the performance [68]. This behavior is the effect of a trade-off of the filtering action of $H_D(\omega)$ on both the ASE- and the XPM-induced estimated phase noise spectrum. If the spectrum of the ASE-induced estimated phase noise (which we overlooked in the above analysis) is almost flat on the bandwidth of the signal, the larger $M$ is, the smaller is the phase error variance. On the other hand, if the phase estimation error has a low-pass spectrum (such as the one induced by XPM or by the lasers phase noise [60]), the smaller $M$ is, the smaller is the variance.

The presented approach can be useful to derive simple rules for the design of the phase estimation stage of coherent receivers. Also note that if the XPM is by far the dominant impairment, the standard differential demodulation of DQPSK is optimal.

This is in good agreement with the results in [69].

### 3.3.4 Checks Against Simulation

To verify the accuracy and the limits of the XPM variance formula (3.8), we ran Monte Carlo simulations to directly estimate the variance of the received phase. We tested a WDM system composed of a central NRZ-QPSK channel at a variable baudrate $10 \leq R_s \leq 50$Gbaud, having $N$=2 NRZ-OOK 10Gb/s channels on each side (5 channels total), with a minimum frequency spacing $\Delta f$ of either 50 or 100GHz. The line was composed of $N$=15 identical spans of 100km of either NZ-DSF fiber ($D_{tx}$=3.83ps/nm, $\alpha$=0.22dB/km, $\gamma$=1.5$\frac{1}{W \cdot km}$@ 1550nm) or SMF ($D_{tx}$=17ps/nm, $\alpha$=0.22dB/km, $\gamma$=1.4$\frac{1}{W \cdot km}$@ 1550nm) and the compensating fibers were linear. The in-line residual dispersion per span was set to $D_{in}$=100ps/nm, and the pre-compensation was selected using the SLR. The total dispersion $D_{tot}$ was set to zero, i.e. to the optimal value for PSK, by tuning the post-compensation. Note that for non-zero values of $D_{tot}$ also the effect of the intensity noise caused by XPM should be taken into account [82, 83].

In the SSFM simulations, we solved the coupled propagation equations for each channel in the single-polarization case, neglecting the FWM beat terms. This amounts to assuming co-polarized WDM channels, which is a worst case for XPM, and neglecting polarization effects. Another implication of our SSFM method is that simulated results for large baudrates $R_s$ such that $R_s + R_{OOK}$ exceeds the channel spacing $\Delta f$ neglect the effect of the spectral overlap of the PSK channel with the neighboring OOK channels during propagation [84]. The number of simulated symbols in the FFT window was fixed to 1260 for the QPSK channel, with 60 samples per symbol. Such a number was chosen such that the ratios $\frac{R_s}{R_{OOK}} = [1, 1.5, 2, 2.5, 3, 3.5, 4, 4.5, 5]$ give an integer number of OOK bits within the FFT window. The minimum number of OOK symbols is thus 252, when the QPSK baudrate is 50Gbaud. The single-polarization receiver was either an incoherent differential receiver or a coherent receiver with feed-forward phase estimation, both with an optical filter with one-sided bandwidth $B_o = 2R_S$ and no electrical filter.

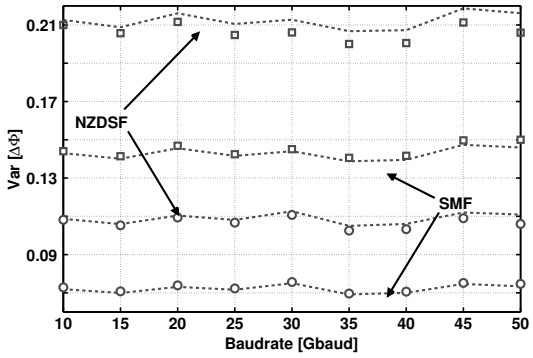


Figure 3.13: XPM-induced phase variance on the reference (D)QPSK channel before $H_D(\omega)$ in a 15-span 5-channel hybrid DM system with either NZ-DSF or SMF transmission fiber, $D_{in}$=100 ps/nm, $D_{pre}$=SLR, $D_{tot}$=0. SSFM simulation (symbols) and XPM filter prediction (dashed). Channel spacing: $\Delta f$=50GHz (squares); $\Delta f$=100GHz (circles).

In all the Monte Carlo simulations, we evaluated the phase variance of every symbol in the sequence separately, taking only the central sample, and subtracting the phase associated with the transmitted symbol. The propagation was repeated 50 times, each time changing the random delay and the random pattern of the OOK channels. We estimated the variance separately on each symbol because, even after subtracting the transmitted phase, the average received phase was different from symbol to symbol, since the mean nonlinear phase induced by XPM depends on the transmitted patterns. After measuring the variance separately on every symbol, we computed the mean of the collected variances. We verified that our procedure produces essentially the same results as the more intuitive procedure in which the phase variance from all the symbols in one simulation is evaluated, and then the average of the phase variance from all the repeated simulations is taken; however our procedure has a faster convergence to the desired confidence level.

We first measured the phase variance of the received reference channel after the optical filter but before demodulation, where the QPSK and DQPSK signals are iden-

tical. We compared the SSFM-simulated variance with the theoretical results of (3.8) when setting $H_D\omega) \equiv 1$. In this case, $C_{OOK}(f)$ was estimated from the actual OOK waveforms by taking the average of the sample PSDs (i.e. their periodograms) collected during the SSFM simulation. This is because, for short to moderate length bit sequences, $C_{OOK}(f)$ may have non-negligible variations from its ergodic limit (3.6).

The results are reported in Fig. 3.13 for the case of both NZ-DSF and SMF transmission fiber, using either 50GHz or 100GHz channel spacing. The launched average power for all channels was $P_{\text{in}}$=2dBm in each case, corresponding to a cumulated nonlinear phase $\phi_{\text{NL}}$=0.22rad [97]. SSFM simulations in this case did not include SPM. Hence, the predictions of the model are very close to simulation in all the tested scenarios. Note that the slight dependence of $\text{Var}[\Delta\phi]$ on the baudrate is only caused by the random fluctuations of the Monte Carlo estimates of the PSD $C_{OOK}(f)$ due to the finite bit-sequence. Replacing it with its theoretical limit (3.6) would yield flat curves at every power level, since $R_S$ doesn't appear in $H_{XPM,p}(f)$ and $C_{OOK}(f)$ is independent of the baudrate of the reference QPSK channel.

Fig. 3.14 shows instead the estimated phase variance after the differential filter versus QPSK channel baudrate, for both DQPSK reception (left graph), and coherent QPSK reception with $M$=5 (right graph). Solid lines refer to theory (3.8), while symbols to SSFM simulations. We also tested the same 15-span DM system at a lower $P_{\text{in}}$=0dBm, and the results (not reported) were qualitatively similar but with a much better fit.

By comparison with Fig. 3.13, we now note a strong dependence of $\text{Var}[\Delta\phi]$ on the baudrate, which is clearly due to the action of the differential filter. This effect was already observed in [84], but ascribed to the walk-off effect. Even in this case the predictions of the theory (3.8) are rather close to the SSFM simulations when SPM is neglected.

Having numerically verified the effectiveness of the filter-based approach, we now turn to testing the SP approximations in (3.2) and (3.4). One limit of the "Blachman" formula (3.1) is that the two noisy fields at times $t$ and $t-T$ are assumed to be independent, while for increasing walk-off the correlation time of the phase process $\Delta\phi(t)$ can be much longer than the symbol time $T_s$, thus clearly violating the indepen-

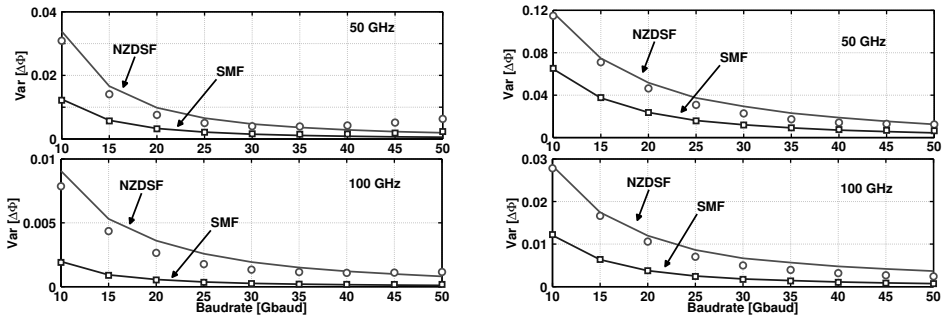


Figure 3.14: XPM induced phase variance on DQPSK (left) or coherent QPSK ($M$=5, right) reference channel at $P_{in}$=2dBm versus QPSK channel baudrate. Same WDM 15-span DM system as before, with $D_{in}$=100ps/nm, $D_{pre}$=SLR, $D_{tot}$=0, channel spacing 50GHz (top) and 100GHz (bottom), while the transmission fiber is either NZ-DSF or SMF. SSFM simulations without SPM (symbols) and XPM filter predictions (3.8) (solid).

dence assumption. Such correlations, by our experience, usually increase the penalty beyond the value predicted by (3.1). Another expected source of discrepancy with the actual penalty is the Gaussian assumption for the statistics of $\Delta\phi(t)$, which typically also leads to an over-estimation of penalty. Also, the analytical fits (3.2), (3.4) yield a penalty that slightly exceeds the predictions of the "Blachman" formulas (3.1), (3.3) at large XPM variance. Hence we expect the model to overestimate the penalty with respect to simulations.

To verify the match of the analytical formulas (3.2), (3.4) evaluated with the analytical variance (3.8) against the SSFM simulated SP, we analyzed the same 15-span DM transmission systems already tested for the numerical results on phase variance. The SP was computed at BER=$10^{-5}$ using the fast semi-analytical Karhunen-Loéve (KL) method for DQPSK [17], while in the case of coherent QPSK with feed-forward phase estimation, in the absence of a reliable semi-analytical BER estimation method, we computed the SP at BER=$10^{-3}$ using direct Monte Carlo error counting. We repeated the simulations 10 times, by varying the OOK random patterns and the delay between the channels. Again, $P_{in}$ was 2dBm. Fig. 3.15 shows the obtained curves,

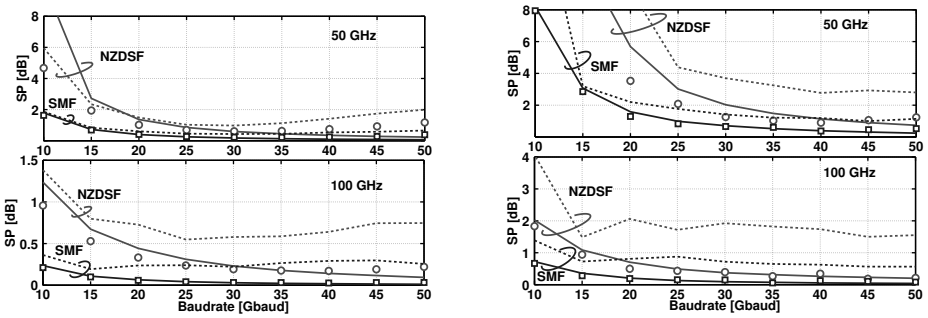


Figure 3.15: XPM induced SP on DQPSK (left graphs) and coherent QPSK ($M$ =5, right graphs) reference channel for a 5-channel 15-span hybrid DM system with $D_{in}$=100 ps/nm, $D_{pre}$=SLR, $D_{tot}$=0 and average input power $P_{\in}$=2dBm/ch. The channel spacing is 50GHz (top) or 100GHz (bottom), while the fiber is either NZ-DSF or SMF. Theoretical SP (3.2), (3.4) (solid); simulated SP without SPM (symbols); simulated SP with SPM (dashed).

where again solid lines denote theory (3.2), (3.4), symbols are simulations without SPM, while dashed lines are the "true" simulated SP including SPM.

From the figure we see that the theoretical fits (3.2), (3.4) give a reasonable match with simulations without SPM for SP values up to $\sim$2 dB, but can lead to large overestimates at higher penalties (top figures). We verified that when the theoretical SP diverges form the simulated one, it is mainly due to the fact that the XPM-filter fails to give an exact prediction of the phase variance. In fact, substitution of the SSFM calculated phase variance in (3.2) , (3.4) yields a more precise estimation of the SP, especially at higher baudrates.

When including SPM (dashed lines) the SP penalty increases because the SPM-induced (D)QPSK phase distortion causes an increase of the phase variance at higher baudrates. Such effect is not included in the theoretical model. If the channels are spaced by 50GHz, the effect of XPM is stronger and thus the theoretical prediction is more accurate, at least up to about 30Gbaud. At higher baudrates, the XPM is largely suppressed while the effect of SPM, which increases with the baudrate, gets more and more dominant. When the channels are spaced at 100GHz, the XPM penalty is

reduced and our approximation is less precise also at lower baudrates. Finally note that for DQPSK there is a minimum of the penalty around 30Gbaud, while for coherent QPSK (which we showed to be more vulnerable to the XPM induced distortion) such a minimum is still not reached within the shown range of baudrates.

## 3.4 Conclusions

In the first section of this chapter, we presented numerical simulations that support the conclusion that PDM-QPSK is a very promising format that will enable to deliver bitrates up to 100Gb/s per channel. However in order to ensure enhanced tolerance against cross channel non-linear impairments and thus extend the reach, the phase estimation process is a critical component that should be carefully engineered. On the other hand, at 40Gb/s, PDM-QPSK is strongly affected by XPM while, with proper DM design, DQPSK has proven to be the best choice among the considered formats for this bitrate in ultra long haul systems.

In the second section we analyzed the different impact of OOK and NZ-DPSK 10Gb/s channels on a 40Gb/s DQPSK channel. Upgrading 10Gb/s OOK channels to NF-DPSK requires to replace some 10G linecards, but proves to be a viable alternative for the upgrade of deployed WDM systems. For the implementation of the proposed scheme, a narrow optical filter with a 3-dB bandwidth of about 6.5GHz is needed at the receiver and the laser frequency drift needs to be limited (e.g., to within $\sim$2GHz), thus requiring wavelength tracking. The slightly more complex setup is compensated for by a largely reduced XPM, which is the main impairment in such hybrid systems for $D_{in}$ as high as 100ps/nm. NF-DPSK is thus a good option for deployed system with low $D_{in}$, where the influence of XPM increases dramatically. For higher values of this key parameter ($D_{in}$) OOK gives acceptable performance, making the upgrade unattractive. However, for a wide range of $D_{in}$ (e.g., $|D_{in}| <$100ps/nm), even with the consideration of the inter-channel NLPN induced on DQPSK channels, the DQPSK performance improves when the 10G OOK channels are converted to NF-DPSK.

Finally in the third section we provided a theoretical model able to explain the

detailed mechanism of the XPM-induced performance degradation by neighboring 10Gb/s OOK channels on both incoherent DQPSK and coherent QPSK with feed-forward phase estimation. We have: (i) derived IM-XPM filters, similar to the IM-IM filters derived in the past to study XPM penalty in OOK channels; (ii) proved, by check against simulations when only XPM is active, that all that matters for the sensitivity penalty evaluation is the XPM variance induced on the test channel by OOK channels; (iii) provided novel SP formulas for both incoherent DQPSK and coherent QPSK; (iv) explained the reason why XPM-induced SP decreases with the baudrate of the phase modulated channel. We traced back the origin mostly to the action of the generalized differential filter $H_D(f)$, which is present both in DQPSK and in feed-forward phase-estimated coherent QPSK. The differential filter suppresses the low-frequency portion of XPM, more effectively when the baud-rate of the phase modulated channel is larger than the bit rate of the 10Gb/s OOK channels. Such an analysis also explains why coherent QPSK, when the feed-forward phase estimation is performed on more than one symbols, is more impaired by XPM than DQPSK at the same baudrate. Note that, although our analysis is performed for simplicity in a single-polarization setting, still one can infer results on performance of polarization division multiplexed (PDM) coherent QPSK by using the effective baud-rate of the QPSK channel. We therefore predict that at 40Gb/s coherent QPSK channels with polarization division multiplexing (10Gbaud) would be even more impaired by 10Gb/s OOK channels. DQPSK (20Gbaud) would be a better solution, but still would require some guard-band from 10Gb/s OOK channels to avoid any impact on the maximum achievable reach, especially over NZ-DSF. On the other hand, at 100Gb/s, PDM-QPSK (25Gbaud) would both allow the design of WDM systems with 50GHz spacing and would be less impaired by neighboring channels thanks to the increased baudrate. Finally note that effects such as nonlinear polarization rotation and its interplay with PMD are not included in the analysis and should be investigated before a final complete picture of the performance degradation due to XPM is obtained.

# Appendix A

Consider the $k$-th span of length $\ell_k$ of an $N$-span DM optical link. At the DM link input consider a CW input probe signal at wavelength $\lambda_s$, having a small enough power to neglect self-phase modulation effects, along with an on-off keying (OOK) modulated pump signal at wavelength $\lambda_p$ having power whose Fourier transform is $P_p(0,\omega)e^{-j\frac{\omega^2}{2}\beta_{pre}}$, where $\beta_{pre} = \beta_{2,pre}\ell_{pre}$ [ps$^2$] is the GVD cumulated in the link pre-compensation fiber of length $\ell_{pre}$, and $P_p(0,\omega)$ is the input pump Fourier transform.

Following the same reasoning as in [90–92], the pump power at coordinate $z$ within the $k$-th span in the retarded time frame of the signal, using the GVD induced IM-IM small signal conversion [100], has Fourier transform

$$P_p(z,\omega) = P_p(0,\omega)e^{j\omega d_a(k)}e^{[-\alpha+j\omega d_{sp,k}]z}\cdot\cos\left[\frac{\omega^2}{2}(\beta_a(k)+\beta_{2,k}z)\right] \tag{A.1}$$

due to walk-off ($d_{sp,k} \cong D_k\Delta\lambda_{sp}$ is the walk-off parameter, being $D_k$ the fiber dispersion and $\Delta\lambda_{sp} = \lambda_s - \lambda_p$ the channel spacing), fiber attenuation parameter $\alpha$, and GVD parameter $\beta_{2,k}$. Here $\beta_a(k) = \beta_{pre} + \sum_{i=1}^{k-1}\beta_{s,j}$ is the dispersion accumulated from system input (including pre-compensation) till the span input, being $\beta_{s,i}$ the accumulated GVD [ps$^2$] in the i-th span after in-line compensation, while $d_{a(k)=d_{sp,pre}}\ell_{pre} + \sum_{i=1}^{k-1} d_{a,i}$ is the accumulated walk-off from system input to span input, being $d_{a,i}$ the accumulated walk-off in the $i$-th span after in-line compensation. In writing (A.1) we are also assuming for simplicity that: i) all spans have the same input power, i.e. the in-line amplifiers recover all span losses; ii) the in-line dispersion compensating fibers are purely linear devices. The probe phase induced at $z$ through XPM by propagation of such a pump over an infinitesimal segment $dz$ has Fourier transform $d\Theta(z\omega) = -2\gamma P_p(z,\omega)dz$. Such a phase modulation enters, if the nonlinear effects of the remaining line segment are neglected, an equivalent pure-GVD trunk composed of the remaining $\ell_k - z$ km of fiber within the k-th span, followed by the remaining spans to the DM system end. Such a purely linear trunk produces by PM-PM

GVD conversion at the DM system output an infinitesimal output XPM of [91, 100]: $d\Theta_{XPM}(\omega) = \cos(\frac{\omega^2}{2}(\beta_r - \beta_a(k) - \beta_{2,k}z)d\Theta(z,\omega)$,where $\beta_r$ [$ps^2$] is the residual (i.e., total) dispersion accumulated over the entire DM link (which does include also a post-compensating fiber when present), hence $(\beta_r - \beta_a(k) - \beta_{2,k}z)$ is the dispersion cumulated from the local coordinate $z$ within span $k$ till the DM system end. Integrating over all infinitesimal contributions from $z$=0 to $z = \ell_k$ on span $k$ one finally gets the output cross phase due to span $k$ as: $\Theta^{(k)}_{XPM}(\omega) = \int_0^{\ell_k} d\Theta_{XPM}(\omega) = H^{(k)}_{XPM}(\omega)P_p(0,\omega)$, where the $k$-th span IM-XPM filter is:

$$\begin{aligned} H^{(k)}_{XPM}(\omega) &= -2\gamma e^{j\omega d_a(k)} \int_0^{\ell_k} \cos[\frac{\omega^2}{2}(\beta_a(k) + \beta_{2,k}z)] \\ &\cdot \cos(\frac{\omega^2}{2}(\beta_r - \beta_a(k) - \beta_{2,k}z))e^{(-\alpha + j\omega d_{sp,k})z}dz. \end{aligned} \tag{A.2}$$

The total output XPM on probe channel in this linearized model is the sum of the contributions of all $N$ spans: $\Theta_{XPM}(\omega) = \sum_{k=1}^{N} H^{(k)}_{XPM}(\omega)P_p(0,\omega)$. Solving the integral in (A.2) gives the explicit global IM-XPM filter:

$$\begin{aligned} H_{XPM}(\omega) = -2\gamma \sum_{k=1}^{N} e^{j\omega d_a(k)} \frac{1}{4} \cdot \Bigg\{ e^{j(\beta_r - 2\beta_a(k))\frac{\omega^2}{2}} \frac{1 - e^{-(\alpha + j(\omega^2\beta_{2,k} - \omega d_{sp,k}))\ell_k}}{\alpha + j(\omega^2\beta_{2,k} - \omega d_{sp,k})} \quad + \\ + e^{-j(\beta_r - 2\beta_a(k))\frac{\omega^2}{2}} \frac{1 - e^{-(\alpha - j(\omega^2\beta_{2,k} + \omega d_{sp,k}))\ell_k}}{\alpha - j(\omega^2\beta_{2,k} + \omega d_{sp,k})} + 2\cos(\beta_r \frac{\omega^2}{2}) \frac{1 - e^{-(\alpha - j\omega d_{sp,k})\ell_k}}{\alpha - j\omega d_{sp,k}} \Bigg\} \end{aligned} \tag{A.3}$$

If we assume long spans ($\ell_k \gg \frac{1}{\alpha}$), a uniform channel spacing so that $\lambda_s - \lambda_p = (s-p)\Delta\lambda$, with $\Delta\lambda = \frac{\lambda^2}{2\pi c}\Delta\omega > 0$, and assume that our reference channel is $s$=0, then equation (A.3) becomes:

$$\begin{aligned} H_{XPM}(\omega) = -\frac{\gamma}{2\alpha} e^{j\omega p\beta_{pre}\Delta\omega} \cdot \Bigg\{ \frac{e^{j\frac{\omega^2}{2}(\beta_r - 2\beta_{pre})} \sum_{k=1}^{N} e^{-j[\omega - p\Delta\omega]\omega\beta_s(k-1)}}{1 + j\frac{\beta_2}{\alpha}\omega(\omega - p\Delta\omega)} + \\ + \quad \frac{e^{-j\frac{\omega^2}{2}(\beta_r - 2\beta_{pre})} \sum_{k=1}^{N} e^{j[\omega + p\Delta\omega]\omega\beta_s(k-1)}}{1 - j\frac{\beta_2}{\alpha}\omega(\omega + p\Delta\omega)} + \frac{(e^{j\frac{\omega^2}{2}\beta_r} + e^{-j\frac{\omega^2}{2}\beta_r}) \sum_{k=1}^{N} e^{j\omega p\beta_s\Delta\omega(k-1)}}{1 - j\frac{\beta_2}{\alpha}\omega p\Delta\omega} \Bigg\}. \end{aligned} \tag{A.4}$$

Define now $x \triangleq e^{jW\beta_s}$, and introduce the following *interference* term:

$$I_p(W) \triangleq \frac{1}{N}\sum_{k=0}^{N-1} x^k = e^{jW\beta_s\frac{N-1}{2}}\frac{\sin(W\frac{\beta_s N}{2})}{N\sin(W\frac{\beta_s}{2})}. \tag{A.5}$$

Also define a *walk-off* term as

$$H_{Wp}(W) = \frac{1}{1-j\frac{\beta_2}{\alpha}W} \tag{A.6}$$

and finally define the following filter:

$$\begin{aligned} H_p(\omega) &\triangleq e^{j\omega p\Delta\omega\beta_{pre}} I_p(\omega p\Delta\omega) H_{Wp}(\omega p\Delta\omega) \\ &+ e^{j\omega(\omega+p\Delta\omega)\beta_{pre}} I_p(\omega(\omega+p\Delta\omega))\cdot \\ &\cdot H_{Wp}(\omega(\omega+p\Delta\omega)). \end{aligned} \tag{A.7}$$

It is now easy to see that, using the new filter (A.7), the IM-XPM filter in (A.5) can finally be expressed as in (3.5), with $\Phi_{NL} = N\frac{\gamma}{\alpha}P_{\text{in,p}}$.

# Chapter 4

# Assessing and mitigating nonlinear effects in 100Gb/s coherent optical communications

In this chapter we focus on the study of nonlinear impairments in 100Gb/s PDM-QPSK systems using coherent reception. We compare transmitter configurations based on a single carrier or a dual-carrier setup [101]. Then we focus on the assessing of the penalties in this kind of systems; the peculiar impairments of polarization multiplexed signals, in fact, require a review of the testing techniques developed for direct detection. Specifically, we test different PMD emulation schemes.

## 4.1 100Gb/s PDM-QPSK transmission in Single carrier and dual-carrier configuration

Referring to 100Gb/s transmissions, an alternative to the traditional approach of modulating a single carrier at 100Gb/s for every channel, is the transmission of two subcarriers, both modulated at 50Gb/s, in the same wavelength slot [102]. This solution would halve the required bandwidth for opto-electronic devices at both the transmit-

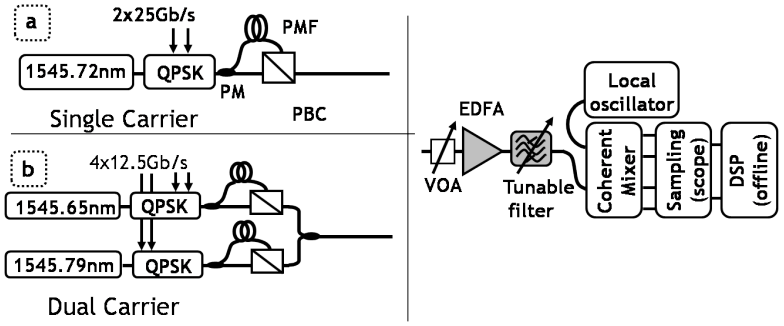


Figure 4.1: SC (a) and DC (b) configuration of the transmitter (left). Coherent receiver setup (right).

ter and the receiver (especially ADCs), at the cost of doubling the number of the components.

In this section we compare through experiments the tolerance of single-carrier (SC) and dual carrier (DC) 100Gb/s PDM-QPSK to narrow optical filtering and we analyze the performance of the two considered solutions when propagating in WDM configuration on non-zero dispersion shifted fiber (NZ-DSF). We want the test to be representative of a realistic upgrade scenario and thus the neighboring channels will be in turn on-off keying (OOK) modulated at 10Gb/s or partial differential phase shift keying [103] (P-DPSK) modulated at 40Gb/s.

Fig. 4.1 (left) shows the transmitter setup for SC (a) and DC (b) configurations. SC was realized with a laser source ($\lambda_c$=1545.72nm) modulated by a QPSK modulator operating at 25GBaud, fed by two $2^{15}$-1 long PRBS. Polarization multiplexing was emulated by splitting the modulated signal, delaying one path by thousands of symbols using a polarization maintaining fiber (PMF), and recombining it by using a polarization beam combiner (PBC). In DC configuration two different laser sources were employed. The fine adjustment of their wavelength allowed to set the desired sub-carrier frequency offset. The equivalent central wavelength was the same $\lambda_c$ as in the SC case. The two sources were injected into two different QPSK modulators operating at 12.5Gbaud, fed by four $2^{15}$-1 long PRBS. Polarization multiplexing

was emulated for both sub-carriers in the same way as for the SC case leading to two PDM-QPSK signals at 50Gb/s. These two signals were then coupled together to make a 100Gb/s DC-PDM-QPSK signal. It should be noted that, due to technical limitations of the equipments, we did not add bit-rate overhead, as would be required by forward error correcting codes and protocol (generally considered to be $\sim$12% at 100Gb/s).

The set-up of the receiver is depicted in Fig. 4.1 (right). It comprised a variable optical attenuator, an EDFA, a narrow optical tunable filter and a coherent receiver, connected to a 50GSample/s real-time oscilloscope. For each measurement, we stored several waveforms totalizing 2Msamples per channel. The stored data were then off-line processed [6]. The numerical process included several steps: resampling at twice the symbol rate, possible dispersion compensation through FIR filtering, digital clock recovery, polarization demultiplexing through 7-tap adaptive filtering based on CMA, carrier-phase estimation using the Viterbi and Viterbi algorithm, and finally symbol identification for BER calculation, which is then converted into $Q^2$-factor. In the SC case the local oscillator was always centered on $\lambda_c$ while in DC case it was centered on one of the two sub-carriers central wavelength. Two separate acquisitions were performed for storing both sub-carriers data and the channel BER results from the averaging of the BERs obtained at each subcarrier. Fig. 4.2a shows the optical spectra of the two solutions, measured with an 80MHz resolution bandwidth complex spectrum analyzer.

Fig. 4.2b shows the results of a preliminary test in which the impact of the offset of the two sub carriers in the DC case has been investigated. A narrow sub-carrier spacing of 15GHz gives up to 2dB penalty. A large one would penalize this solution in case of narrow filtering along the line. In the following, we tuned the offset to 18GHz, which is found to be the narrowest one giving negligible penalty ($\leq$0.2dB). This choice set the sub-carrier wavelengths to 1545.65nm and 1545.79nm respectively.

With this configuration, the $Q^2$-factor was measured for various filter settings. Initially, the filter 3dB bandwidth was varied in the range 0.40-0.15nm. Fig. 4.3a shows $Q^2$-factor penalty of SC (squares) and DC (circles) versus filter width. The insets represent the spectra at 21GHz of both cases with the same scale as in Fig. 4.2b.

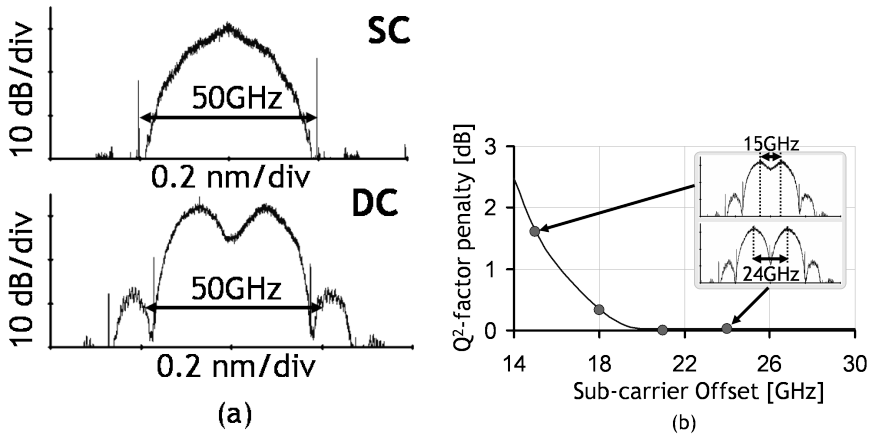


Figure 4.2: SC and DC spectra when sub-carrier spacing is set to 18 GHz (a). $Q^2$-factor penalty vs. sub-carrier offset for DC configuration (b)

We observe almost no impact on the sensitivity penalty in the range 35-50GHz of filter width. The 1dB penalty is at 21GHz and 25GHz for SC and DC configurations respectively. In correspondence of a 21GHz filtering SC looses 20% of the energy while DC the 40%. Next we varied the filter position, keeping its 3dB bandwidth constant at 43GHz, in order to highlight misalignment effects with respect to the ones coming from narrow filtering. The results are depicted in Fig. 4.3b for SC (square) and DC (circles) cases; the 1dB-penalty is located at 100pm and 70pm respectively. The slight asymmetry of the two curves is due to filter imperfections. Even if both solutions present no penalty inside the interval $\pm$40pm, the DC case is clearly more sensitive to filter misalignment, which can become a significant impairment when cascading reconfigurable add-drop modules (ROADMs).

For transmission experiments, we used 80 lasers distributed on a 50GHz grid in the range [1530.31-1562.61 nm] and divided into even and odd channels. The test channel central frequency was again 1545.72 nm and was injected into the even comb using a coupler. The two combs were then passed through a polarization scrambler and combined using an interleaver. The setup of the test channel was the same as previously described for both SC and DC configurations. The neighboring channels

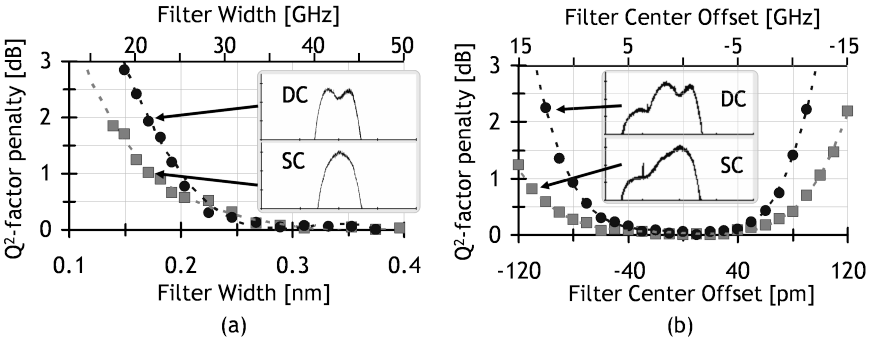


Figure 4.3: $Q^2$-factor penalty versus optical filter width for SC (square) and DC (circles) cases. The insets show the two spectra, which are cut by narrow filtering w.r.t the unfiltered ones of Fig 4.2a. (a). $Q^2$-factor penalty versus filter center misalignment for SC (square) and DC (circles) cases. The spectra deformed by a 100pm misalignment of the optical filter are represented in the insets (b).

could be modulated (even and odd separately), using either 10Gb/s OOK or 40Gb/s P-DPSK. When neighboring channels were OOK modulated, we left 50GHz bandgaps. (i.e. one empty channel slot) in order to be able to achieve optimal performance above the FEC codes limit, for both SC and DC. The transmitter setup is depicted in Fig. 4.4a, while Fig. 4.4c shows the resulting WDM spectra when neighboring channels are OOK and P-DPSK modulated.The transmission setup is represented in Fig. 4.4b. The WDM signal was boosted through a dual stage EDFA that incorporated pre-compensating fibers. The recirculating loop comprised four 100-km spans of NZ-DSF, amplified by dual-stage EDFAs comprising dispersion compensating fibers . The tunable narrow optical filter was always kept aligned with the central frequency of the channel under test and its width was set to 50GHz.

Fig. 4.5 shows the experimental results for SC (left) and DC (right) in single channel configuration (squares), with 40Gb/s P-DPSK neighbors (triangles) and with 10Gb/s OOK neighbors (circles). All the curves represent the measured $Q^2$-factor after 800km versus the average injected power per channel.

The single channel curves (squares) show an optimal $Q^2$-factor of around 13dBm

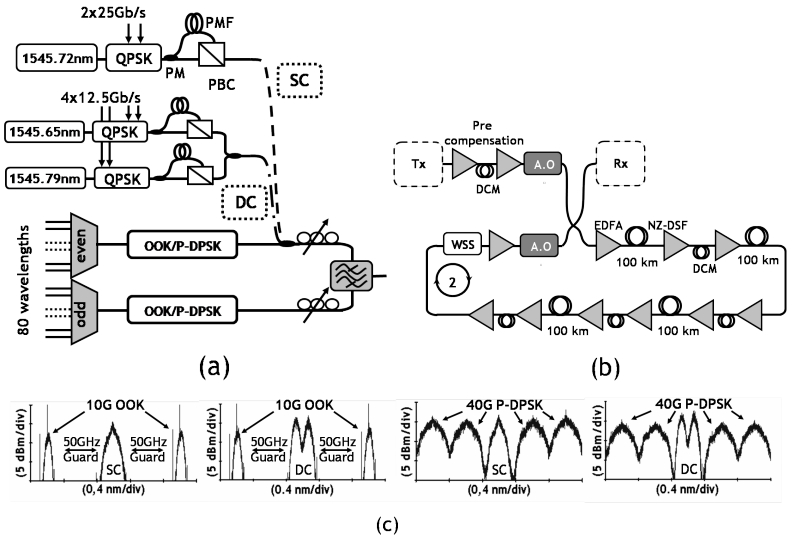


Figure 4.4: Transmitter setup in propagation configuration (a). Recirculating loop setup (b). WDM spectra of the central SC or DC 100Gb/s channel and their 4 closest neighbors when 10Gb/s OOK modulated and 40Gb/s P-DPSK modulated (c).

for SC and 12dBm for DC; the nonlinear threshold (NLT, defined as the power that maximizes the $Q^2$-factor) is also 1dB better for SC (1dBm vs. 0dBm). This proves that SC is more tolerant to intrachannel nonlinear effects. When co-propagating with 40Gb/s P-DPSK channels (triangles), both SC and DC configurations undergo similar degradations w.r.t. the single channel case (1dB in $Q^2$-factor and 2dB in NLT). This 1dB penalty is limited and should be further decreased when propagating on SMF; thus the upgrade from 40Gb/s DPSK modulated channels to 100Gb/s channels should not pose severe engineering challenges. Also note that we expect similar tendencies when all the channels are either SC or DC (homogeneous WDM), because, even if at a different bitrate, neighboring channels would be still phase modulated. On the other hand, the impact of 10Gb/s OOK modulated neighboring channels (circles) is very important ($\sim$3.5dB penalty w.r.t. single channel for both DC and SC). This is because QPSK modulated signals are strongly impacted by the cross phase modulation (XPM) induced by amplitude modulated signals [69, 104]. Without band-gaps,

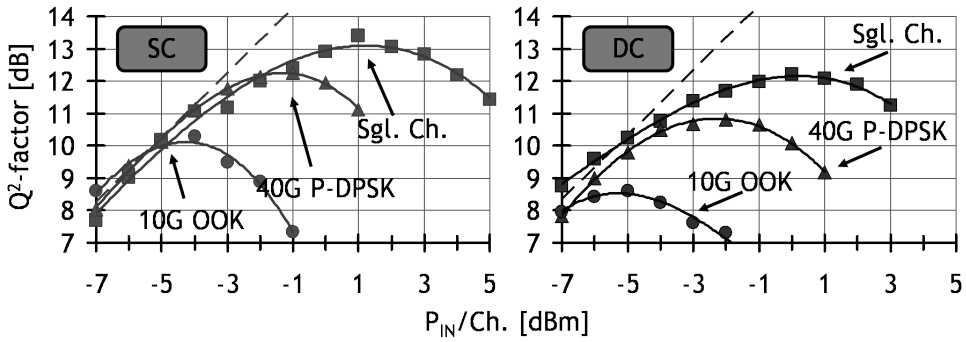


Figure 4.5: $Q^2$-factor vs. average injected power per channel for SC (left) and DC (right) in single channel configuration (squares) and when propagating along with 40Gb/s P-DPSK channels (triangles) or 10Gb/s OOK channels (circles).

the optimal $Q^2$-factor for the DC case was below the FEC threshold; we thus inserted the 50GHz band-gaps in order to reduce the impact of XPM. With the selected channel configuration, SC yields a $Q^2$-factor of $\sim$10dB, while DC reaches $\sim$8.5dB at best. This result can be explained by the fact that reducing the symbolrate of a phase modulated signal also reduces its tolerance to XPM [73, 84].

## 4.2 Nonlinear PMD emulation in 100Gb/s PDM-QPSK systems

The correct emulation of PMD has been the subject of theoretical and experimental studies for many years [105–107]. Today, PMD emulators are available as compact lab instruments. As long as single polarization, directly detected signals are considered, the distortion induced by linear PMD is one of the main sources of penalty. This is especially true at very high baudrates (> 10Gbaud) [108], both for intensity modulated and phase modulated transmissions [2]. When PMD-induced linear distortion is dominant, the position of a PMD emulator in an experimental setup is indifferent, and the emulator is usually placed at the output of the transmitter or before the receiver for simplicity. However in transmission systems employing PDM and coherent detec-

tion, both the amplitude and the phase of the signal are available at the receiver. The linear PMD can be thus effectively compensated in the electrical domain using DSP algorithms [34]. In these systems, linear PMD is not a concern, even for extremely large values of differential group delay (DGD), while other polarization-related effects, like cross-polarization modulation (XPolM) [109–111], are major sources of penalty. These distortions are due to the interaction between PMD (or even simple birefringence) and Kerr effect and thus they are intrinsically nonlinear and distributed along the line [112].

A very practical problem when assessing through experiments the penalty induced by these distortions is that, while deployed fibers can have very large amounts of PMD, new generation fibers are typically used in the laboratories. These fibers have a very small PMD coefficient due to an improved production process and PMD should be somehow emulated in the experimental setup using PMF sections or appropriate devices composed of a number of programmable waveplates. In this scenario a correct emulation of the PMD-related effects does not only depend on the characteristics of the PMD emulator, but also on its position in the experimental setup. It is thus interesting to analyze the impact of the line parameters (transmission fiber, dispersion management, etc.) on the accuracy of the PMD estimation, using different emulation schemes.

In this section we present the results of extensive simulations from which we derive some simple rules to be used in experimental investigations of PMD/nonlinear effects (NL) interactions. Specifically, we estimate the PDFs of the $Q^2$-factor for the selected configurations, comparing different emulation techniques with the real case of in-line distributed PMD. This way it is possible to verify if the emulation schemes are able to capture the distributed nature of PMD/NL interactions. For this kind of work, numerical simulations provide a simple and reproducible testbed, not affected by the instabilities of a real lab recirculating loop.

The basic setup is depicted in Fig. 4.6. We always tested the central of 9 channels, all modulated with PDM quadrature phase shift keying (QPSK) at 112Gb/s. The channels were spaced by 50GHz and modulated using a random pattern. The phase noise of the lasers was neglected

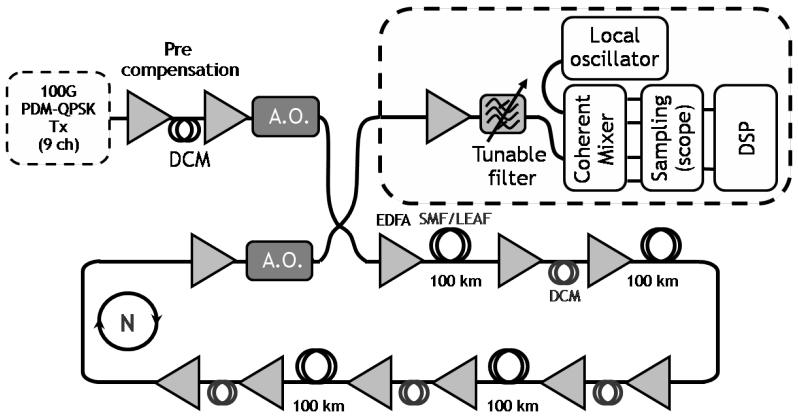


Figure 4.6: Basic simulative setup configuration used in the simulations.

and the input states of polarization (ISOP) of the channels were randomly selected over the Poincaré sphere at each run. The signal was then propagated over a recirculating loop composed of four 100-km spans of either NZ-DSF ($D$=4ps/nm/km, $S$=0.085ps/nm$^2$/km, $\alpha$=0.2dB/km, $A_{eff}$=72$\mu$m$^2$, $n_2$=2.7x10-20) or SMF ($D$=17ps/nm/km, $S$=0.057ps/nm$^2$/km, $\alpha$=0.2dB/km, $A_{eff}$=80$\mu$m$^2$, $n_2$=2.5x10-20). The loop could in turn be dispersion managed (DM) or unmanaged (noDM). In the first case, we used a single-periodic map with non-zero residual dispersion per span ($D_{in}$) and the pre-compensating fiber was selected using the "straight line rule" [76]. In the second case, no dispersion compensation was performed along the loop and the pre-compensating dispersion was omitted. The propagation was modeled solving the coupled nonlinear Schrödinger equation (CNLSE) through the split step Fourier method. To account for birefringence and PMD, each span was modeled as a concatenation of 50 random waveplates. The number of recirculations could be 1, 3 or 5, totaling 400, 1200 or 2000km. In all cases the propagation was noiseless and the equivalent noise of the link was loaded at the receiver (equivalent amplifier). We thus ignored the effects of nonlinear phase noise, which has been shown to be almost negligible in this kind of systems [113]. Before the receiver, we perfectly compensated for linear effects, i.e. chromatic dispersion and PMD, by inverting the Jones

matrix of the simulated channel. This step replaced electronic compensation in the coherent receiver. This choice allowed us to concentrate exclusively on the penalty arising from linear/nonlinear interactions along the link, neglecting any effect related to the non-ideal nature of DSP based compensation. At the receiver, the central channel was selected using a $2^{nd}$ order superGaussian optical filter with 56GHz bandwidth, then the signal beated with the local oscillator, was detected by ideal photodiodes at the output of a dual-polarization 90° hybrid and was ideally sampled at twice the baudrate. We neglected the phase noise of the local oscillator and we assumed perfect frequency alignment between the signal and the local oscillator. The phase was estimated using a standard Viterbi&Viterbi algorithm with 9 taps. We formed a Monte Carlo estimate of the BER by stopping the simulation when 100 errors were counted. Then the estimated BER was converted to $Q^2$-factor. For each combination of fiber type, dispersion map and distance, we tested three different values of average DGD: 4ps, corresponding to a link with moderate PMD; an intermediate 8ps case; and 20ps, which, especially for shorter links, is a very large amount of DGD. In total we thus considered 36 possible combinations of length/fiber/dispersion map/DGD.

We first needed to assess the true impact of PMD/NL interactions, and needed, for every configuration, a value of the average power per channel ($P_{in}$) that produces significant nonlinear effects. We will then estimate the $Q^2$-factor PDF at that value of injected power. To this aim, we simulated the so-called "bell curves" for all the 36 possible combinations. These curves give the measured $Q^2$-factor versus $P_{in}$, at a fixed noise figure of the equivalent amplifier at the end of the link. Hence, increasing the injected power also improves the received optical signal to noise ratio (OSNR). In all the curves, there is a maximum $Q^2$-factor at a value of $P_{in}$ which is commonly referred to as the nonlinear threshold (NLT). The length of the transmitted random pattern was 1024 symbols and for each value of $P_{in}$ we averaged the BER over 15 possible ISOP/fiber realizations in order to account for the variability induced by the PMD. Fig. 4.7 shows the bell curves for the case of a 1200km link using NZ-DSF. When using dispersion management, we saw that the total DGD had a positive impact on performance, since the DGD-induced depolarization that reduced the impact of XPolM [113]. The measured $Q^2$-factor for the noDM case was instead

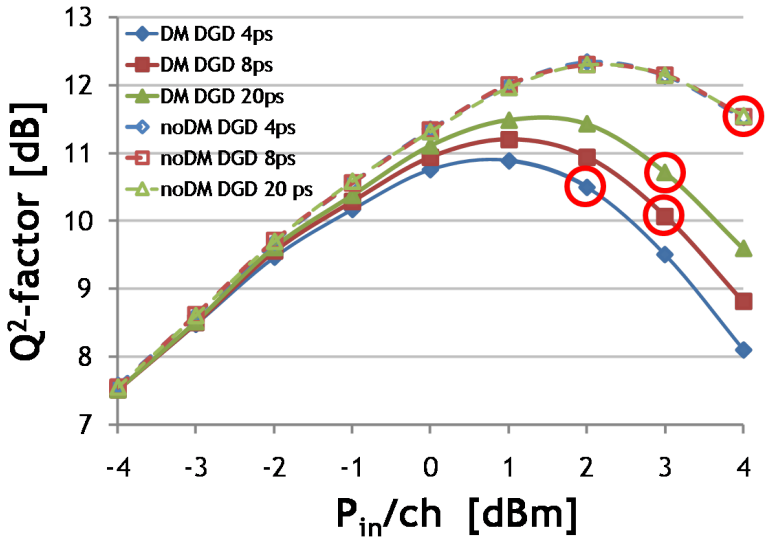


Figure 4.7: Bell curve for a 1200km link using NZ-DSF. Red circles: selected $P_{in}$ for the six reported configurations.

almost independent of the DGD. These results, valid for all tested combinations of distance/transmission fiber, are consistent with the results in [113]. Once these bell-curves were available, we chose for all the 36 combinations the value of $P_{in}$ to be used when estimating the $Q^2$-factor PDF. We select the $P_{in}$ that yields a $Q^2$-factor penalty (w.r.t the $Q^2$-factor at the NLT) of around 0.5-1dB in order to operate in the nonlinear regime, but close to realistic values of $P_{in}$. Also, given the selected power, we adjusted the NF of the equivalent amplifier at the receiver in order to work at $Q^2$-factors around 10-11dB; this was done to both work at practical $Q^2$-factor and to limit the computational time required by the simulations.

We compared three PMD emulation schemes which could be easily used in a laboratory: (**Tx case**) Place a multi-section PMD emulator at the transmitter. In this case the emulator could be accommodated within a dual stage booster along with the pre-compensating fibers, as in Fig. 3 (top). (**Loop case**) Place a multi-section emulator in the loop, such that the signal crosses it at each roundtrip. In this case the emulator

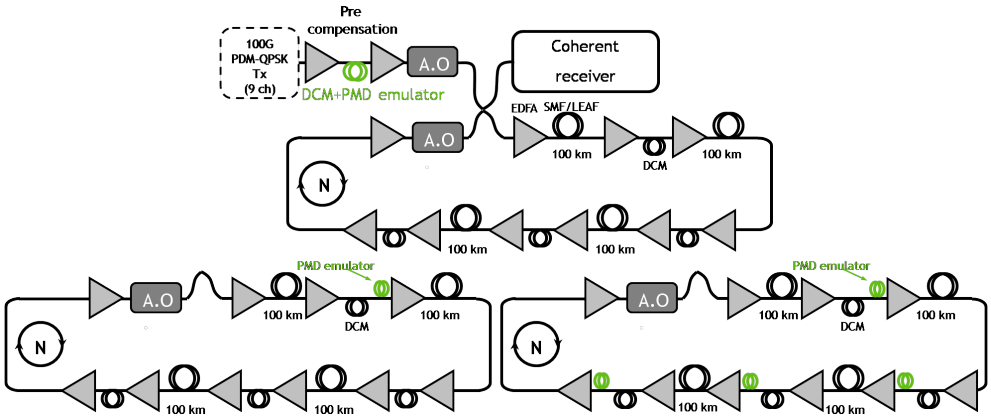


Figure 4.8: PMD emulator at the transmitter (top), one emulator trunk at each loop roundtrip (bottom, left) and one emulator trunk at each span (bottom, right).

could be placed either in a dual stage amplifier together with the compensating fiber (as in Fig. 3, bottom left) or, when no DM is used, in a dedicated dual stage with the power equalizer used to compensate for the amplifier gain profile. (**Span case**) Place a multi-section emulator in the dual stage amplifier at each span, along with the compensating fibers (Fig. 3, bottom right). These three schemes have an increasing complexity, but they also provide an increasing precision in catching the distributed effect of PMD/NL interaction. We want to derive some simple rules to understand when a certain complexity is "enough" for the system we want to study. We thus compared for each of the 36 considered configurations, the three proposed emulation schemes against the true case of distributed in-line PMD. Each multi-stage PMD emulator consisted of 10 randomly oriented waveplates. We simulated 500 random realizations of the PMD emulator settings at each evaluation of the $Q^2$-factor in order to estimate its PDF. For these tests we used a shorter pattern (256 symbols) in order to speed up the simulations [114].

Given the vast amount of tested cases, it would be impractical to present all the obtained PDF curves. We will summarize the most meaningful PDF trends with some examples provided in Figs. 4.9 and 4.10: (**a**) The larger the number of spans and/or

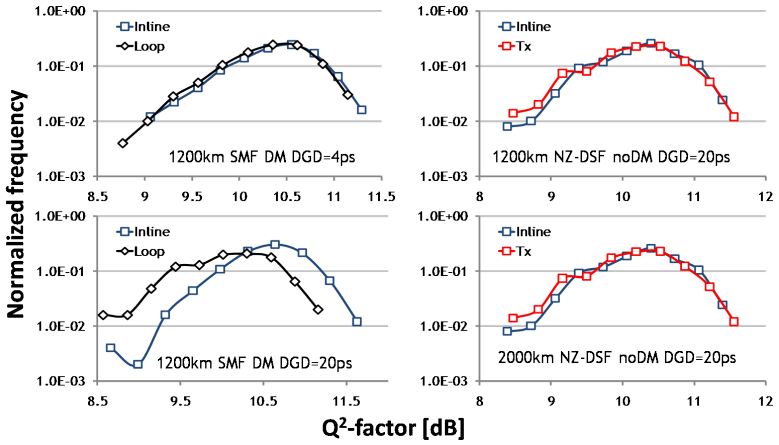


Figure 4.9: 1200km link, SMF, DM, DGD=4ps (top, left), 1200km link, NZ-DSF, noDM, DGD=20ps (top, right), 1200km link, SMF, DM, DGD=20ps (bottom, left), 2000km link, NZ-DSF, noDM, DGD=20ps (bottom, right).

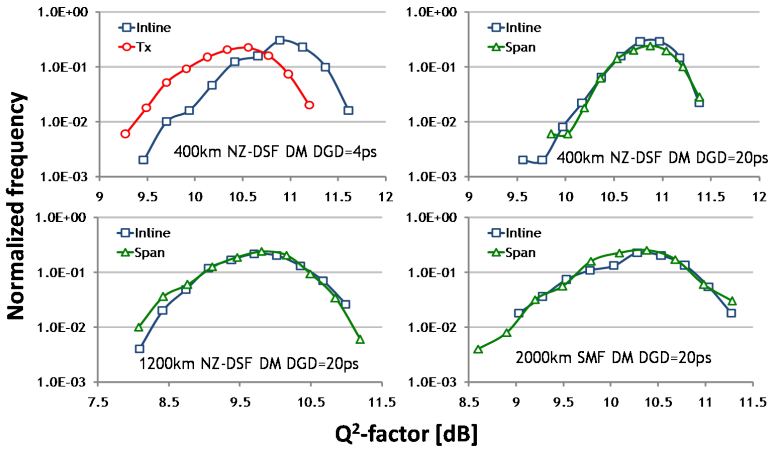


Figure 4.10: 400km link, NZ-DSF, DM, DGD=4ps (top left), 400km link, NZ-DSF, DM, DGD=20ps (top right), 1200km link, NZ-DSF, DM, DGD=20ps (bottom left), 2000km link, SMF, DM, DGD=20ps (bottom right).

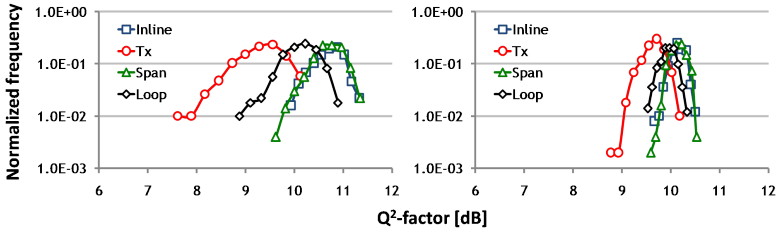


Figure 4.11: $Q^2$-factor PDF for 1200km DM NZ-DSF link with DGD=20ps, with (left) $P_{in}$=NLT and (right) $P_{in}$=NLT-2dB.

the PMD of the link are, the larger is the number of emulator sections needed to reproduce PMD in the system. Looking at Fig. 4.9 (left) it is clear that using one emulator section per loop is enough for a 1200km link of SMF fiber with DM and 4ps of DGD, but not for the same system with 20ps of DGD. This is quite intuitive since the PMD is spatially distributed and thus when it gets very large, it is necessary to increase the number of emulators in order to correctly account for its effects. (**b**) PMD emulation at the transmitter is always accurate for dispersion unmanaged systems (Fig. 4.9, right column). This is because here GVD largely dominates over PMD and thus a very simple emulation scheme is sufficient to provide accurate results. (**c**) When considering dispersion managed systems, PMD emulation at the transmitter is always inaccurate in all the considered tests, even on short links with a small amount of PMD (Fig. 4.10, top left). We conclude that when DM is present, PMD/NL has a clear impact and an accurate emulation scheme is required. (**d**) With DM, independently of the transmission fiber, also using one emulator at each loop round trip can lead to inaccurate PMD estimation for large values of DGD even for 1200km links (Fig. 4.9 bottom left). (**e**) The only emulation scheme that proved to be accurate and reliable in all the 36 tested configurations is the one using a PMD emulator at each span. If an increased complexity of the PMD emulation setup is acceptable, it guarantees precise estimation of the effect of PMD in a variety of link configurations (Fig. 4.10, right and bottom left).

To complete the analysis we tested the impact of two more parameters. First

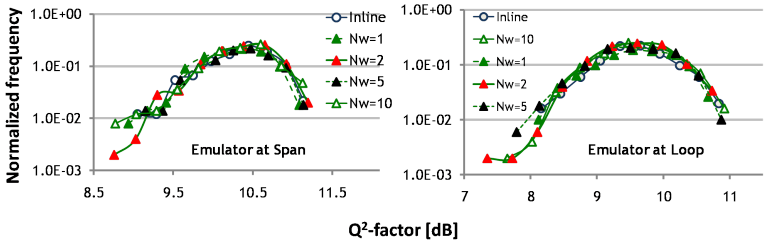


Figure 4.12: Impact of the number of waveplates per emulator for a 2000km DM link on SMF fiber with: (left) DGD=20ps, (one emulator per span): (right) DGD=4ps, (one emulator per loop, right).

we verified that our conclusions hold also at lower values of $P_{in}$. In fact, we tested our system using a $P_{in}$ larger than the NLT to enhance the PMD/NL interactions, but it is interesting to confirm that our results are also valid at the NLT or even at lower powers. Fig. 4.11 shows results for a 1200km, NZ-DSF system with DM and DGD=20ps, for two different input powers. On the left $P_{in}$=NLT, while on the right $P_{in}$=NLT-2dB. In both cases the conclusion that neither an emulator at the Tx, nor one per loop are enough to emulate the NL/PMD interactions (cfr. Fig. 4.9, bottom, left for SMF) holds at the NLT and is still valid at lower powers. Another test is to consider the impact of the number of waveplates at each emulator on the PDF. We decided to use 10 waveplates per emulator in our simulations in order to reproduce higher order PMD. However it would be very interesting to use just one PMF, i.e. one waveplate with a given DGD, to reduce the hardware. Fig. 4.12 shows results with a variable number of waveplates ($N_w$=1, 2, 5, 10) for a 2000km DM link on SMF fiber, with DGD=20ps, and one emulator at each span (left plot) and with DGD=4ps, and one emulator at each loop. In both cases using a single waveplate is equivalent to the use of an emulator with 10 waveplates. We thus understand that the PMD/NL interaction in each fiber span is dominated by 1st order PMD.

## 4.3 Conclusions

In this chapter we have compared the performance of single-carrier and dual-carrier PDM-QPSK at 100Gb/s both in back-to-back after narrow optical filtering and when co-propagating over 800km of NZ-DSF in single channel and with 10Gb/s and 40Gb/s neighbors. In back-to-back we found that the single-carrier optical solution is more tolerant against the filtering impairments of typical optical networks. After propagation in single channel configuration, the maximum $Q^2$-factor is 1dB better for SC than DC. Neighboring 40Gb/s P-DPSK channels induce a limited penalty of around 1dB in both configurations. When co-propagating with 10Gb/s channels, the DC solution is slightly more impacted. We thus conclude that SC is not only more tolerant to linear filtering than DC, but also that it is more tolerant to intrachannel nonlinear effects and to XPM induced by 10Gb/s OOK modulated channels.

We also analyzed different solutions to emulate PMD/NL interaction in 100Gb/s PDM-QPSK systems using numerical simulations. We showed that the optimal emulation scheme depends on many factors such as transmission fiber, dispersion map, total distance, and DGD, and should be carefully selected to avoid wrong performance estimation. As a general rule, when using dispersion management, a PMD emulator should be placed at least at each loop roundtrip. For large values of DGD this is insufficient and an emulator should be placed at every span. With noDM, the effect of PMD is minor due to the extremely large cumulated dispersion. Placing the emulator at the transmitter assures correct emulation of the PMD in all the tested cases. The same conclusions still apply when using input powers around the NLT. The number of waveplates per emulator can be reduced to 1 (PMF fiber), since the PMD/NL is dominated by 1st order PMD.

# Chapter 5

# 40Gb/s and 100Gb/s undersea coherent optical communication systems

In this section we will discuss the benefits brought by coherent detection to submarine transmission systems at 40Gb/s and 100Gb/s. We will start from an introduction to state of the art 40Gb/s PDM-BPSK-based systems, then we will report recent results obtained comparing RZ carving schemes for 40Gb/s undersea transmission and finally will present the results of a recent experiment regarding 100Gb/s submarine systems [42].

## 5.1 Undersea coherent communications: present and perspectives

Today commercial submarine optical transmission systems are mostly based on 10Gb/s OOK channels, with a channel count as high as 100 (using C/C+ band) for the systems with highest capacity. The maximum capacity per fiber in undersea communications is thus around 1Tb/s. 10Gb/s OOK channels provide a good tolerance to

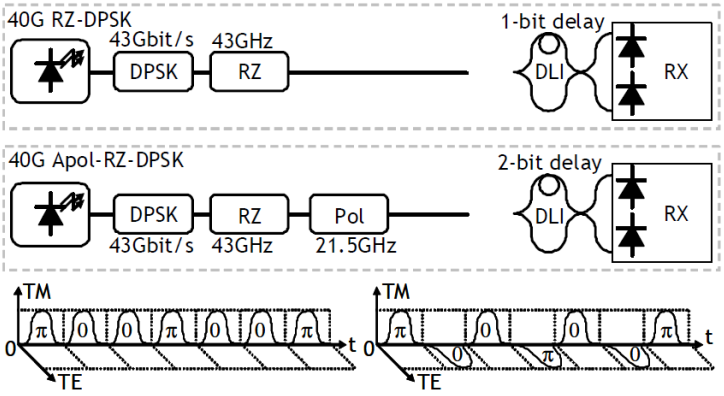


Figure 5.1: Tx/RX scheme for RZ-DPSK (top) and APol-RZ-DPSK (top) modulation formats at 43.7Gb/s. Diagrams showing the effect of the alternate polarization on the optical power (bottom).

noise, allowing both transatlantic (∼6300km) and transpacific (∼9000km) transmissions. Moreover these systems have a very limited complexity of both transmitter and receiver, which reduces the costs and simplifies the maintenance. Recently, DPSK has been introduced [115] at 10Gb/s; thanks to its increased tolerance to noise (3dB better sensitivity when using balanced detection), DPSK allows to increase the reach of a system or the span length, thus reducing the number of installed amplifiers in a system.

In order to further improve the total capacity of an installed system, two approaches are possible. It is possible to extend the bandwidth of the amplifiers to the L band, enabling a larger number of channels (up to around 200). However C+L band EDFA amplifiers pose serious issues in undersea communications because of the large power consumption of such devices and of the increased complexity. Another approach is to increase the spectral efficiency of the system. Again, this can be achieved either reducing the channel spacing without altering the bitrate of every single channel (es. 10Gb/s channels at 25GHz spacing) or increasing the bitrate to 40Gb/s per channel.

In 2004, alternate polarization RZ-DPSK (APol-RZ-DPSK) has been propsed as a candidate for 40Gb/s transmissions. Fig. 5.1 (top) shows the transmitter and receiver schemes of standard RZ-DPSK and of Apol-RZ-DPSK. In the first case a 43Gb/s Mach-Zehnder modulator generates a DPSK signal and a following RZ pulse carver driven by a 43GHz clock generates RZ pulses. At the receiver side a 1-bit delay line interferometer (DLI) feeds two balanced photodiodes. In the Apol-RZ-DPSK case there is one more modulator, which generates bit-to-bit changes in the state of polarization. This GaAs based polarization modulator, fed by a half bit-rate clock (21.7GHz), is precisely tuned in order to force orthogonal states of polarization in adjacent bits. For this reason at the receiver side a 2-bit DLI is needed and a specific encoding should be used. The diagrams at the bottom of Fig. 5.1 represent the optical power versus time for both TE and TM polarization states. On the right side it is reported the standard RZ-DPSK and on the left side the Apol. It can be noticed the narrow shape of optical pulses performed by the pulse carver and the fact that the state of polarization of two adjacent bits is always orthogonal. This property will enhance the tolerance to nonlinear effects as it will be shown in the results.

These modulation formats have been tested [116] in a recirculating 510km-long loop made of +D/-D/+D UltraWave fibre and all-Raman amplification with backward pumping. Fig. 5.2 (top) shows the $Q^2$-factor for all the channels with Apol-RZ-DPSK modulation format at 9180km (18 loop rountrip), where they are all greater than 11.5dB, and 11220km (22 loop rountrip), where the worst channel measures 9.9dB of $Q^2$-factor. In Fig. 5.2 (bottom) the power of a single channel is varied in order to test the nonlinear threshold for both modulation formats. APol system outperforms traditional DPSK transmission by more than 2dB in term of maximum $Q^2$-factor. Even if 40Gb/s Apol- RZ-DPSK has an excellent reach, it has a moderate spectral efficiency because it requires 100GHz channel spacing. A system with 10Gb/s per channel with 25GHz spacing would have the same spectral efficiency [117].

It is clear that without any improvement in spectral efficiency, 40Gb/s undersea systems are not sustainable from an economic point of view. This is the reason why, eve if the technology is available since 2004, no commerical 40Gb/s systems have yet been deployed. In the last couple of years, however, the revamp of coherent de-

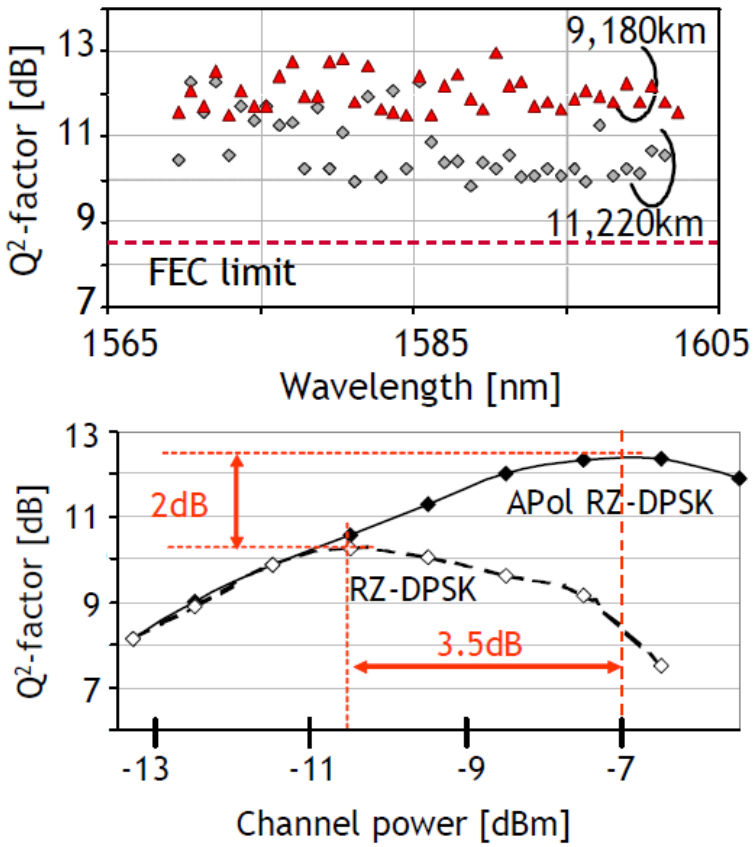


Figure 5.2: $Q^2$-factor after 9180km (with margins) and 11220km (without margins) for all 40 channels(top) with Apol RZ-DPSK. Comparison between Apol-RZ-DPSK and RZ-DPSK (bottom).

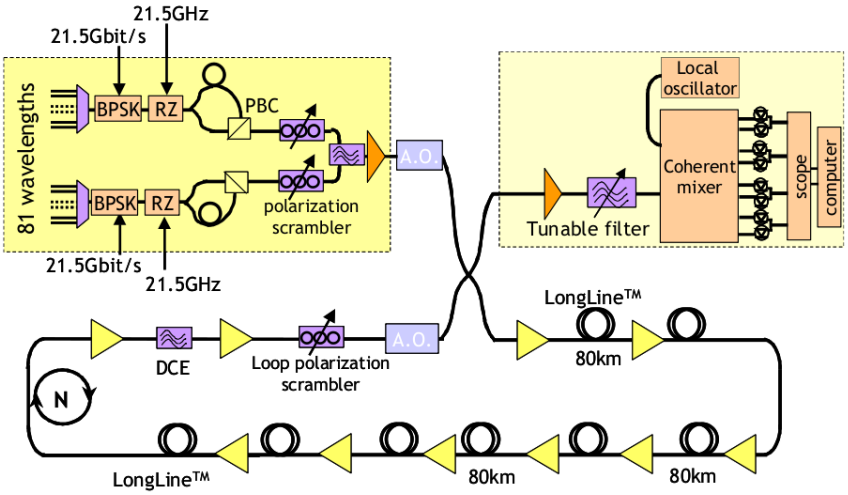


Figure 5.3: Experimental set-up of the 640km long recirculating [courtesy of G. Charlet].

tection opened new perspectives for 40Gb/s submarine transmission. In 2008 for the first time a transpacific transmission 8960 was demonstrated at 40GHz, with 50GHz spacing and EDFA only amplification (the use of Raman in submarine systems still poses huge challenges due to the lerge number of required pumps), using PDM-BPSK modulation format [41].

In this experiment (whose test-bed depicted in Fig. 5.3 eighty-one lasers spanning over a 50GHz frequency grid and split into two 100GHz-spaced sub-combs of odd and even channels were involved. Each sub-comb passed into a Mach-Zehnder Modulator driven at 21.5Gbit/s, including 7% overhead for forward error-correction emulation, and fed with $2^{15}$ -1-bit PRBS. The output light was sent into a pulse carver in order to generate 21Gb/s RZ-BPSK optical data and finally polarization multiplexing was emulated splitting the signal into two copies, one of them being delayed by approximately 100 bits with respect to the other, before being recombined into a PBC to yield 43Gb/s RZ-PDM-BPSK channels. The resulting multiplex was sent over a recirculating loop composed of eight 80km-long spans of Draka LongLine fiber ($\alpha$ ~0.184 dB/km, $A_{eff}$ ~120$\mu$m$^2$. Standard, 980nm-pumped, single-stage, subma-

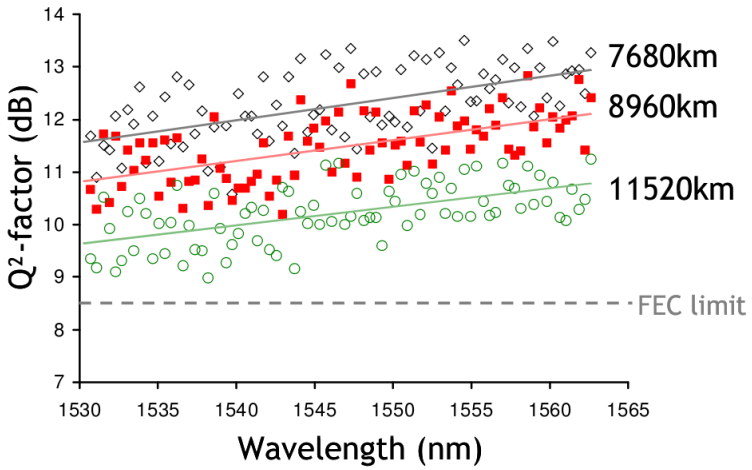


Figure 5.4: $Q^2$-factor, from BER measurements, of 81 channels at 7,680km (open diamonds), 8,960km (red full squares) and 11,520km (circles) [courtesy of G. Charlet].

rine EDFAs with 17dBm output power were used to compensate for each span loss. At the receiver side, the signal was sent to the coherent receiver that used digital signal processing for discriminating the phase/polarisation states but also for compensating the large cumulated chromatic dispersion (up to 230,000ps/nm).

Three distances were considered, 7680km, 8960km and 11,520km, respectively (see Fig.5.4). Slightly better BERs were observed in the upper part of the wavelength band than in the lower part ($\sim$1dB tilt), due to the poorer noise figure of the EDFAs and also to the slightly higher fibre attenuation in the lower part of the C-Band. After 8960km, the transmission didn't have enough margin (minimum $Q^2$-factor was around 10dB), but still it proved the feasibility of submarine trasmission at 40Gb/s over a 50GHz grid for the first time.

What is very interesting of this experiment is that it clearly highlights the moltitude of benefits enabled by coherent reception: first of all, PDM-BPSK has a better sensitivity than DPSK and thus it allows to extend the reach of a system. But more important, coherent reception coupled with DSP processing allows to redisign the transmission link, introducing several improvements:

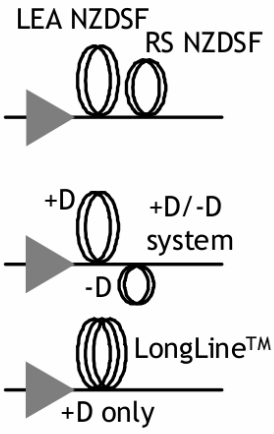


| Average loss | Length | NLP |
|---|---|---|
| 0.20dB /km | 75 km | $\Phi_0$ |
| 0.20dB/km | 75 km | 0.78 $\Phi_0$ |
| 0.185dB/km | 80 km | 0.55 $\Phi_0$ |

Figure 5.5: Average loss, length and relative nonlinear phase (NLP) of a 15dB span of NZDSF, DSMF, and LongLine.

- The absence of dispersion compensation makes possible the use of single stage EDFA amplifiers, and thus the noise figure of every amplifier can be reduced of around 0.5-1dB with respect to dual-stage amplifiers. As a consequence the received OSNR is improved of the same quantity
- Dispersion unmanaged links where shown to be very effective in improving the tolerance of the signal to nonlinear distortions, thus improving the NLT of the system and allowing to transmit larger powers [118].
- The digital post-compensation of the chromatic dispersion makes possible the use of spans composed of positive dispersion fibres only, taking full benefit of their excellent qualities.

Expecially the last point is a major advance brought by DSP-based compensation of the GVD. To better understand the importance of this tecnological advance, consider Fig. 5.5, where the average loss, the length and the nonlinear phase of three different kinds of fibre: NZ-DSF, dispersion slope matched fiber (DSMF, a fiber com-

monly used in undersea systems), and LongLine are reported for a hypothetical span of 15dB. The total cumulated nonlinear phase over LongLine is 1.5dB less than the one of a traditional DSMF based system while span length can increase by 5km. This means that LongLine can support higher power levels than traditional submarine fibers and at the same time allows to reduce the number of repeaters in the link. Large effective area fibres are still under heavy development and could futher improve in few years, becoming a must-have component for going towards 40Gbit/s or even 100Gbit/s trans-oceanic systems.

## 5.2 Undersea 100Gb/s PDM-QPSK transmissions

The first submarine cable using optical amplification was designed to operate with a single channel at 5Gb/s and was installed in 1995. In the meantime, experiments in the labs started to highlight the benefits of WDM, also at 5Gb/s, with a growing number of channels, while the channel spacing was gradually reduced. However, the first commercial cable using WDM was deployed with channels only at 2.5Gb/s. Almost simultaneously, the first 10Gb/s WDM transmissions were reported in the labs, but the first commercial system of this kind was laid only in 2000. Three years later, data at Nx40Gb/s were sent over a transoceanic distance for the first time in a loop testbed. Nonetheless, no cable operating at 40Gb/s have been announced yet, even if the achievable information spectral density already seems higher at 40Gb/s than at 10Gb/s. The highest information spectral density reported to date at distances in excess of 6000km was 0.65bit/s/Hz [119] at 10Gb/s channel rate and 0.8bit/s/Hz at 40Gb/s [41, 120],respectively.

In this section we describe the first WDM transmission using 100Gb/s channel rate over a transoceanic distance. The main motivation for migrating to 100Gb/s is to increase the total capacity, which implies to achieve a high information spectral density, i.e. the data rate in a given spectral band, expressed in bit/s/Hz. To achieve such a high bitrate we use PDM-QPSK-modulation and coheret reception. Our 72 100Gb/s-channels (7.2Tb/s total capacity) are packed along a 50GHz channel grid, which represents an information spectral density of 2bit/s/Hz for the system, i.e. 2.5

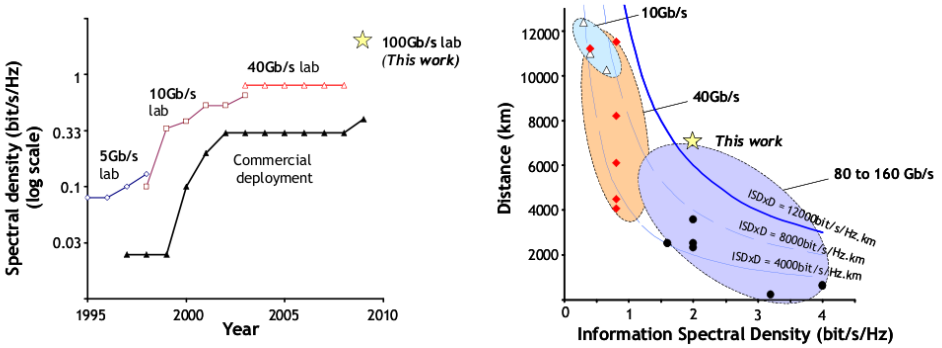


Figure 5.6: Evolution of information spectral density of undersea links in the laboratories (over 6000km) and in commercial systems (left); Distance versus information spectral density of WDM lab transmissions with more than 1Tbit/s capacity (right).

times more than the best result at 40Gb/s and 5 times more than in the commercial submarine cables relying on 10Gb/s technology. Fig. 5.6 depicts the evolution of spectral density in submarine systems over the last 15 years and the distance vs. information spectral density of WDM lab experiments with more than 1Tb/s of capacity.

The experimental test-bed is schematized in Fig. 5.7. It involved 72 DFB lasers, ranging from 1535.25nm to 1562.64nm spaced 50GHz apart, which were combined into two spectrally-interleaved wavelength combs. The two combs were passed into two separate QPSK modulators, fed with $2^{15}$-1 bit-long sequences at 28Gb/s, assuming 7% FEC overhead. The output from each modulator was split along two PMF paths. The QPSK data along one path were delayed by hundreds of symbols, before being polarization-multiplexed with the QPSK data along the other path through a PBC, to produce PDM-QPSK channels at 112Gbit/s. The odd and even channels were then spectrally interleaved through a 50GHz interleaver, boosted through a dual-stage amplifier before being injected into the recirculating loop.

The loop consisted of eight 80km-long spans of LongLine fiber, characterized by 120$\mu$m$^2$ effective area, 0.184dB/km loss, polarization mode dispersion (PMD) value below 0.04ps/km, and was free of any dispersion-compensating fiber. The fiber

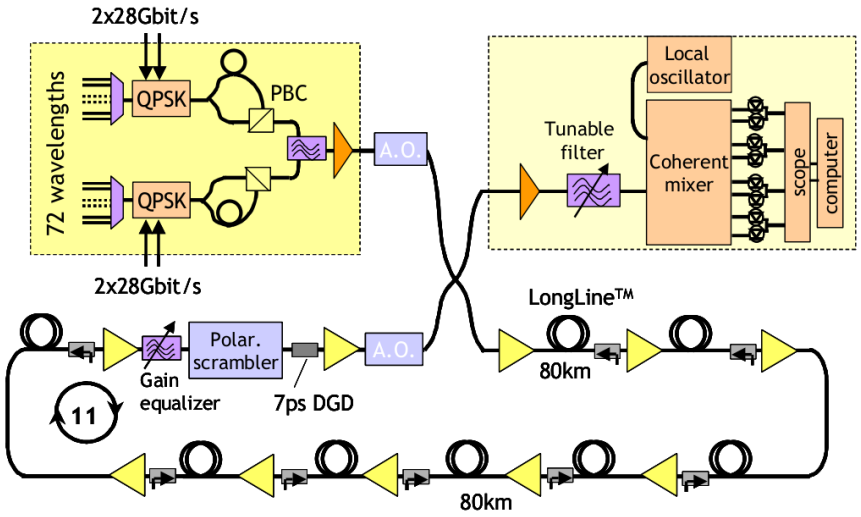


Figure 5.7: Experimental loop set-up depicting the transmitter based on 72x100Gb/s channel, a 8-span recirculating loop incorporating hybrid Raman-Erbium amplifiers, a dynamic gain equalizer and a loop synchronous polarization scrambler, and the coherent receiver.

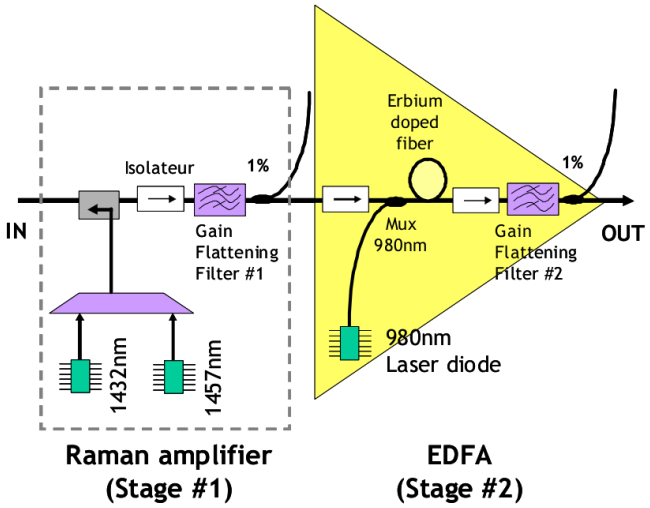


Figure 5.8: Schematic of a line optical repeater using hybrid Raman-Erbium amplification.

spans were separated by 980nm-pumped EDFAs, assisted by Raman pre-amplifiers. Each Raman pre-amplifier was designed to provide ∼10dB on-off gain, thanks to 600mW backward-injected power at wavelengths 1432nm and 1457nm, as schematized in Fig. 5.8. It was spliced to the next EDFA through a gain-flattening filter (GFF), while the EDFA was spliced to the following fiber section through another GFF. Both GFFs were used to equalize the power distribution across the multiplex. Further power adjustment was performed thanks to a dynamic gain equalizer (DGE), inserted at the end of the recirculating loop. The loop also incorporated a loop polarization scrambler and a polarization maintaining fiber with 7ps DGD, such that the cumulated PMD (or mean DGD) after 11 round trips was ∼23ps, i.e. much larger than commonly found in submarine links. At the receiver end, each channel could be isolated from the rest of the multiplex by a tunable filter, and sent to the coherent receiver. The electrical waveforms were sampled, digitized and stored by sets of 2Msamples. They were then processed off-line in a computer, for re-sampling at 2 samples/symbol (56Gsamples/s), digital chromatic dispersion compensation, po-

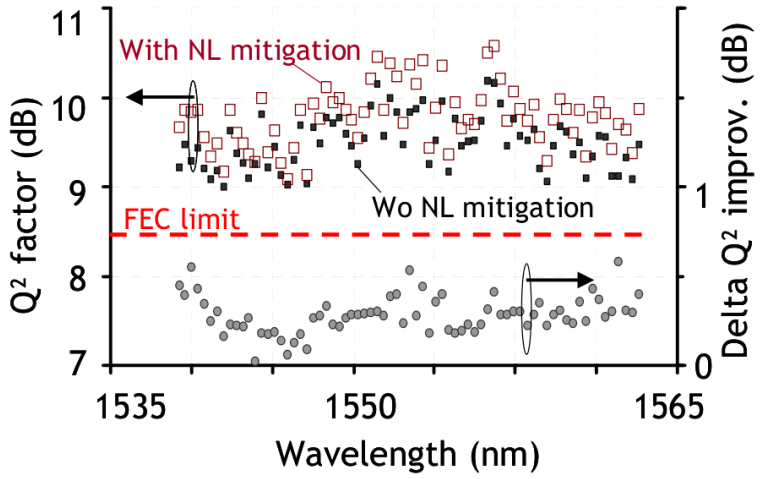


Figure 5.9: Measured $Q^2$-factor of the 72 channels at 7040km without nonlinearity mitigation algorithm (top dark point), with non linear mitigation algorithm (top white square). $Q^2$-factor improvement due to nonlinearity mitigation (bottom grey disk, right scale).

larization demultiplexing, equalization, and carrier-phase estimation/subtraction. All chromatic dispersion accumulated within the transmission was digitally compensated by using a 1500 taps FIR filter.

The BERs of all channels were measured and converted into $Q^2$-factors. The $Q^2$-factors of the 72 channels are plotted in Fig. 5.9. The average $Q^2$-factor is 9.4dB, while the best is 10.2dB. The worst performing channel still has 9.0dB $Q^2$-factor, i.e. 0.5dB above the limit yielding $10^{-13}$ BER after correction, assuming today's commercial 10Gb/s FEC techniques with 7% overhead. In order to improve the transmission performance, we next investigated the benefits of performing digital non linear mitigation using an inverse, backward-propagation, SSFM algorithm [121], instead of dispersion compensation. The algorithm used eighty-eight steps, as many as the transmission spans. In each step, chromatic dispersion was first compensated, then Kerr non linearity was mitigated (based on a scalar, single-channel approach), from the last span to the first span successively. With this scheme, the receiver algorithm

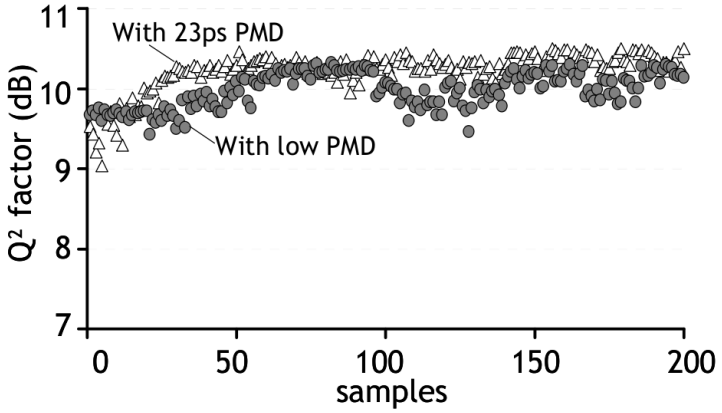


Figure 5.10: $Q^2$-factor fluctuations recorded at 1545.72nm with (white triangle) and without (grey disk) 7ps DGD element inserted, at 6400km.

complexity was considerably increased and practical implementation would be complex. Note that here, the algorithm was applied to a polarization multiplexed signal and not to a singly polarized channel as in [121]. The $Q^2$-factors improvement was measured for all channels and is shown in Fig. 5.9, too. It is relatively moderate, from 0.03dB to 0.58dB. The mean improvement is 0.26dB, probably not worth the extra receiver complexity.

Insight on the $Q^2$-factors (dB) stability is given in Fig. 5.10. At wavelength 1545.72nm, two hundred successive waveforms of 2 million bits were recorded after 6400km and processed independently. We voluntarily used low speed (<1KHz) in-loop asynchronous polarization scrambling such that, across the 40$\mu$s-long waveforms, the PMD/polarization-dependent loss conditions almost do not change, while they change significantly from one recorded waveform to the next. The measurements were performed twice, with and without the 7ps DGD element in the loop, respectively. The $Q^2$-factors fluctuations are slightly larger when DGD is inserted, as depicted in Fig 5.10. However, we believe that $Q^2$-factors fluctuations should be primarily attributed to polarization-dependent loss and loop-specific effects,rather than

to the PMD itself.

## 5.3 Conclusions

In this chapter we discussed the impact of coherent reception on submarine transmissions. We described the advantages of coherent systems with respect to traditional directly detected systems in ultralong haul submarine links and analyzed the enabling techniques behind this improvement. Then we reported an experimental demonstration of the first submarin transmission at 100Gb/s per channel.

Submarine 100Gb/s transmissions are possible with current technology, as demonstrated by other test like [45, 122], but require the use of Raman aplification and a DSP processor at the receiver able to compensate the total dispersion of the link. For this reasons, 100Gb/s transmission over such long links are not still commercially available and will require years of further tests and researches before they will be ready for the deployment.

# Bibliography


[1] E. Desurvire, "Capacity demand and technology challenges for lightwave systems in the next two decades," *J. Lightw. Technol.*, vol. 24, no. 12, pp. 4697–4710, Dec. 2006.

[2] P. J. Winzer and R.-J. Essiambre, "Advanced modulation formats for high-capacity optical transport networks," *J. Lightw. Technol.*, vol. 24, no. 12, pp. 4711–4728, Dec. 2006.

[3] A. Gnauck, X. Liu, X. Wei, D. Gill, and E. Burrows, "Comparison of modulation formats for 42.7-Gb/s single-channel transmission through 1980 km of SSMF," *IEEE Photon. Technol. Lett.*, vol. 16, no. 3, pp. 909–911, Mar. 2004.

[4] S. Bigo, G. Charlet, and E. Corbel, "What has hybrid phase/intensity encoding brought to 40Gbit/s ultralong-haul systems," in *Proc. European Conference on Optical Communications ECOC 2004*, Stockholm, Sweden, paper Th2.5.1, 2004.

[5] A. Gnauck and P. Winzer, "Optical phase-shift-keyed transmission," *J. Lightw. Technol.*, vol. 23, no. 1, pp. 115–130, Jan. 2005.

[6] R. Griffin, R. Johnstone, R. Walker, J. Hall, S. Wadsworth, K. Berry, A. Carter, M. Wale, J. Hughes, P. Jerram, and N. Parsons, "10 Gb/s optical differential quadrature phase shift key (DQPSK) transmission using GaAs/AlGaAs integration," in *Proc. Conference on Optical Fiber Communication OFC 2002*, Anaheim, CA, USA, paper FD6-3, 2002.

[7] H. Kim and R.-J. Essiambre, "Transmission of 8x20 Gb/s DQPSK signals over 310-km SMF with 0.8-b/s/Hz spectral efficiency," *IEEE Photon. Technol. Lett.*, vol. 15, no. 5, pp. 769–771, May 2003.

[8] G. P. Agrawal, *Fiber-optic communication systems*, 3rd ed. Wiley&Sons, 2002.

[9] G. J. Milburn, M. D. Levenson, R. M. Shelby, S. H. Perlmutter, R. G. DeVoe, and D. F. Walls, "Optical-fiber media for squeezed-state generation," *J. Opt. Soc. Am. B*, vol. 4, no. 10, pp. 1476–1489, Oct. 1987.

[10] H. A. Haus and Y. Lai, "Quantum theory of soliton squeezing: a linearized approach," *J. Opt. Soc. Am. B*, vol. 7, no. 3, pp. 386–392, Mar. 1990.

[11] G. P. Govind P. Agrawal, *Nonlinear fiber optics*. New York: Academic, 2001.

[12] J. Leibrich, C. Wree, and W. Rosenkranz, "CF-RZ-DPSK for suppression of XPM on dispersion-managed long-haul optical WDM transmission on standard single-mode fiber," *IEEE Photon. Technol. Lett.*, vol. 14, no. 2, pp. 155–157, Feb. 2002.

[13] X. Liu, "Nonlinear effects in phase shift keyed transmission," in *Proc. Conference on Optical Fiber Communication OFC 2004*, Los Angeles, CA, USA, paper ThM4, 2004.

[14] J. P. Gordon and L. F. Mollenauer, "Phase noise in photonic communications systems using linear amplifiers," *Opt. Lett.*, vol. 15, no. 23, pp. 1351–1353, Dec. 1990.

[15] K.-P. Ho, "Probability density of nonlinear phase noise," *J. Opt. Soc. Am. B*, vol. 20, no. 9, pp. 1875–1879, Sept. 2003.

[16] ——, "Statistical properties of nonlinear phase noise," *ArXiv Physics eprints*, Mar. 2003.

[17] P. Serena, A. Orlandini, and A. Bononi, "Parametric-gain approach to the analysis of single-channel DPSK/DQPSK systems with nonlinear phase noise," *J. Lightw. Technol.*, vol. 24, no. 5, pp. 2026–2037, May 2006.

[18] H. Kim and A. Gnauck, "Experimental investigation of the performance limitation of DPSK systems due to nonlinear phase noise," *IEEE Photon. Technol. Lett.*, vol. 15, no. 2, pp. 320–322, Feb. 2003.

[19] T. Mizuochi, K. Ishida, T. Kobayashi, J. Abe, K. Kinjo, K. Motoshima, and K. Kasahara, "A comparative study of DPSK and OOK WDM transmission over transoceanic distances and their performance degradations due to nonlinear phase noise," *J. Lightw. Technol.*, vol. 21, no. 9, pp. 1933–1943, Sept. 2003.

[20] T. Okoshi, "Recent advances in coherent optical fiber communication systems," *J. Lightw. Technol.*, vol. 5, no. 1, pp. 44–52, Jan 1987.

[21] T. Kimura, "Coherent optical fiber transmission," *J. Lightw. Technol.*, vol. 5, no. 4, pp. 414–428, Apr 1987.

[22] T. Okoshi and K. Kikuchi, *Coherent Optical Fiber Communications*. Boston: Kluwer Academic.

[23] R. Linke and A. Gnauck, "High-capacity coherent lightwave systems," *J. Lightw. Technol.*, vol. 6, no. 11, pp. 1750–1769, Nov. 1988.

[24] P. S. Henry and S. D. Persoinick, *Coherent Lightwave Communications*. Piscataway, NJ: IEEE Press, 1990.

[25] S. Betti, G. de Marchis, and E. Iannone, *Coherent Optical Communication Systems*. New York: Wiley, 1995.

[26] T. Hodgkinson, R. Harmon, and D. Smith, "Demodulation of optical DPSK using in-phase and quadrature detection," *Electron. Lett.*, vol. 21, no. 19, pp. 867–868, Sept. 1985.

[27] A. Davis, M. Pettitt, J. King, and S. Wright, "Phase diversity techniques for coherent optical receivers," *J. Lightw. Technol.*, vol. 5, no. 4, pp. 561–572, Apr. 1987.

[28] L. Kazovsky, "Phase- and polarization-diversity coherent optical techniques," *J. Lightw. Technol.*, vol. 7, no. 2, pp. 279–292, Feb. 1989.

[29] A. Kersey, A. Yurek, A. Dandridge, and J. Weller, "New polarisation-insensitive detection technique for coherent optical fibre heterodyne communications," *Electronics Letters*, vol. 23, no. 18, pp. 924–926, Aug. 1987.

[30] T. Okoshi and Y. Cheng, "Four-port homodyne receiver for optical fibre communications comprising phase and polarisation diversities," *Electron. Lett.*, vol. 23, no. 8, pp. 377–378, Apr. 1987.

[31] B. Glance, "Polarization independent coherent optical receiver," *J. Lightw. Technol.*, vol. 5, no. 2, pp. 274–276, Feb. 1987.

[32] S. Tsukamoto, D.-S. Ly-Gagnon, K. Katoh, and K. Kikuchi, "Coherent demodulation of 40-Gbit/s polarization-multiplexed QPSK signals with 16-GHz spacing after 200-km transmission," in *Proc. Conference on Optical Fiber Communication OFC 2005*, Anaheim, CA, USA, paper PDP29, 2005.

[33] D.-S. Ly-Gagnon, S. Tsukamoto, K. Katoh, and K. Kikuchi, "Coherent detection of optical quadrature phase-shift keying signals with carrier phase estimation," *J. Lightw. Technol.*, vol. 24, no. 1, pp. 12–21, Jan. 2006.

[34] J. Renaudier, G. Charlet, M. Salsi, O. Pardo, H. Mardoyan, P. Tran, and S. Bigo, "Linear fiber impairments mitigation of 40-Gbit/s polarization-multiplexed QPSK by digital processing in a coherent receiver," *J. Lightw. Technol.*, vol. 26, no. 1, pp. 36–42, Jan. 2008.

[35] C. Laperle, B. Villeneuve, Z. Zhang, D. McGhan, H. Sun, and M. O'Sullivan, "WDM performance and PMD tolerance of a coherent 40-Gbit/s dual-polarization QPSK transceiver," *J. Lightw. Technol.*, vol. 26, no. 1, pp. 168–175, Jan. 2008.

[36] K. Roberts, M. O'Sullivan, K.-T. Wu, H. Sun, A. Awadalla, D. Krause, and C. Laperle, "Performance of dual-polarization QPSK for optical transport systems," *J. Lightw. Technol.*, vol. 27, no. 16, pp. 3546–3559, Aug. 2009.

[37] J. Renaudier, G. Charlet, B. Pardo, H. Mardoyan, P. Tran, M. Salsi, and S. Bigo, "Experimental analysis of 100Gb/s coherent PDM-QPSK long-haul transmission under constraints of typical terrestrial networks," in *Proc. European Conference on Optical Communication ECOC 2008*, Bruxelles, Belgium, paper Th.2.A.3, 2008.

[38] M. Alfiad, M. Kuschnerov, T. Wuth, T. Xia, G. Wellbrock, E.-D. Schmidt, D. van den Borne, B. Spinnler, C. Weiske, E. de Man, A. Napoli, M. Finkenzeller, S. Spaelter, M. Rehman, J. Behel, M. Chbat, J. Stachowiak, D. Peterson, W. Lee, M. Pollock, B. Basch, D. Chen, M. Freiberger, B. Lankl, and H. de Waardt, "111-gb/s transmission over 1040-km field-deployed fiber with 10G/40G neighbors," *IEEE Photon. Technol. Lett.*, vol. 21, no. 10, pp. 615–617, May 2009.

[39] M. Alfiad, D. van den Borne, S. Jansen, T. Wuth, M. Kuschnerov, G. Grosso, A. Napoli, and H. de Waardt, "111-gb/s POLMUX-RZ-DQPSK transmission over LEAF: Optical versus electrical dispersion compensation," in *Proc. Conference on Optical Fiber Communication OFC 2009*, San Diego, CA, USA, paper OThR4, 2009.

[40] G. Charlet, J. Renaudier, H. Mardoyan, P. Tran, O. Pardo, F. Verluise, M. Achouche, A. Boutin, F. Blache, J.-Y. Dupuy, and S. Bigo, "Transmission of 16.4-bit/s capacity over 2550 km using PDM-QPSK modulation format and coherent receiver," *J. Lightw. Technol.*, vol. 27, no. 3, pp. 153–157, Feb. 2009.

[41] G. Charlet, M. Salsi, H. Mardoyan, P. Tran, J. Renaudier, S. Bigo, M. Astruc, P. Sillard, L. Provost, and F. Cerou, "Transmission of 81 channels at 40Gbit/s over a transpacific-distance erbium-only link, using PDM-BPSK modulation, coherent detection, and a new large effective area fibre." in *Proc. European*

*Conference on Optical Communication ECOC 2008*, Bruxelles, Belgium, paper Th.3.E.3, 2008.

[42] G. Charlet, M. Salsi, P. Tran, M. Bertolini, H. Mardoyan, J. Renaudier, O. Bertran-Pardo, and S. Bigo, "72&00gb/s transmission over transoceanic distance, using large effective area fiber, hybrid Raman-Erbium amplification and coherent detection," in *Proc. Conference on Optical Fiber Communication OFC 2009*, San Diego, CA, USA, paper PDPB6, 2009.

[43] A. Sano, E. Yamada, H. Masuda, E. Yamazaki, T. Kobayashi, E. Yoshida, Y. Miyamoto, R. Kudo, K. Ishihara, and Y. Takatori, "No-guard-interval coherent optical OFDM for 100-Gb/s long-haul WDM transmission," *J. Lightw. Technol.*, vol. 27, no. 16, pp. 3705–3713, Aug. 2009.

[44] S. Chandrasekar, X. Liu, B. Zhu, and D. W. Peckham, "Transmission of a 1.2-Tb/s 24-carrier no-guard-interval coherent OFDM superchannel over 7200-km of ultra-large-area fiber," in *Proc. European Conference on Optical Communication ECOC 2009*, Wien, Austria, paper PD2.6, 2009.

[45] M. Salsi, H. Mardoyan, P. Tran, C. Koebele, E. Dutisseuil, G. Charlet, and S. Bigo, "155x100Gbit/s coherent PDM-QPSK transmission over 7,200km," in *Proc. European Conference on Optical Communication ECOC 2009*, Wien, Austria, paper PD2.5, 2009.

[46] P. Winzer and A. Gnauck, "112-Gb/s polarization-multiplexed 16-QAM on a 25-GHz WDM grid," in *Proc. European Conference on Optical Communication ECOC 2008*, Bruxelles, Belgium, paper Th.3.E.5, 2008.

[47] X. Zhou, J. Yu, M. Huang, Y. Shao, T. Wang, P. Magill, M. Cvijetic, L. Nelson, M. Birk, G. Zhang, S. Y. Ten, H. B. Matthew, and S. K. Mishra, "32Tb/s (320x114Gb/s PDM-RZ-8QAM transmission over 580km of SMF-28 ultra-low-loss fiber," in *Proc. Conference on Optical Fiber Communication OFC 2009*, San Diego, CA, USA, paper PDPB4, 2009.

[48] A. H. Gnauck, P. J. Winzer, C. R. Doerr, and L. L. Buhl, "10x112-Gb/s PDM-16-QAM transmission over 630km of fiber with 6.2-b/s/Hz spectral efficiency," in *Proc. Conference on Optical Fiber Communication OFC 2009*, San Diego, CA, USA, paper PDPB8, 2009.

[49] H. Sun, K.-T. Wu, and K. Roberts, "Real-time measurements of a 40 Gb/s coherent system," *Opt. Express*, vol. 16, no. 2, pp. 873–879, Jan. 2008.

[50] J. Armstrong, "OFDM for optical communications," *J. Lightw. Technol.*, vol. 27, no. 3, pp. 189–204, Feb. 2009.

[51] S. J. Savory, "Digital filters for coherent optical receivers," *Opt. Express*, vol. 16, no. 2, pp. 804–817, Jan. 2008.

[52] F. Gardner, "A BPSK/QPSK timing-error detector for sampled receivers," *IEEE Trans. Commun.*, vol. 34, no. 5, pp. 423–429, May 1986.

[53] M. Kuschnerov, F. Hauske, E. Gourdon, K. Piyawanno, B. Lankl, and B. Spinnler, "Digital timing recovery for coherent fiber optic systems," in *Proc. Conference on Optical Fiber Communication OFC 2008*, San Diego, CA, USA, paper JThA63, 2008.

[54] H. Louchet, K. Kuzmin, and A. Richter, "FFT-based digital clock recov very for coherent transmission systems with multilevel modulation formats," in *Proc. European Conference on Optical Communication ECOC 2009*, Wien, Austria, paper 7.3.5, 2009.

[55] S. Betti, F. Curti, G. De Marchis, and E. Iannone, "A novel multilevel coherent optical system: 4-quadrature signaling," *J. Lightw. Technol.*, vol. 9, no. 4, pp. 514–523, Apr. 1991.

[56] D. Godard, "Self-recovering equalization and carrier tracking in two-dimensional data communication systems," *IEEE Trans. Commun.*, vol. 28, no. 11, pp. 1867–1875, Nov. 1980.

[57] R. C. Johnson, P. Schniter, T. J. Endres, J. D. Behm, D. R. Brown, and R. A. Casas, "Blind equalization using the constant modulus criterion: A review," *Proc. of the IEEE*, no. 10, pp. 1927–1950, Oct. 1998.

[58] H. Louchet, K. Kuzmin, and A. Richter, "Improved DSP algorithms for coherent 16-QAM transmission," in *Proc. European Conference on Optical Communication ECOC 2008*, Bruxelles, Belgium, paper Tu.1.E.6, 2008.

[59] A. Viterbi, "Nonlinear estimation of PSK-modulated carrier phase with application to burst digital transmission," *IEEE Trans. Inf. Theory*, vol. 29, no. 4, pp. 543–551, July 1983.

[60] E. Ip and J. Kahn, "Feedforward carrier recovery for coherent optical communications," *J. Lightw. Technol.*, vol. 25, no. 9, pp. 2675–2692, Sept. 2007.

[61] J. G. Proakis and D. G. Manolakis, *Digital Signal Processing: Principles, Algorithms, and Applications*. Prentice Hall, 1996.

[62] M. Seimetz, "Performance of coherent optical square-16-QAM-systems based on IQ-transmitters and homodyne receivers with digital phase estimation," in *Proc. Conference on Optical Fiber Communication OFC 2006*, San Diego, CA, USA, paper NWA4, 2006.

[63] A. Leven, N. Kaneda, U.-V. Koc, and Y.-K. Chen, "Frequency estimation in intradyne reception," *IEEE Photon. Technol. Lett.*, vol. 19, no. 6, pp. 366–368, Mar. 2007.

[64] C. Fürst, J.-P. Elbers, M. Camera, H. Wernz, H. Griesser, S. Herbst, F. Cavaliere, A. Ehrhardt, D. Breuer, D. Fritzsche, S. Vorbeck, M. Schneiders, W. Weiershausen, R. Leppla, J. Wendler, M. Schrödel, T. Wuth, C. Fludger, T. Duthel, B. Milivojevic, and C. Schulien, "43 Gb/s RZ-DQPSK DWDM field trial over 1047 km with mixed 43 Gb/s and 10.7 Gb/s channels at 50 and 100 GHz channel spacing," in *Proc. European Conference on Optical Communication ECOC 2006*, Cannes, France, paper Th4.1.4, 2006.

[65] H. Griesser, J.-P. Elbers, H. Wernz, and C. Fürst, "43 Gb/s RZ-DQPSK Transmission over a 660 km 10.7 Gb/s DWDM Link," in *Proc. European Conference on Optical Communication ECOC 2006*, Cannes, France, paper Th1.6.6, 2006.

[66] S. Chandrasekhar and X. Liu, "Impact of channel plan and dispersion map on hybrid DWDM transmission of 42.7-Gb/s DQPSK and 10.7-Gb/s OOK on 50-GHz grid," *IEEE Photon. Technol. Lett.*, vol. 19, no. 22, pp. 1801–1803, Nov. 2007.

[67] S. Bigo, G. Charlet, O. B. Pardo, and J. Renaudier, "Characterization of the impact of non-linear effects in coherent transmission experiments," in *Digest of the IEEE/LEOS Summer Topical Meetings 2008*, Acapulco, Mexico, 2008.

[68] O. Bertran-Pardo, J. Renaudier, G. Charlet, H. Mardoyan, P. Tran, and S. Bigo, "Nonlinearity limitations when mixing 40-Gb/s coherent PDM-QPSK channels with preexisting 10-Gb/s NRZ channels," *IEEE Photon. Technol. Lett.*, vol. 20, no. 15, pp. 1314–1316, Aug. 2008.

[69] M. Bertolini, P. Serena, N. Rossi, and A. Bononi, "Numerical Monte Carlo comparison between coherent PDM-QPSK/OOK and incoherent DQPSK/OOK hybrid systems," in *Proc. European Conference on Optical Communication ECOC 2008*, Bruxelles, Belgium, paper P.4.16, 2008.

[70] ——, "Monte Carlo estimation of PDM-QPSK/OOK and DQPSK/OOK hybrid systems tolerance against nonlinear effects," *IEEE Photon. Technol. Lett.*, vol. 21, no. 1, pp. 15–17, Jan. 2009.

[71] ——, "Narrow filtered DPSK: an attractive solution for hybrid systems," in *Proc. European Conference on Optical Communication ECOC 2008*, Bruxelles, Belgium, paper P.4.15, 2008.

[72] ——, "XPM reduction in hybrid 10G/40G transmission using 10-Gb/s narrow-filtered DPSK modulation," *Opt. Express*, vol. 17, no. 8, pp. 5919–5924, Mar. 2009.

[73] M. Bertolini, P. Serena, G. Bellotti, and A. Bononi, "On the XPM-induced distortion in DQPSK-OOK and coherent QPSK-OOK hybrid systems," in *Proc. Conference on Optical Fiber Communication OFC 2009*, San Diego, CA, USA, paper OTuD4, 2009.

[74] A. Bononi, M. Bertolini, P. Serena, and G. Bellotti, "Cross-phase modulation induced by OOK channels on higher-rate DQPSK and coherent QPSK channels," *J. Lightw. Technol.*, vol. 27, no. 18, pp. 3974–3983, Sept. 2009.

[75] M. Lefrancois, F. Houndonougbo, T. Fauconnier, G. Charlet, and S. Bigo, "Cross comparison of the nonlinear impairments caused by 10Gbit/s neighboring channels on a 40Gbit/s channel modulated with various formats, and over various fiber types," in *Proc. Conference on Optical Fiber Communication OFC 2007*, Anaheim, CA, USA, paper JThA44, 2007.

[76] Y. Frignac, J.-C. Antona, and S. Bigo, "Enhanced analytical engineering rule for fast optimization dispersion maps in 40 Gbit/s-based transmission," in *Proc. Conference on Optical Fiber Communication OFC 2004*, San Diego, CA, USA, paper OTuN3, 2004.

[77] D. Penninckx, H. Bissessur, P. Brindel, E. Gohin, and F. Bakhti, "Optical differential phase shift keying (DPSK) direct detection considered as a duobinary signal," in *Proc. European Conference on Optical Communication ECOC 2001*, Amsterdam, Netherlands, paper We.P.40, 2001.

[78] I. Lyubomirsky and C.-C. Chien, "DPSK demodulator based on optical discriminator filter," *IEEE Photon. Technol. Lett.*, vol. 17, no. 2, pp. 492–494, Feb. 2005.

[79] E. Forestieri and G. Prati, "Narrow filtered DPSK implements order-1 CAPS optical line coding," *IEEE Photon. Technol. Lett.*, vol. 16, no. 2, pp. 662–664, Feb. 2004.

[80] H. Griesser and J.-P. Elbers, "Influence of cross-phase modulation induced nonlinear phase noise on DQPSK signals from neighbouring OOK channels,"

in *Proc. European Conference on Optical Communication ECOC 2005*, Glasgow, United Kingdom, paper Tu1.2.2, 2005.

[81] K.-P. Ho, "Error probability of DPSK signals with cross-phase modulation induced nonlinear phase noise," *IEEE J. Sel. Topics Quantum Electron.*, vol. 10, no. 2, pp. 421–427, Mar.–Apr. 2004.

[82] R. Luis, B. Clouet, A. Teixeira, and P. Monteiro, "Analytical Modeling of the Cross-Phase Modulation-Induced Degradation in Mixed DPSK and ASK Transmission Systems," in *Proc. International Conference on Transparent Optical Networks ICTON 2007*, Rome, Italy, paper Mo.P.17, 2007.

[83] ——, "Pump-probe analysis of the cross-phase modulation degradation induced by 10 Gbit/s amplitude-shift-keyed signals on 40 Gbit/s DPSK signals," *Opt. Lett.*, vol. 32, no. 19, pp. 2786–2788, Oct. 2007.

[84] O. Vassilieva, T. Hoshida, J.C.Rasmussen, and T. Naito, "Symbol rate dependency of XPM-induced phase noise penalty on QPSK- based modulation formats," in *Proc. European Conference on Optical Communication ECOC 2008*, Bruxelles, Belgium, paper We.1.E.4,2008.

[85] N. Blachman, "The effect of phase error on DPSK error probability," *IEEE Trans. Commun.*, vol. 29, no. 3, pp. 364–365, Mar. 1981.

[86] K.-P. Ho, "The effect of interferometer phase error on direct-detection dpsk and dqpsk signals," *IEEE Photon. Technol. Lett.*, vol. 16, no. 1, pp. 308–310, Jan. 2004.

[87] ——, *Phase Modulated Optical Communication Systems*. New York: Springer, 2005.

[88] T.-K. Chiang, N. Kagi, M. Marhic, and L. Kazovsky, "Cross-phase modulation in fiber links with multiple optical amplifiers and dispersion compensators," *J. Lightw. Technol.*, vol. 14, no. 3, pp. 249–260, Mar. 1996.

[89] A. Bononi, C. Francia, and G. Bellotti, "Impulse response of cross-phase modulation filters in multi-span transmission systems with dispersion compensation," *Opt. Fiber Technol.*, vol. 4, no. 4, pp. 371–383, Apr. 1998.

[90] M. Varani, G. Bellotti, A. Bononi, and C. Francia, "Analysis of cross-phase modulation induced intensity noise in high-speed dispersion compensated transmission systems," in *Proc. IEEE Lasers and Electro-Optics Society Annual Meeting LEOS '98*, Orlando, FL, USA, 1998.

[91] A. Bononi, G. Bellotti, M. Varani, and C. Francia, "SPM/XPM induced intensity distortion in WDM systems," in *Optical Networking*, A. Bononi, Ed. London, UK: Springer-Verlag, 1999, pp. 383–398.

[92] A. Cartaxo, "Cross-phase modulation in intensity modulation-direct detection wdm systems with multiple optical amplifiers and dispersion compensators," *J. Lightw. Technol.*, vol. 17, no. 2, pp. 178–190, Feb. 1999.

[93] R. Hui, Y. Wang, K. Demarest, and C. Allen, "Frequency response of cross-phase modulation in multispan wdm optical fiber systems," *IEEE Photon. Technol. Lett.*, vol. 10, no. 9, pp. 1271–1273, Sept. 1998.

[94] A. Cartaxo, "Impact of modulation frequency on cross-phase modulation effect in intensity modulation-direct detection wdm systems," *IEEE Photon. Technol. Lett.*, vol. 10, no. 9, pp. 1268–1270, Sept. 1998.

[95] G. Bellotti, M. Varani, C. Francia, and A. Bononi, "Intensity distortion induced by cross-phase modulation and chromatic dispersion in optical-fiber transmissions with dispersion compensation," *IEEE Photon. Technol. Lett.*, vol. 10, no. 12, pp. 1745–1747, Dec. 1998.

[96] R. Killey, H. Thiele, V. Mikhailov, and P. Bayvel, "Prediction of transmission penalties due to cross-phase modulation in wdm systems using a simplified technique," *IEEE Photon. Technol. Lett.*, vol. 12, no. 7, pp. 804–806, July 2000.

[97] A. Bononi, P. Serena, and M. Bertolini, "Unified analysis of weakly-nonlinear dispersion-managed optical transmission systems from perturbative approach," *C. R. Physique*, vol. 9, pp. 947–962, 2008.

[98] R. Luis and A. Cartaxo, "Analytical characterization of spm impact on xpm-induced degradation in dispersion-compensated wdm systems," *J. Lightw. Technol.*, vol. 23, no. 3, pp. 1503–1513, Mar. 2005.

[99] A. Bononi, P. Serena, and A. Orlandini, "A unified design framework for single-channel dispersion-managed terrestrial systems," *J. Lightw. Technol.*, vol. 26, no. 22, pp. 3617–3631, Nov.15, 2008.

[100] J. Wang and K. Petermann, "Small signal analysis for dispersive optical fiber communication systems," *J. Lightw. Technol.*, vol. 10, no. 1, pp. 96–100, Jan. 1992.

[101] M. Bertolini, M. Salsi, G. Charlet, H. Mardoyan, P. Tran, O. Bertran-Pardo, J. Renaudier, and S. Bigo, "Single-carrier vs. dual-carrier transmission of 100Gb/s coherent PDM-QPSK over NZ-DSF fibre," in *Proc. European Conference on Optical Communication ECOC 2009*, Wien, Austria, paper 2.3.1, 2009.

[102] T. Xia, G. Wellbrock, M. Pollock, W. Lee, D. Peterson, D. Doucet, J. Sitch, K. Ghazian, P. Bryan, and P. Rochon, "92-Gb/s field trial with ultra-high PMD tolerance of 107-ps DGD," in *Proc. Conference on Optical Fiber Communication OFC 2009*, San Diego, CA, USA, paper NThB3, 2009.

[103] B. Mikkelsen, C. Rasmussen, P. Mamyshev, and F. Liu, "Partial DPSK with excellent filter tolerance and OSNR sensitivity," *Electron. Lett.*, vol. 42, no. 23, pp. 1363–1364, Nov. 2006.

[104] J. Renaudier, O. Bertran-Pardo, H. Mardoyan, P. Tran, G. Charlet, S. Bigo, M. Lefrancois, B. Lavigne, J.-L. Auge, L. Piriou, and O. Courtois, "Performance comparison of 40G and 100G coherent PDM-QPSK for upgrading dis-

persion managed legacy systems," in *Proc. Conference on Optical Fiber Communication OFC 2009*, San Diego, CA, USA, paper NWD5, 2009.

[105] C. D. Poole and J. A. Nagel, "Polarization effects in lightwave systems," in *Optical Fiber Telecommunications IIIA*, I. P. Kaminov and T. L. Kochs, Eds. San Diego, CA: Academic Press., 1997, ch. 6.

[106] A. Dal Forno, A. Paradisi, R. Passy, and J. von der Weid, "Experimental and theoretical modeling of polarization-mode dispersion in single-mode fibers," *IEEE Photon. Technol. Lett.*, vol. 12, no. 3, pp. 296–298, Mar. 2000.

[107] R. Khosravani, J. Lima, I.T., P. Ebrahimi, E. Ibragimov, A. Willner, and C. Menyuk, "Time and frequency domain characteristics of polarization-mode dispersion emulators," *IEEE Photon. Technol. Lett.*, vol. 13, no. 2, pp. 127–129, Feb. 2001.

[108] F. Buchali and H. Bulow, "Adaptive pmd compensation by electrical and optical techniques," *J. Lightw. Technol.*, vol. 22, no. 4, pp. 1116–1126, Apr. 2004.

[109] M. Karlsson and H. Sunnerud, "Effects of nonlinearities on PMD-induced system impairments," *J. Lightw. Technol.*, vol. 24, no. 11, pp. 4127–4137, Nov. 2006.

[110] C. Xie, "Interchannel nonlinearities in coherent polarization-division-multiplexed quadrature-phase-shift- keying systems," *IEEE Photon. Technol. Lett.*, vol. 21, no. 5, pp. 274–276, Mar. 2009.

[111] M. Winter, C.-A. Bunge, D. Setti, and K. Petermann, "A statistical treatment of cross-polarization modulation in DWDM systems," *J. Lightw. Technol.*, vol. 27, no. 17, pp. 3739–3751, Sept. 2009.

[112] O. Bertran-Pardo, J. Renaudier, G. Charlet, P. Tran, H. Mardoyan, M. Salsi, and S. Bigo, "Experimental assessment of interactions between nonlinear impairments and polarization-mode dispersion in 100-Gb/s coherent systems versus receiver complexity," *IEEE Photon. Technol. Lett.*, vol. 21, no. 1, pp. 51–53, Jan. 2009.

[113] P. Serena, N. Rossi, and A. Bononi, "Nonlinear penalty reduction induced by PMD in 112 Gbit/s WDM PDM-QPSK coherent systems," in *Proc. European Conference on Optical Communication ECOC 2009*, Wien, Austria, paper 10.4.3, 2009.

[114] J.-C. Antona, E. Grellier, A. Bononi, S. Petitrenaud, and S. Bigo, "Revisiting binary sequence length requirements for the accurate emulation of highly dispersive transmission systems," in *Proc. European Conference on Optical Communication ECOC 2008*, Bruxelles, Belgium, paper We.1.E.3, 2008.

[115] E. Golovchenko, L. Rahman, B. Bakhshi, D. Kovsh, F. Idrovo, and S. Abbott, "Field deployment of WDM 10 Gb/s capacity over 10,757 km of reconfigured portion of SAM-1 cable system," in *Optical Fiber Communication Conference OFC 2007*, San Diego, CA, USA, paper PDP27, 2007. [Online]. Available: http://www.opticsinfobase.org/abstract.cfm?URI=OFC-2007-PDP27

[116] G. Charlet, E. Corbel, J. Lazaro, A. Klekamp, R. Dischler, P. Tran, W. Idler, H. Mardoyan, A. Konczykowska, F. Jorge, and S. Bigo, "WDM bit-to-bit alternate-polarisation RZ-DPSK transmission at 40x42.7Gbit/s over transpacific distance with large Q-factor margin," in *Proc. European Conference on Optical Communication ECOC 2008*, Stockholm, Sweden, paper Th4.4.5, 2004.

[117] J.-X. Cai, D. G. Foursa, C. R. Davidson, Y. Cai, G. Domagala, H. Li, L. Liu, W. Patterson, A. Pilipetskii, M. Nissov, and N. Bergano, "A DWDM demonstration of 3.73Tb/s over 11,000km using 373 RZ-DPSK channels at 10Gb/s," in *Optical Fiber Communication Conference*, Atlanta, GE, USA, paper PDP22, 2003. [Online]. Available: http://www.opticsinfobase.org/abstract.cfm?URI=OFC-2003-PD22

[118] V. Curri, P. Poggiolini, A. Carena, and F. Forghieri, "Dispersion compensation and mitigation of nonlinear effects in 111-Gb/s WDM coherent PM-QPSK systems," *IEEE Photon. Technol. Lett.*, vol. 20, no. 17, pp. 1473–1475, Sept. 2008.

[119] L. Becouarn, G. Vareille, P. Pecci, and J. Marcerou, "3Tbit/s transmission (301DPSK channels at 10.709Gb/s) over 10270km with a record efficiency of 0.65(bit/s)/Hz," in *Proc. European Conference on Optical Communication ECOC 2003*, Rimini, Italy, paper Th 4.3.2, 2003.

[120] I. Morita and N. Edagawa, "50GHz-spaced 64x42.7Gbit/s transmission over 8,200km using prefiltered CS-RZ DPSK signal and EDFA repeaters," in *Proc. European Conference on Optical Communication ECOC 2003*, Rimini, Italy, paper Th 4.3.1, 2003.

[121] E. Ip and J. Kahn, "Compensation of dispersion and nonlinear impairments using digital backpropagation," *J. Lightw. Technol.*, vol. 26, no. 20, pp. 3416–3425, Oct. 2008.

[122] H. Masuda, E. Yamazaki, A. Sano, T. Yoshimatsu, T. Kobayashi, E. Yoshida, Y. Miyamoto, S. Matsuoka, Y. Takatori, M. Mizoguchi, K. Okada, K. Hagimoto, T. Yamada, and S. Kamei, "13.5-Tb/s (135 x 111-Gb/s/ch) No-Guard-Interval coherent OFDM transmission over 6,248 km using SNR maximized second-order DRA in the extended L-band," in *Proc. Conference on Optical Fiber Communication OFC 2009*, San Diego, CA, USA, paper PDPB5, 2009.

# Publications


[1] M. Magnani, M. Salsi, A. Bononi, and **M. Bertolini**, "Misure comparative di prestazione di catene di amplificatori a semiconduttore con e senza stabilizzazione di guadagno," *in Proc. Fotonica 2007*, Mantova, Italy, paper A8.2, 2007.

[2] P. Serena, N. Rossi, **M. Bertolini** and A. Bononi, "A stratified sampling Monte Carlo algorithm for efficient BER measurement and its application to DQPSK terrestrial systems," *in Proc. European Conference on Optical Communications ECOC 2008*, Bruxelles, Belgium, paper We.1.E.2, 2008.

[3] **M. Bertolini**, P. Serena, N. Rossi, and A. Bononi, "Narrow filtered DPSK: an attractive solution for hybrid systems," *in Proc. European Conference on Optical Communications ECOC 2008*, Bruxelles, Belgium, paper P.4.15, 2008.

[4] **M. Bertolini**, P. Serena, N. Rossi, and A. Bononi, "Numerical Monte Carlo comparison between coherent PDM-QPSK/OOK and incoherent DQPSK/OOK hybrid systems," *in Proc. European Conference on Optical Communications ECOC 2008*, Bruxelles, Belgium, paper P.4.16, 2008.

[5] A. Bononi, P. Serena, and **M. Bertolini**, "Unified analysis of weakly-nonlinear dispersion-managed optical transmission systems using the perturbative approach," *Comptes Rendus - Physique*, vol. 9, no. 9-10, pp. 947-962, Nov.-Dic. 2008 .

[6] **M. Bertolini**, P. Serena, N. Rossi, and A. Bononi, "Monte Carlo estimation of PDM-QPSK/OOK and DQPSK/OOK hybrid systems tolerance against nonlinear effects," *IEEE Photon. Technol. Lett.*, vol. 21, no. 1, pp. 15-17, Jan. 2009.

[7] **M. Bertolini**, P. Serena, G. Bellotti, and A. Bononi, "On the XPM-induced distortion in DQPSK-OOK and coherent QPSK-OOK hybrid systems," *in Proc. of Optical Fiber Communication Conference OFC 2009*, San Diego, CA, USA, paper OTuD4, 2009.

[8] G. Charlet, M. Salsi, P. Tran, **M. Bertolini**, H. Mardoyan, J. Renaudier, O. Bertan-Pardo, S. Bigo, "72x100Gb/s transmission over transoceanic distance, using large effective area fiber, hybrid Raman-Erbium amplification and coherent detection," *in Proc. of Optical Fiber Communication Conference OFC 2009*, San Diego, CA, USA, paper PDPB6, 2009.

[9] G. Bellotti, A. Bononi, P. Serena, and **M. Bertolini**, "Analisi delle distorsioni indotte da XPM in sistemi ibridi DQPSK-OOK e QPSK-OOK," *in Proc. Fotonica 2009*, Pisa, Italy, paper A5.3, 2009.

[10] **M. Bertolini**, P. Serena, N. Rossi, and A. Bononi, "XPM reduction in hybrid 10G/40G transmission using 10-Gb/s narrow-filtered DPSK modulation," *Opt Express*, vol. 17, no. 8, pp. 5919-5924, Apr. 2009

[11] P. Serena, N. Rossi, **M. Bertolini** and A. Bononi, "Stratified sampling Monte Carlo algorithm for efficient BER estimation in long-haul optical transmission systems," *J. Lightw. Technol.*, vol. 27, no. 13, pp.2404-2411, Jul. 2009

[12] **M. Bertolini**, M. Salsi, G. Charlet, H. Mardoyan, P. Tran, O. Bertran-Pardo, J. Renaudier, and S.n Bigo, "Single-carrier vs. dual-carrier transmission of 100Gb/s coherent PDM-QPSK over NZ-DSF fibre," *in Proc. European Conference on Optical Communications ECOC 2009*, Wien, Austria, paper 2.3.1, 2009.

[13] J. Renaudier, O. Bertran-Pardo, G. Charlet, M. Salsi, **M. Bertolini**, H. Mardoyan, P. Tran, and S. Bigo, "On the required number of WDM channels when

assessing performance of 100Gb/s coherent PDM-QPSK overlaying legacy systems," *in Proc. European Conference on Optical Communications ECOC 2009*, Wien, Austria, paper 3.4.5, 2009.

[14] O. Bertran-Pardo, J. Renaudier, G. Charlet, M. Salsi, **M. Bertolini**, H. Mardoyan, P. Tran, C. Koebele, and S. Bigo, "System benefits of temporal polarization interleaving with 100Gb/s coherent PDM-QPSK, " *in Proc. European Conference on Optical Communications ECOC 2009*, Wien, Austria, paper 9.4.1, 2009.

[15] M. Salsi, **M. Bertolini**, and G. Charlet., "Taking long repeatered submarine systems to 40 Gbit/s and beyond," emphin Proc. European Conference on Optical Communications ECOC 2009, Wien, Austria, invited paper 9.7.3, 2009.

[16] O. Bertran-Pardo, J. Renaudier, G. Charlet, M. Salsi, **M. Bertolini**, H. Mardoyan, P. Tran, C. Koebele, and S. Bigo, "PDM-QPSK: on the system benefits arising from temporally interleaving polarization tributaries at 100Gb/s," *Opt. Express*, vol. 17, n. 22, pp.19902-19907, Oct. 2009.

[17] O. Bertran-Pardo, J. Renaudier, G. Charlet, P. Tran, H. Mardoyan, M. Salsi, **M. Bertolini**, and S. Bigo, "Insertion of 100Gb/s coherent PDM-QPSK channels over legacy optical networks relying on low chromatic dispersion fibres," *IEEE Globecom 2009 Optical Networks and Systems Symposium*, Honolulu, HA, USA, Nov. 2009.

[18] A. Bononi, **M. Bertolini**, P. Serena, and G. Bellotti, "Cross-phase modulation induced by OOK channels on higher-rate DQPSK and coherent QPSK channels," to be published on *J. Lightw. Technol.*

[19] J. Renaudier, O. Bertran-Pardo, G. Charlet, M. Salsi, **M. Bertolini**, H. Mardoyan, P. Tran, and S. Bigo, "Investigation on WDM nonlinear impairments arising from the insertion of 100Gb/s coherent PDM-QPSK over legacy optical networks," to be published on *IEEE Photon. Technol. Lett.*

# Acknowledgements

There are many people that helped me during these three years, in many different ways. All of them have contributed somehow to this these.

First I would like to thank my family and my girlfriend Claudia for their continuous support, advices, and unconditional love.

I want to thank my advisor Prof. Alberto Bononi for giving me the excellent opportunity to work in his group, for his commitment, inspiration and precious advices. He also allowed me to work abroad during my Ph.D., opening me a world of experiences and opportunities. In Parma I had the chance to work with wonderful people: Prof. Paolo Serena, Prof. Armand Vannucci, Nicola Rossi, Donato Sperti and, last but not least, Massimiliano Salsi (which will make an appearance later in this page).

I want to thank Prof. Leslie Rusch for welcoming me in his group at UniversitÉLaval where I could lay the bases of the work described in this these. In Quebec I worked with Francesco Vacondio and Amirhossein Ghazisaeidi whit whom I had a very fruitful although short interaction.

Finally I want to thank all the people at Alcatel-Lucent Bell Labs France. All of them made my 6 months in France an amazing experience. I would like to thank Sébastien Bigo for letting me work in his group, for his support and wise suggestions. Gabriel Charlet for the supervision, for bearing with my (so many) errors and teaching me how to work in a laboratory. Massimiliano Salsi, Oriol Bertran Pardo, Jeremie Renaudier and Clemens Koebele for creating such a friendly environment, for the enriching discussions and all the fantastic moments outside the working hours.